

Metabolic variation in cultured cells treated with differentially functionalised gold nanoparticles (GNPs)

AC Roets
22790918

Dissertation submitted in partial fulfilment of the requirements
for the degree *Magister Scientiae* in *Biochemistry* at the
Potchefstroom Campus of the North-West University

Supervisor: Dr Z Lindeque

Co-supervisor: Dr F Taute

May 2017

i) Abstract

Gold nanoparticles (GNPs) and differentially functionalised or ligand exchanged GNPs (Lig-GNPs) present promising advantages in a variety of fields. Surface functionalisation of GNPs with ligands is believed to improve the biocompatibility of the GNPs. However, the effects of these particles on biological systems remain unclear due to contradictions and several limitations in the literature, such as unstandardised protocols. Standardised methods and compatibility of assays with GNPs are essential in accurately determining the overall effect of GNPs on biological systems. Metabolomics analysis may present answers to the possible effects observed in the literature as it presents the metabolites, which are the closest to the functional phenotype of a biological system. However, research in these two fields as a combination is greatly limited. This study reveals the metabolic variation that occurs in HepG2 cells when treated with PVP-GNPs, PSSNa-GNPs and Citrate-GNPs by using standardised, pre-evaluated protocols. The results show that even though differentially functionalised GNPs seem to improve the biocompatibility of the particles, GNPs do induce variation on metabolome level; however, the variation is not necessarily linked with cytotoxicity. This field presents opportunities to further elucidate the effects that GNPs may have on biological systems.

Keywords: Biocompatibility, Gold nanoparticles, HepG2, Ligand functionalisation, Metabolomics, Variation.

ii) Acknowledgements

Thank you to my amazing two Supervisors, Dr. Zander Lindeque and Dr. Francois Taute, for all your patience, extraordinary guidance and effort. You truly are an inspiration to the students you lead. I really enjoyed working with you. Thank you to everyone who helped with various components of the study: Mr. Peet Jansen van Rensburg, for your assistance with the analytical equipment (GC-MS and LC-MS/MS), Dr. Shayne Mason for the help with the NMR, Mr. Johan Hendricks for the ICP-MS analysis. Dr. Anine Jordaan for the TEM images. Ms. Elcke du Plessis for your help with the editing, references and bibliography.

To my friends, Nadia Koen, Christinah Motshwane, Gontsiwe Mouthloatse, Chantell van der Merwe and Danielle Mulder, for keeping me sane, fed, active and loved. My Familiy, Mom, Dad and my two awesome brothers, for your support and unconditional love. Also for pretending to follow when I am speaking about my project- I love you to bits. Thank you Jason Matthyser, the love of my life, my pillar, my candle in the dark: for nagging me constantly to finish. You are the most amazing person I have ever met.

Thank You, Lord Almighty Father for Your never ending grace and love, for giving me the opportunity to serve through science, for equipping me, for blessing me with wonderful, talented people. "For by him were all things created, that are in heaven, and that are in earth, visible and invisible, whether they be thrones, or dominions, or principalities, or powers: all things were created by him, and for him:¹⁷ And he is before all things, and by him all things consist."-**Colossians 1:16-1**

iii) Table of contents

i) Abstract	2
ii) Acknowledgements	3
iii) Table of contents	4
iv) List of tables	10
v) List of figures	12
vi) List of equations	15
vii) Abbreviations	16
Chapter 1: Introduction	19
Chapter 2: Literature review	21
2.1 Introduction	21
2.2 A brief overview of nanoparticles	22
2.3 Concise history of GNPs	24
2.4 Applications of GNPs	24

2.4.1 Targeted drug delivery	24
2.4.2 DNA- and protein-binding agents	25
2.5 Synthesis of GNPs.....	27
2.5.1 Methods of synthesis.....	27
2.5.2 Size-dependent synthesis	28
2.5.3 Separation and sample clean-up.....	30
2.6 GNP Characterisation.....	32
2.6.1 Ultraviolet-visible (UV-Vis) spectroscopy	32
2.6.2 Dynamic light scattering (DLS).....	33
2.6.3 Transmission electron microscopy (TEM)	34
2.7 Surface modifications.....	35
2.8 The effects of GNPs on biological systems	38
2.8.1 Impacts on cells based on the chemical properties of GNPs	38
2.8.2 Effect on the cellular metabolome	40
2.9 Metabolomics.....	44
2.9.1 Applications, approaches, advantages and disadvantages	44

2.10 Problem statement	51
2.11 Aim and objectives	52
2.12 Study design	53
Chapter 3: Nanochemistry	55
3.1 Introduction	55
3.2 Methods	56
3.2.1 GNP synthesis	56
3.2.2 Sample clean-up	56
3.2.3 GNP characterisation	56
3.2.4 Ligand exchange	61
3.3 Results and discussion	66
3.3.1 GNP synthesis and characterisation	66
3.3.2 Ligand exchange standardisation & characterisation	71
3.3.3 Ligand exchange stability evaluation	77
3.4 Summary	79
Chapter 4: Cell Biology – Pilot study	80

4.1 Introduction	80
4.2 Methods	80
4.2.1 General culturing	80
4.2.2 Trypsinisation, cell counting and cell seeding	80
4.2.3 Treatment of HepG2 cells with Lig-GNPs	82
4.2.4 Cell viability assays	83
4.2.5 Internalisation analysis using inductively coupled plasma mass spectrometry (ICP-MS)	86
4.3 Results and discussion.....	87
4.3.1 WST-1 cell viability/cytotoxicity assay results	87
4.3.2 APOPercentage (Apo %) apoptosis assay results	91
4.3.3 Internalisation Results.....	95
4.4 Conclusive summary	98
Chapter 5: Metabolomics.....	100
5.1 Introduction	100
5.2 Materials and methods	102

5.2.1 Seahorse XF ⁹⁶ analysis	102
5.2.2 Metabolomics analysis.....	104
5.3 Results and discussion.....	110
5.3.1 Seahorse XF ⁹⁶ analysis.....	110
5.3.2 Metabolomics analysis.....	113
5.4 Conclusive summary	131
Chapter 6: Conclusion.....	132
Addendum A: Bibliography	136
Addendum B: Concentration evaluation of GNPs	145
Addendum C: Ligand exchanged GNPs	147
Addendum D: Stability analysis.....	149
Addendum E: Cell viability assays	155
WST-1 data	155
Addendum F: Metabolomics data	157
Addendum G: Materials, suppliers and preparation of stock solutions.	162
Materials and suppliers	162

Stock solutions and buffers	164
Addendum H: Comet assay results reported by Mulder et al., (2016)	166
Addendum I: Ligand exchange ppm-mol calculations	168
Addendum J: Seahorse XF analysis elaborated protocol	172

iv) List of tables

Table 2-1: Ligands that are used as coating materials for GNPs (Lig-GNPs).....	36
Table 2-2: A summative table of the effect of GNPs on the cellular metabolome reported in the literature.....	41
Table 2-3: Identification levels of metabolites	46
Table 3-1: The absorbance values determined using UV-Vis spectrometry and the correlating diameter (d) of GNPs (in nm; adapted from Haiss et al., (2007)).....	62
Table 3-2: The size dependent decadic extinction coefficient values at 540 nm.....	59
Table 3-3: The Ligand:GNP ratio that was added to each pH group.....	59
Table 3-4: Ligands with their stock solutions, favourable pH for ligand exchange, and final concentration in GNP-solution.	63
Table 3-5: A summary of the compounds and concentrations/pH values used to determine the stability of GNPs in a physiological environment.	65
Table 3-6: Summary of the calculated size and concentration of GNPs based on the OD of the particles and calculations	68
Table 3-7: The OD ₄₅₀ and maximum absorbance values (OD ₅₂₀) of the Lig-GNPs....	72
Table 3-8: RF values of Lig-GNPs which migrated through the agarose gel.....	74
Table 3-9: The hydrodynamic diameter of Lig-GNPs measured by DLS.	75
Table 3-10: A summary of the aqueous stability ranges of the Lig-GNPs.....	78
Table 4-1: The quantities of PBS, trypsin, cells and media used for each container...	82

Table 4-2: Treatment conversion from nM to ppm.	83
Table 4-3: Controls included for the WST-1 cell viability assay.	84
Table 4-4: Lig-GNPs dosages selected for the main study based on the IC ₃₀ values obtained by the WST-1 cytotoxicity assay.	88
Table 4-5: The FI values of the Lig-GNPs at the selected time points.....	94
Table 4-6: The gold atoms present in each Lig-GNP sample.....	95
Table 5-1: Compounds applied during the analysis.....	103
Table 5-2: Programmed mobile phase gradient used for separating butylated amino acids and acylcarnitines.	108
Table 5-3: The p-values of compounds significantly altered in the exometabolome	115
Table 5-4: ID levels, p-values and significant difference of each treatment group, compared with the VC, measured with Fisher's LSD.	117
Table 5-5: A summary of the affected metabolism class, metabolites, ID levels and p- values of all the Lig-GNP treatment groups.	125

v) List of figures

Figure 2-1: The Localised Surface Plasmon Resonance (LSPR)..	22
Figure 2-2: Targeted drug delivery application of rheumatoid arthritis.	25
Figure 2-3: Colorimetric detection of proteins by using GNPs.	26
Figure 2-4: A schematic presentation of the two general methods used to synthesise GNPs..	28
Figure 2-5: The relationship between the FC of citrate (required for the synthesis of GNPs) and the GNP's diameter.	29
Figure 2-6: Separation of GNPs by using sucrose gradient centrifugation.	31
Figure 2-7: Normalised absorbance values illustrating the difference in plasmon peaks between different morphologies and sizes of nanoparticles.	33
Figure 2-8: The correlation between particle size and intensity because of the hydrodynamic diameter..	34
Figure 2-9: Mitochondrial respiration and the parameters measured using the Seahorse XF96 analyser.	50
Figure 2-10: The study design.	54
Figure 3-1: The absorbance spectrum of citrate capped GNPs measured in the 300-700 nm wavelength range.	67
Figure 3-2: TEM results showing the morphology and diameter of citrate capped GNPs..	69

Figure 3-3: The size distribution graph indicating the % signal intensity measured by DLS.....	70
Figure 3-4: Absorbance spectra of the differentially functionalised GNPs used in this study.....	72
Figure 3-5: Agarose gel electrophoresis of Lig-GNPs at pH8, 50 V for 45 minutes. .	73
Figure 3-6: The size and orientation differences between a PSSNa-GNP and a BSA-GNP.....	76
Figure 4-1: The % cytotoxicity after treatment with a range of different concentrations of Lig-GNPs.....	89
Figure 4-2 HepG2 cells analysed with the APOPercentage apoptosis dye reagent ...	92
Figure 4-3: The FI values of PVP-GNP and PSSNa-GNP treated cells over 24hours.	93
Figure 4-4: The percentages of Lig-GNPs in a) the cells, b) the PBS-wash and c) the media.....	96
Figure 5-1 Schematic representation of the metabolomics analysis performed..	104
Figure 5-2: Mitochondrial OCR of HepG2 cells after 3 hours of Lig-GNP treatment.	111
Figure 5-3: One-way ANOVA results showing the maximal respiration and spare respiratory capacity.....	112
Figure 5-4: Box plots illustrating the differences in compound concentrations.....	114
Figure 5-5: PCA scores plot of compounds altered within the exometabolome	116
Figure 5-6: Box plots illustrating the differences in compound concentrations.....	120

Figure 5-7: PCA scores plot of the metabolites altered within the endometabolome.	121
Figure 5-8: One way ANOVA statistical analysis on the treated groups	123
Figure 5-9: PCA score plot of the three Lig-GNP treatment groups	124
Figure 5-10: Metabolic pathway and box plots of altered compounds	138
Figure 5-11: Metabolic pathway and box plots of altered compounds associated with the TCA cycle and amino acids.....	139

vi) List of equations

Equation 2-1: Fractional concentration (FC).....	31
Equation 3-1: Calculation of Cit-GNP size using the OD obtained from UV-Vis spectrometry.....	63
Equation 3-2: Determination of GNP concentration.....	64
Equation 4-1: Calculation of % cytotoxicity from WST-1 data.....	93
Equation 4-2: Normalisation of baseline apoptosis.	94

vii) Abbreviations

BSA	-	Bovine serum albumin
BSTFA	-	N,O-Bistrifluoroacetamide
MMPCs	-	Cationic mixed monolayer protected gold clusters
Cit-GNPs	-	Citrate capped gold nanoparticles
cRPMI	-	Complete RPMI cell culture media
ddH ₂ O	-	Ultra-pure water
DLS	-	Dynamic light scattering
EDTA	-	Ethylene-diamine-tetra-acetic acid
EROD		Ethoxyresorufin O-deethylase
FBS	-	Foetal bovine serum
FC	-	Fractional concentration
FI	-	Fold increase
GNPs	-	Gold nanoparticles
GSH	-	Glutathione, reduced
GSSG	-	Glutathione, oxidized
HCl	-	Hydrochloric acid
HEPES	-	4 -(2-hydroxyethyl)-1-piperazineethanesulfonic acid
HepG2	-	Hepatocellular carcinoma cells
HPLC	-	High performance liquid chromatography
IC	-	Inhibition concentration

ICP-MS	-	Inductively coupled plasma mass spectrometry
Lig-GNPs	-	Ligand exchanged gold nanoparticles or functionalised gold nanoparticles
LSD	-	Least significant difference
LSPR	-	Localised surface plasmon resonance
MMPCs	-	Cationic mixed monolayer protected gold clusters
MOX	-	Methoxyamine hydrochloride
MOPS	-	3-(N-morpholino) propanesulfonic acid
MUA	-	11-Mercaptoundecanoic acid
NAC	-	N-acetyl-L-cysteine
NaCl	-	Sodium chloride
NaOH	-	Sodium hydroxide
NIR	-	Near-infrared
nm	-	Nanometre
nM	-	Nanomolar
OBD	-	Oxford Dictionary of Biochemistry and Molecular Biology
OCR	-	Oxygen consumption rate
OD	-	Optical density
PBS	-	Phosphate buffered saline
PEG	-	Polyethylene glycol
PEI	-	Polyethylenimine
PROD		pentoxylresorufinO-deethylase
PSSNa	-	Poly-(sodium styrene-sulfonate)
PVP	-	Polyvinylpyrrolidone

TCZ	-	Tocilizumab
TEM	-	Transmission electron microscopy
TMCS	-	Trimethylsilyl chloride
UV-Vis	-	Ultraviolet-visible
VC	-	Vehicle control

Chapter 1: Introduction

Research on nanomaterial safety has received an increasing amount of attention. Gold nanoparticles (GNPs) and the effect thereof on biological systems has been a valid concern since the development of nanobased pharmaceutical applications and research in nanomedication. GNP-based applications have presented beneficial outcomes in targeted drug delivery, treatment of various diseases (including cancer and rheumatoid arthritis), colorimetric diagnostics with antibody-gold conjugation (Di Pasqua et al., 2009), and research involving GNPs as binding agents for DNA and proteins (Tsai et al., 2005). However, effects on cellular function is observed in the literature (Alkilany & Murphy, 2010). Therefore, research on the effects of these particles is considered to be a great priority in the pharmaceutical industry, since there are currently FDA-approved nanodrugs which have been effective up to this point (Pillai, 2014). Moreover, research elaborating on the effects of GNPs on biological systems in the literature is found to be contradicting or inconclusive (Alkilany & Murphy, 2010). Several challenges are faced by researchers due to protocols that are not standardised, yet are being used to evaluate cellular responses (Kong et al., 2011). The methods used to determine cell viability produce false positive or negative results because of interference of the GNPs with the assays used (Kong et al., 2011). These contradictory results could present obstacles in the future, unless sufficient research is done on the subject and protocols are standardised.

The effect GNPs have on the metabolome of living organisms is currently overlooked. Seeing that the metabolome is the final downstream product of the genome, transcriptome and proteome, it can display any potential effects GNPs have on the other biochemistry levels. Metabolomics can give a good indication if (so-called bio-inert) GNPs affect living systems; and, to a lesser extent, how it affects it. The metabolites in a cell are also the closest relation to the phenotype of the cell and can therefore provide very valuable information regarding the cellular environment (Gioria et al., 2015). With the limited amount of overall research available in the field of metabolomics and nanoparticles, it was decided to test the effect of GNPs on the metabolome of cells grown in culture. Moreover, the effect of differentially

coated GNPs is also lacking despite their use in certain applications. The effect of differentially functionalised GNPs was also studied.

Chapter 2 elaborates on the findings in the literature, which includes an overview on GNPs, applications, synthesis, characterisation and the effects on living systems observed in the literature. Moreover, the advantages and equipment used for metabolomics analysis are also included. The chapter concludes with the problem statement, aims and objectives, and a brief study design.

In Chapter 3, the methods used and results found with regards to the nanochemistry section of the study are discussed. The section includes the synthesis of GNPs, functionalisation of GNPs via ligand exchange, characterisation, and evaluation in terms of stability in the physiological environment.

Chapter 4 consists of the cell biology work which included cell culturing, viability assessment and cellular uptake. Two independent cell viability assays were performed, which included the WST-1 cytotoxicity assay (dosage response to determine the IC_{30} values) and the APOPercentage apoptosis assay to evaluate programmed cell death of the treated cells.

The effect of GNPs on the metabolome of cells was determined by evaluating cell viability in correlation with a metabolic profile of the cells that are treated with differentially functionalised GNPs. In Chapter 5, the methods and results of the metabolomics analysis are discussed. Based on the results in Chapter 4, HepG2 cells were treated accordingly and the cellular metabolome was evaluated. Firstly, the mitochondrial respiration was measured with the Seahorse XF96 analyser to determine whether the oxygen consumption rate (OCR) was altered as a result of the treatment. Afterwards, metabolomics analysis was done to investigate whether changes in the metabolome occur. The metabolised cell culture media (exometabolome) was analysed via NMR; and the internal cellular environment was analysed (endometabolome) via untargeted GC-MS analysis as well as targeted LC-MS/MS analysis on amino acids and acylcarnitines. Chapter 6 describes the conclusion and future perspectives of the study.

Chapter 2: Literature review

2.1 Introduction

This chapter gives an overview on GNPs as a whole, and includes a brief description of the chemical properties, history, applications, synthesis, and sample clean-up. Characterisation methods used in the literature to evaluate sizes and shapes of nanomaterials are also discussed. Furthermore, GNPs have a chemical affinity towards ligands, which can bind to their surface and alter the chemical properties of the GNPs. This characteristic is one of the main reasons why GNPs act as such an effective drug delivery vehicle in many applications. Ligand exchange between GNPs and ligands used for this purpose will be discussed and evaluated in terms of their chemical properties and their effect on cells. Contradictions and downfalls in the literature will also be investigated. The second part of this chapter directs attention to metabolomics. A concise description is given, explaining why metabolomics is a powerful tool that can be used to study the combination of these two fields of interest, namely the effect of GNPs on biological systems and the metabolome of such systems. The last section focuses on similar studies done and the questions that still remain unanswered. Finally, the chapter will be concluded with the aims and objectives of this study.

2.2 A brief overview of nanoparticles

Gold-nanoparticles (GNPs) are small gold structures with at least 1 dimension on the nanometre (nm) scale. The term “nano” can be defined as an extremely small structure between the range of 1 nm-100 nm which is applied in the field of nanoscience and nanotechnology (Sadik et al., 2014). GNPs are clusters of gold atoms which have notable characteristics and different physiochemical properties owing to their small size, such as catalytic reactivity due to their large surface area relative to their weight (Sadik et al., 2014).

GNPs possess unique properties as a result of their small size and are optically characterised by brilliant colours in solution due to intense absorption and scattering in the visible and NIR (Near-infrared) spectral regions (Chanana & Liz-Marzán, 2012). The colour changes from red to deep blue according to differences in size and morphology of the particles (Brust & Kiely, 2002). This unique optical observation is caused by the localised surface plasmon resonance (LSPR), which refers to the oscillation of electrons in the electrical field. The concept of the LSPR is illustrated in Figure 2-1. The dielectric nature of the environment around the particles also influences its physical properties, for instance: the inter-particle distance; the coating material on the particle; and the dispersion medium or solvent (Chanana & Liz-Marzán, 2012).

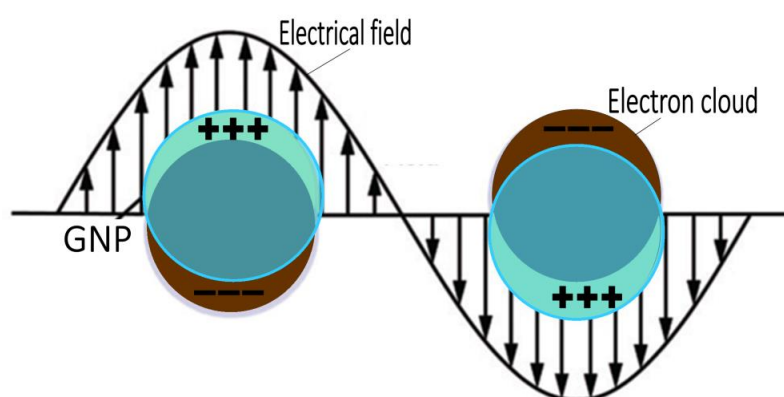


Figure 2-1: The Localised Surface Plasmon Resonance (LSPR). In an electric field, there is a slight separation between the positively charged metal core and the negatively charged electron cloud. The difference in charge causes the electrons to bounce back and forth in the electric field, which causes the unique optical properties observed in a GNP solution (adapted from Cobley et al., 2011).

It is historically believed that gold is chemically inert. This is true for gold in bulk state, however, it is found that in nanoparticle form, gold is highly reactive and has catalytic properties (Daniel & Astruc, 2004). A catalyst is defined by the Oxford Dictionary of Biochemistry and Molecular Biology (ODB) as any substance that increases the rate of a chemical reaction but is itself unchanged at the end of the reaction. Catalysts are usually present in very low concentrations relative to those of the substances whose reaction they are catalysing (Cammack et al., 2006). It is known in the literature that GNPs catalyse electrochemical redox reactions such as oxidising CO and CH₃OH, as well as the reduction of O₂ molecules (Daniel & Astruc, 2004). Studies have found that 8 nm size citrate capped GNPs deplete the mitochondrial GSH levels and induced apoptosis in HL7702 cells. They conclude that this may be due to the ability of GNPs to alter the redox status of the cells (Gao et al., 2011). Li et al. (2010) found that 20 nm foetal bovine serum (FBS) coated GNPs re-suspended in phosphate buffered saline (PBS) induced changes in 84 human oxidative stress pathway genes by at least one-fold. These studies all show the strong catalytic reactivity that GNPs have and the potential effects that may cause intercellular changes.

GNPs have had significant applications throughout history which has led to recent pharmaceutical breakthroughs. These advantageous properties present applications in the field of colorimetric research (Tsai et al., 2005) and targeted drug delivery in treatment of pathogenic diseases and cancer (Lee et al., 2014). Moreover, the synthesis, coating, and characterisation of GNPs involve simple techniques that are cost-effective, repeatable and robust (Daniel & Astruc, 2004; Ghosh et al., 2011; Horovitz et al., 2007; Seitz et al., 2003; Wang & Ma, 2009).

2.3 Concise history of GNPs

Around the fourth or fifth century, GNPs in the form of “soluble gold” appeared in China and Egypt. Ruby glass production and ceramic colouring using colloidal gold became famous. An example thereof is the Lycurgus cup which appeared green in reflected light and red in transmitted light. Another historical application of colloidal gold is the dye of silk in 1794. In the middle ages, colloidal gold was discovered to have curative medicinal properties for heart diseases, epilepsy, venereal problems, dysentery, and tumours, as well as diagnostic properties for other diseases such as syphilis. The formation of colloidal gold by reduction and the optical properties thereof was reported by Farady in 1857 (Daniel & Astruc, 2004).

2.4 Applications of GNPs

GNPs are currently used for numerous pharmaceutical and research-related advantages (Goodman et al., 2004). These applications include drug delivery for cancer therapy (Cheng et al., 2008) and treatment of rheumatoid arthritis (Lee et al., 2014) as well as specific binding agents for DNA and proteins (McIntosh et al., 2001; Li et al., 2005; Tsai et al., 2005). GNPs are also applied in a broader range of fields such as cosmetics, fuel cell technology, food additives, electronics and biocidal packaging (Sadik et al., 2014).

2.4.1 Targeted drug delivery

Since the development of nanotechnology, cancer and other treatments have shown to be successful due to the useful chemical properties of GNPs (Pillai, 2014). One of these powerful characteristics is the anti-angiogenic effects of GNPs by means of inhibition of heparin-binding glycoproteins, therefore, preventing the succeeding proliferative signalling effects of the tumour (Mukherjee et al., 2005). Moreover, GNPs have shown to present effective drug delivery in photodynamic cancer therapy. This form of cancer therapy involves light-excitabile photosensitisers that are able to transfer energy to oxygen in surrounding

tissue which produces highly reactive oxygen species (ROS), which in turn can directly induce necrosis or apoptosis of cancerous tissue (Cheng et al., 2008).

Lee et al. (2014) used GNPs as a drug delivery mechanism by forming a complex with hyaluronate and Tocilizumab (TCZ) to successfully treat rheumatoid arthritis. TCZ is an immunosuppressive drug that acts as an inhibitor of the interleukin-6 receptor, which is involved in the pathogenesis of rheumatoid arthritis. Hyaluronate has lubricative effects which protect cartilages against the damaging effects of rheumatoid arthritis. Figure 2-2 illustrates how GNPs are used to form a complex with TCZ in the treatment of rheumatoid arthritis.

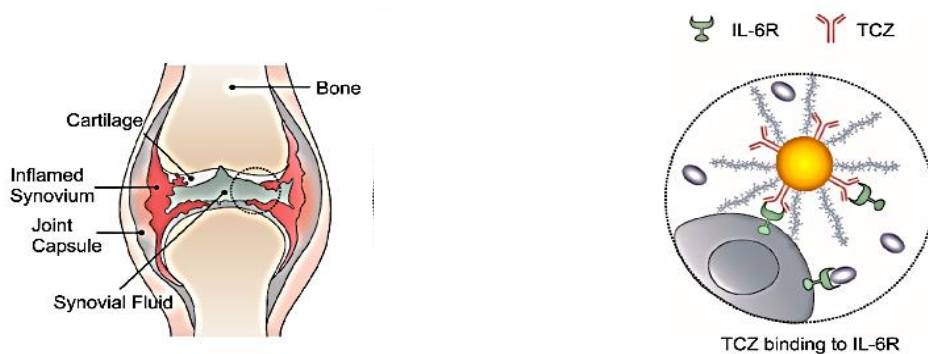


Figure 2-2: Targeted drug delivery application of rheumatoid arthritis. TCZ is bound to the surface of a GNP. The TCZ binds to the interleukin-6 receptor, and competition for binding occurs between the interleukin molecules and the TCZ on the surface of the GNP. Thus, the complex molecule inhibits the pathogenesis of rheumatoid arthritis by acting as an immunosuppressant (adapted from Lee et al., 2014).

2.4.2 DNA- and protein-binding agents

a) DNA

GNPs have also been used in molecular biology as DNA-binding agents. McIntosh et al. (2001) observed that cationic mixed monolayer protected gold clusters (MMPCs) have transcription inhibition properties when interacting with DNA. They functionalised MMPCs with tetra-alkyl-ammonium ligands which interacts based on charge complementarity with

the backbone structure of DNA. This process successfully led to the inhibition of T7 RNA polymerase transcription (McIntosh et al., 2001). The use of GNPs has also shown to improve the specificity in PCR reactions. Li et al. (2005) optimised PCR amplification using inexpensive organic nanomaterials such as GNPs that are highly stable as well as commercially available. These observations indicate that GNPs serve as useful DNA-binding agents.

b) Proteins

A competitive colorimetric assay using GNPs was used by Tsai et al. (2005) to detect protein interactions, specifically binding constants for concanavalin A. This principle is based on wavelength shifts within absorption spectra. Protein-protein interactions such as these play key roles in the functional and structural organisation of living cells (Tsai et al., 2005). Figure 2-3 explains the mechanism involved in colorimetric detection of proteins by using GNPs.

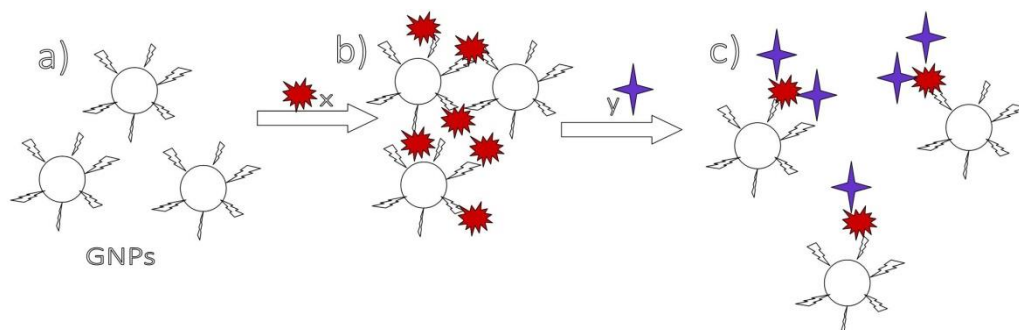


Figure 2-3: Colorimetric detection of proteins by using GNPs. GNPs are treated to attach ligands on the surface of the GNPs. These ligands are capable of binding with a protein, denoted as X (a). This allows proteins to interact with the ligand on the surface of the GNP, which leads to agglomeration due to multivalent ligand-protein interactions. A blue absorbance shift occurs in the solution which can be visually observed and measured with UV-Vis spectrometry (b). However, when a second, putative protein is introduced to the mixture, interaction between the two different proteins will occur, which can reverse the agglomeration noted. As a result, the solution shifts from blue back to its original purple-red colour (c), (adapted from Tsai et al., 2005)

2.5 Synthesis of GNPs

2.5.1 Methods of synthesis

There are mainly two methods most commonly available to synthesise GNPs, namely the Turkevich method (citrate reduction) and the Brust-Schiffrin method. Other related methods involve slight modifications of the above mentioned (Daniel & Astruc, 2004). Figure 2-4 shows the difference between the two general synthesis procedures.

a) Citrate reduction method

Citrate reduction is also known as the Turkevich synthesis method as it was pioneered by Turkevich in 1951. This procedure involves the reduction of chloroauric acid (HAuCl_4) by adding sodium citrate ($\text{Na}_3\text{C}_6\text{H}_5\text{O}_7$) to reduce the Au^{3+} in water. The reaction is endothermic and requires heat for successful synthesis; also, an ambient atmosphere is sufficient (Ghosh et al., 2011; Seitz et al., 2003).

b) Brust-Schiffrin method

The Brust-Schiffrin method is a two phase synthesis method using two immiscible organic liquids such as toluene and water. The mixture is stirred to create an emulsion and a strong reducing agent, sodiumborohydrate (NaBH_4), is added to form the GNPs (Wang & Ma, 2009).

Figure 2-4 gives a basic illustration of the differences between the two main methods of synthesis for GNPs.

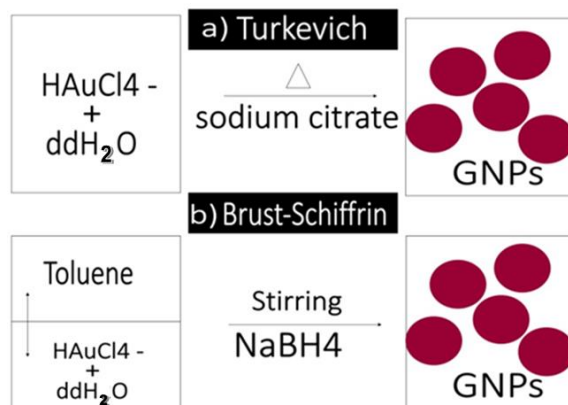


Figure 2-4: A schematic presentation of the two general methods used to synthesise GNPs. (a) Citrate reduction involves heating a mixture chloroauric acid (HAuCl₄) and ddH₂O, and then adding citrate (Na₃C₆H₅O₇) to reduce the Au³⁺ to form GNPs. (b) The Brust-Schiffrin method involves rapid stirring of two immiscible liquids such as toluene and water with HAuCl₄, and the addition of a strong reducing agent such as sodiumborohydrate (NaBH₄) to form the GNPs (Primo et al., 2011).

2.5.2 Size-dependent synthesis

a) Fractional concentration (FC) of citrate

With the citrate reduction method, the ratio between the chloroauric acid and citrate can be used to produce the GNP size of interest. This ratio was investigated by Ghosh et al. (2011), where the synthesis method is standardised successfully. GNPs with the diameter of interest can be produced by calculating the correlating fractional concentration (FC) of citrate that is added during the synthesis. Figure 2-5 is a graph which illustrates which FC of citrate (on the x-axis) is required to produce the desired GNP diameter (in nm) on the y-axis.

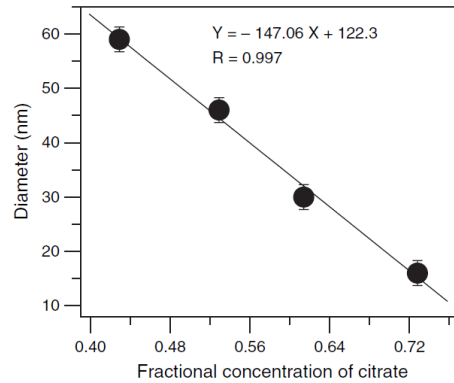


Figure 2-5: The relationship between the FC of citrate (required for the synthesis of GNPs) and the GNP's diameter. The diameter of the GNPs produced during synthesis is mainly dependent on the ratio between the HAuCl_4 and the amount of citrate added (Gosh et al., 2011).

The fractional concentration is calculated based on the concentrations of the reagents by using the following equation of Gosh et al. (2011):

Equation 2-1: Fractional concentration (FC)

$$\text{Fractional concentration (FC) of citrate} = \frac{[\text{citrate}]}{[\text{citrate}] + [\text{HAuCl}_4]}$$

where:

FC is the Fractional concentration of citrate that will be added to the HAuCl_4 solution, $[\text{citrate}]$ is the concentration of the stock solution citrate which is usually 1 % (38.8 mM) and $[\text{HAuCl}_4]$ is the concentration of chloroauric acid used during the synthesis.

2.5.3 Separation and sample clean-up

During the synthesis of inorganic GNPs, a large size distribution is produced. It is therefore important to separate these particles via sample clean-up before further analysis can be performed. Sample clean-up is extremely important, especially when analysing the effects that the particles may have on a living system. For instance, if a sample is not cleaned up, it is uncertain whether the cellular responses are due to the GNPs or simply to ligand present in solution that did not react (Alkilany & Murphy, 2010). An uncleansed sample may be too polydispersed, where the product is a mixture of a wide range of GNP sizes. Firstly, this will not be suitable for dynamic Light Scattering (DLS) measurement when characterising the GNPs, and, secondly, it will also cause differences in reactivity and toxicity (Zhou et al., 2009; Pan et al., 2007). GNPs are separated based on size and morphology (Hanauer et al., 2007). Separation can be done by performing normal centrifugation (Chen et al., 2009) or gel electrophoresis (Hanauer et al., 2007).

a) Centrifugation

Sucrose gradient centrifugation is a differential centrifugation procedure where a sucrose solution is used to separate particles by means of a gradient, based on the particle density and size (Wilson & Walker, 2010). The larger, denser particles will form at the lower end of the tube. This procedure can also be used to effectively separate GNPs. Chen et al. (2009) compared various differential centrifugation techniques to separate GNPs with high purity. Figure 2-6 illustrates the separation of GNPs by using sucrose gradient centrifugation.

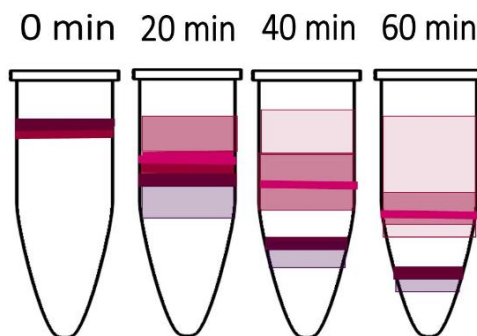


Figure 2-6: Separation of GNPs by using sucrose gradient centrifugation. A range of different concentrations of sucrose is added on top of each other from highest to lowest concentration, for instance 80 %, 60 %, 40 % etc. The sample is then added on top and centrifuged for 20-60 minutes or until the sample has separated. Each layer can then be resuspended separately (adapted from Chen et al., 2007).

The sample can also be cleaned up by normal centrifugation. The sample is pipetted into a centrifuge tube and centrifuged at $2000 \times g$ for 45 minutes or until the solution is clear. The pellet can then be resuspended in a suitable buffer or deionised water, depending on the use of the GNPs afterwards.

b) Gel electrophoresis

Hanauer et al. (2007) demonstrated the separation of GNPs by using gel electrophoresis after coating the particles with suitably charged polymers. The separation is optically monitored by using size- and morphology-dependent techniques and confirmed by using transmission electron microscopy (TEM). These researchers observed that gel electrophoresis presents the advantage of permitting multiple runs on a single gel when compared to other separation techniques, such as: centrifugation, size-exclusion chromatography, high performance liquid chromatography (HPLC), capillary electrophoresis and diafiltration. This advantage is considerable for standardisation of study conditions (Hanauer et al., 2007).

2.6 GNP Characterisation

There are several techniques available to determine the characteristics of GNPs after synthesis. Previously described methods such as centrifugation and gel electrophoresis (Section 2.5.3) can give a rough indication of the size, morphology and charge properties of GNPs. However, a variety of characterisation methods are required for more reliable results. UV-Vis spectroscopy, DLS and TEM are highly effective techniques used for this purpose.

2.6.1 Ultraviolet-visible (UV-Vis) spectroscopy

Certain characteristics of GNPs can be deduced based on the absorbance in the ultraviolet-visible spectral region. A notable property of GNPs is that it reaches a minimum optical density (OD) at 450 nm wavelength as the electron orbitals start to overlap. The maximum value is dependent on the morphology and size of the particles (Figure 2-7) and is used to determine the surface plasmon resonance (Alkilany & Murphy, 2010).

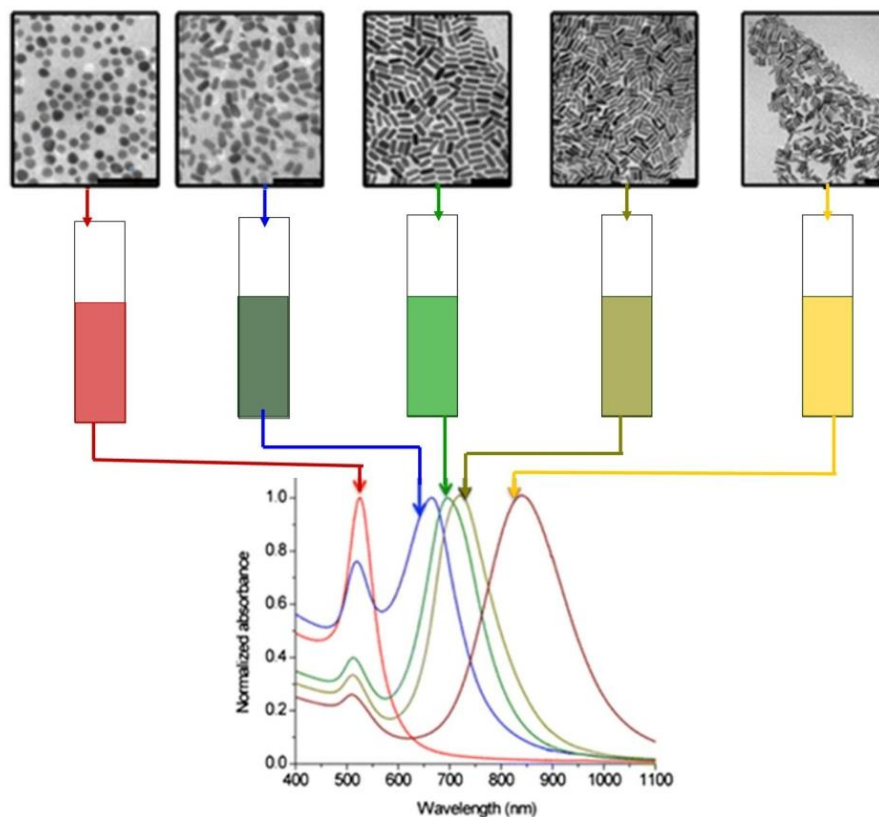


Figure 2-7: Normalised absorbance values illustrating the difference in plasmon peaks between different morphologies and sizes of nanoparticles, measured using UV-Vis spectroscopy and TEM. Spherical GNPs reaches a maximum at 520 nm where smaller, rod shaped particles show a shift in maximum peak to the 800-900 nm spectral region (adapted from Alkilany & Murphy, 2010).

2.6.2 Dynamic light scattering (DLS)

Dynamic light scattering (DLS) is an analytical technique used to determine the geometrical structure and motion state of small particles according to their Brownian motion. The measurement of dynamic behaviour of fluids is accomplished by scattering light from the particles (Goldburg, 1999). This technique is useful when measuring the size of the particles that have been coated with ligand, because it measures the hydrodynamic diameter of the particle as it moves. Figure 2-8 represents the result of measuring a given sized particle and the difference in intensity over time depending on the size of the sample.

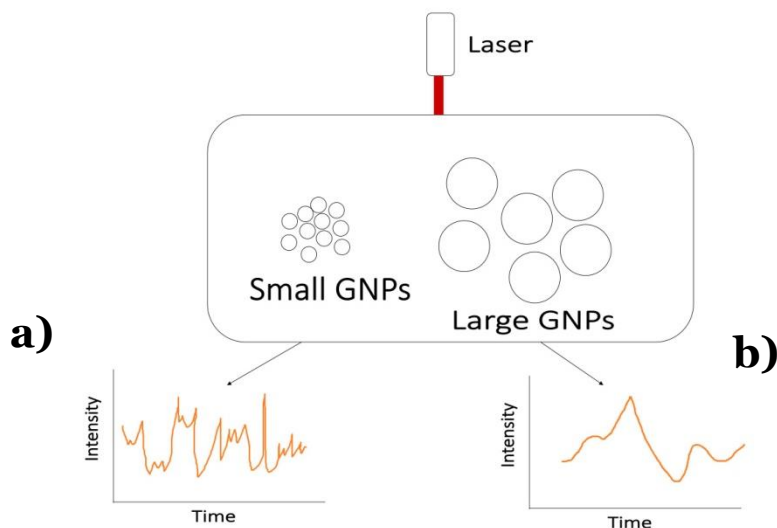


Figure 2-8: The correlation between particle size and intensity because of the hydrodynamic diameter. a) Small particles have a more rapid Brownian motion, therefore, more fluctuations occur. b) Larger particles move slower and have a less rapid Brownian motion, therefore, there are less fluctuations (adapted from Malvern, 2015).

2.6.3 Transmission electron microscopy (TEM)

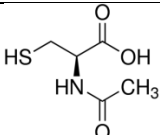
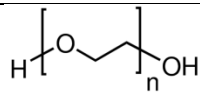

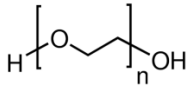
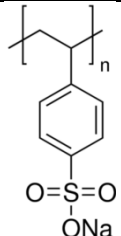
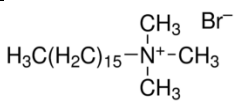
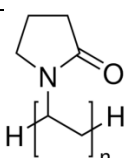
Transmission electron microscopy (TEM) is the most common characterisation method which allows visual confirmation of the GNP core. TEM gives structural, morphological and chemical information on nanoparticles that are individually analysed (Alloyeau et al., 2012). The microscope functions by accelerating electrons to a high energy level which interacts with the electron shells and nuclei of the sample particles, causing diffraction on the crystal lattice. This allows interference patterns to be visualised due to the strong absorbance of electrons by the sample (Alloyeau et al., 2012). Figure 2-7 (Section 2.6.1) presents an illustration of TEM images of different morphologies and sizes.

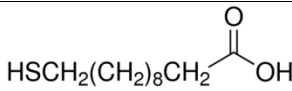
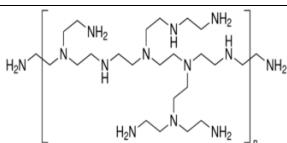
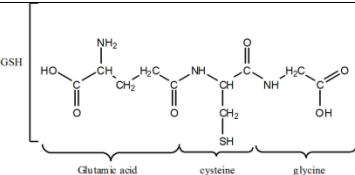
2.7 Surface modifications

Surface modification is the act of modifying the surface of a material by introducing physical, chemical or biological characteristics different from the ones originally found on the surface of a material (Cammack et al., 2006). A ligand can attach to the surface of a particle in different ways. The ODB defines a unidentate as any individual atom, ion, or molecule that is attached coordinately to one central metal atom. A polydentate or multidentate (of a ligand) consists of two or more groups which can be attached to a central atom. Such a ligand is able to form a chelate or a bridge (Cammack et al., 2006).

Based on the ability of GNPs to bind ligands to their surface, ligand exchange is a very useful way to modify the physical, optical, catalytic, electronic and chemical properties of GNPs (Chanana & Liz-Marzán, 2012). Based on the type of coating material, GNPs can be stabilised and solubilised according to the chemical functionality of the coating on the GNP surface (Basiruddin et al., 2010). Therefore, it is important that the most suitable coating material is used to achieve the desired results. The final applications will depend on these properties. A specific coating material on the GNP serves as modification of the surface properties (Zheng et al., 2004). A study by Goodman et al. (2004) on anionic and cationic GNPs evaluated the toxic properties induced by difference in charge according to the coating materials used. There is a wide variety of possible ligands available to coat GNPs. GNPs with ligands attached to their surface are referred to as ligand coated GNPs (Lig-GNPs). Table 2-1 presents a summary of examples of ligands that can be used as coating materials to modify the surface of GNPs.

Table 2-1: Ligands that are used as coating materials for GNPs (Lig-GNPs).

Ligand	Structure	Comments
N-Acetyl-L-Cysteine (NAC)		<ul style="list-style-type: none"> NAC-GNPs are used to detect phenol-containing molecules (Dong et al., 2010; Su et al., 2012). Enhance infra-red signals in detection methods (Ghosh and Bürgi, 2013).
Polyethylene glycol ₆₀₀₀ (PEG)		<ul style="list-style-type: none"> PEG-GNPs are used in cell imaging (Ye et al., 2014). Tumour detection and drug delivery (Bhattacharya et al., 2007; Wang et al., 2011).
Bovine serum albumin (BSA)		<ul style="list-style-type: none"> BSA-GNPs are used as drug delivery vehicles in systemic circulation (Khullar et al., 2012).
PEO Poly(ethylene oxide) 100k		<ul style="list-style-type: none"> Used as a nanoparticle superstructure in photo thermal therapy (Yang et al., 2013).
Poly-Na-sterenesulfonate 70.000 kDa		<ul style="list-style-type: none"> Used as part of a dot-structure for labelling applications (Wang et al., 2002)
Hexadecyltrimethylammonium bromide (CTAB)		<ul style="list-style-type: none"> Used as colorimetric assays for nucleic acids (Saber et al., 2013). Used with Polyethylenimine as a less toxic gene vector (Xu et al., 2013).
Polyvinylpyrrolidone (PVP)		<ul style="list-style-type: none"> PVP-GNPs are used as part of a layered structure for melanoma drug delivery (Labala et al., 2015).

11-Mercaptoundecanoic acid (MUA)	 $\text{HSCH}_2(\text{CH}_2)_8\text{CH}_2\text{COOH}$	<ul style="list-style-type: none"> MUA-GNPs are used for biomedicine, diagnostics, drug delivery and tumour removal (Fraga et al., 2013).
Polyethylenimine (PEI)		<ul style="list-style-type: none"> Used in combination with other polymers and molecules such as CTAB as a successful gene vector that is less toxic (Xu et al., 2013).
Glutathione (GSH)	 <p style="text-align: center;">Glutamic acid cysteine glycine</p>	<ul style="list-style-type: none"> GSH-GNPs are used to mediate drug delivery (Ghosh et al., 2008; Hong et al., 2006).

As summarised in Table 2-1, Lig-GNPs have a wide variety of applications. Some Lig-GNPs seem to have little to no effects on biological systems such as NAC-GNPs, GSH-GNPs and BSA-GNPs, which is an important aspect for applications relating to drug delivery and cancer therapy (Khullar et al., 2012). Polymer Lig-GNPs such as PEG-GNPs also seem to have no effect on cell viability (Gu et al., 2009). However, PEG-GNPs may cause ATP levels and mitochondrial membrane potential to be altered (Leite et al., 2015). Where PVP-GNPs seem to induce changes in A549 and NCIH441 cell lines (Uboldi et al., 2009), MUA-GNPs are considered to have a lesser effect on HepG2 cells and their genome than citrate capped particles (Fraga et al., 2013). The following section will further elucidate these effects.

2.8 The effects of GNPs on biological systems

2.8.1 Impacts on cells based on the chemical properties of GNPs

The effects of nanomaterials such as GNPs have drawn attention to the research field of toxicology. Numerous studies have been performed to establish the effects of GNPs in biological systems. Paino et al. (2012) investigated the cellular and genetic responses of 7-20 nm citrate capped and polyamidoaminedendimer capped GNPs in human hepatocellular carcinoma cells (HepG2) and peripheral blood mononuclear cells. Clean-up was reported in PBS and the cell viability was assessed using the MTT assay. Their results suggest that the particles elicit a negative response on genome- and cellular level (Paino et al., 2012). However, the incubation time of the cells with the GNPs was not mentioned in this article. Pernodet et al. (2006) found that 13 nm citrate-GNPs in different concentrations and exposure times had major adverse effects on the viability of fibroblast cells. Their results suggested that the cells' internal activities have been affected. However, no removal of citrate or sample clean-up was reported in this paper, which could have played a role in the effect observed. Connor et al. (2005) conducted a study to determine the interactions of modified nanoparticles on K562 leukaemia cells. Their data suggests that the nanoparticles themselves are not necessarily responsible for the detrimental observations in cellular function, and that some precursors used in GNP synthesis might be responsible for the noted cytotoxicity instead (Alkilany & Murphy, 2010). From these studies it is clear that there are no standardised protocols being followed, which results in different conclusions being made. Kong et al. (2011) mentioned in a study done to establish the outcome of the effect of nanoparticles that they encountered several challenges due to the lack of standardised protocols in different studies in the literature. Jones & Grainger (2009) discussed methodologies used currently to determine the *in vitro* effects of GNPs and their physiochemical properties. They state that these methods are limited in sensitivity, correlation, and reliability. In their paper they discuss crucial aspects such as possible surface contamination, particle aggregation, cell types, and assays on cells that include viability assays and cell stress assays. These are all important factors to consider when attempting to obtain reliable results (Jones & Grainger, 2009).

Moreover, most of the nanomaterial safety studies in the literature are based on viability assays such as the MTT assay. Kong et al. (2011) referred to studies investigating the reliability of viability assays. Certain methods are based on colorimetric changes such as the MTT assay and propidium iodide fluorescence. However, due to reaction of the MTT assay reagents with GNPs and the observation that some nanoparticle shapes/sizes absorb in the same spectral region as the assay dye, some viability assays produce false positive/negative results and are therefore considered to be unreliable. They suggest that viability assays are to be carefully evaluated and verified with two or more independent tests (Kong et al., 2011).

Because different morphologies, sizes and surface charges of GNPs have different properties, they differ in cytotoxicity depending on the size of the nanoparticles (Pan et al., 2007) and the cell line (Patra et al., 2007; Paino et al., 2012; Pan et al., 2007) and the surface charge of the particle (Goodman et al., 2004). Therefore, the results in the literature are very contradictory concerning this matter (Alkilany & Murphy, 2010).

Pan et al. (2007) discussed how cellular responses towards GNPs are dependent on the size of the particles being used for the study. They noted that 1.4 nm particles were responsible for rapid cell death within 12 hours via necrosis while 1.2 nm GNPs which are closely related affect cell death via apoptosis (Pan et al., 2007). They also reported that connective tissue fibroblasts, macrophages, epithelial cells and melanoma cells are most sensitive to 1.4 nm sized GNPs (Pan et al., 2007). Patra et al. (2007) as well as Paino et al. (2012) also noted that various cell lines are selective in their response towards GNPs. They concluded that HepG2 cells were more sensitive to DNA damage than PBMC (peripheral blood mononuclear cells).

A study done by Fraga et al. (2013) to determine the influence that a surface coating on GNPs has on HepG2 cells demonstrates how the change in properties leads to a change in cytotoxicity in cells. They observed DNA damage in cells treated with citrate capped particles but not in GNPs capped with 11-mercaptopundecanoic acid (MUA). Their data suggests that capping GNPs with a surface coating increases the safety and biocompatibility of GNPs towards biological systems (Fraga et al., 2013). Goodman et al. (2004) suggested that toxicity is based on the surface charge of the GNPs. They found that cationic particles seem to be moderately toxic where anionic particles are non-toxic (Goodman et al., 2004).

2.8.2 Effect on the cellular metabolome

A lot of research is done in line with the cytotoxicity caused by GNPs (Alkilany & Murphy, 2010). However, the studies that focus on metabolic changes or components that may affect the metabolome lack rigorousness. Several studies clearly state that biological samples are affected by the GNPs in various ways; however, none of these studies supply a full metabolic profile of the metabolites that were affected.

For instance, Cho et al. (2010) found that 4 nm and 13 nm PEG-coated particles activated the phase I metabolic enzymes in liver tissue, but they did not measure the metabolites as part of their study. Lasagna-Reeves et al. (2010) investigated renal toxicity in mice caused by bioaccumulation of GNPs in the kidneys. They assessed tissue morphology in the mice organs as well as animal behaviour, and they also tested the serum which includes monitoring metabolites associated with renal failure (such as the levels of urea and creatinine levels in the blood). However, as these are only two metabolites that have been evaluated, their study does not provide an accurate description of what is occurring on metabolome level (Lasagna-Reeves et al., 2010).

Liu et al. (2012) determined the penetration and metabolic toxicity of 10 nm, 30 nm, and 60 nm GNPs on human skin after a 24-hour treatment. They observed that no significant penetration could be detected, and as a result there was no change in the metabolic output of total NAD(P)H levels in the epidermis (Liu et al., 2012).

Huang et al. (2015) investigated the effect that GNPs have on microRNA (miRNA) level. They observed that the GNPs were not cytotoxic after treating the cells for one, four, and eight hours. However, 202 miRNAs were differentially expressed, and the energy metabolism of the cells was affected (Huang et al., 2015). Wang et al. (2012) investigated the metabolic effect of 15 nm GNPs on the energy metabolism of living organisms by using a *Drosophila* larvae model. They used RNA- and protein-analysis to determine a change in lipid levels without elucidating a stress response (Wang et al., 2012).

Bajak et al. (2015) examined cellular responses of Caco-2 cells to GNPs by comparing cellular uptake, RNA expression and cytotoxicity of 5 nm and 30 nm particles. Among

biological processes such as metal binding, the glutathione metabolism was increased and several genes were up-regulated. They concluded that a high concentration (300 μ M) of 5 nm GNPs affects metal and selenium homeostasis and also triggers oxidative stress signalling pathways in these cells (Bajak et al., 2015). Li et al. (2010) established the biological toxicity of GNPs in MRC-5 human lung fibroblast cells. The autophagy proteins were up regulated, lipid peroxidation was indicated and the presence of oxidative damage was confirmed. They also noted that there is a correlation between GNP treatment and antioxidant up regulation, stress-response protein and gene expression. They conclude that these cellular responses may be a defence mechanism against oxidative stress toxicity (Li et al., 2010).

The following table presents different studies done to investigate the effect that GNPs have on biological systems.

Table 2-2: A summative table of the effect of GNPs on the cellular metabolome reported in the literature.

GNP specifications	Study specifications	Metabolomics results	Reference
4 nm & 13 nm PEG-Coated GNPs (no clean-up reported)	Determined metabolic enzyme activity by using ICP-MS, TEM, and EROD and PROD assays.	Metabolic activity of phase 1 metabolic enzymes was increased.	(Cho et al., 2010)
12.5 nm Citrate capped particles (no clean-up reported)	Determined that bioaccumulation of GNPs in different dosages did not induce renal toxicity.	Analysed serum with a biochemical auto-analyser (Type 7170, Hitachi), and found no significant effect.	(Lasagna-Reeves et al., 2010)
21.83 \pm 4.79 nm Citrate capped particles (no clean-up reported)	Investigated the effect of GNPs on miRNA level that mainly regulate 71 biological pathways.	GNPs did not induce ROS, apoptosis or cytoskeletal harm, but affected the energy metabolism of dermal	(Huang et al., 2015)

		fibroblasts.	
15 nm citrate capped, (no clean-up reported)	Used a Drosophila model to investigate the metabolic effect of 15 nm GNPs on the energy metabolism. They used RNA and protein analysis.	GNPs increased lipid levels but did not elicit a stress response.	(Wang et al., 2012)
10 nm, 30 nm and 60 nm citrate capped particles (no clean-up reported)	Determined the penetration and toxicity of 10 nm, 30nm and 60 nm GNPs on human skin after a 24-hour treatment.	NAD(P)H levels were normal, no changes in metabolic output. Epidermis was viable, no penetration occurred.	(Liu et al., 2012)
5 nm and 30 nm (clean-up reported; centrifugal filter)	Investigated transcriptomic changes due to GNPs by analysing RNA (RNA isolation, micro array and PCR)	Cadmium/copper ion binding and glutathione metabolism increased.	(Bajak et al., 2015)
20 nm (clean-up reported; Centrifuge)	Investigated oxidative stress caused by GNPs in MRC-5 human lung fibroblasts	GNPs induce oxidative damage and trigger a defence pathway with stress-response proteins.	(Li et al., 2010)

From this table, it is notable that each finding may have a link to metabolites present in the biological system. However, not once was a metabolite profile obtained to indicate variation on metabolome level.

A previous study at our institution on the effect of GNPs on the organic acid profile of Sprague Dawley rats indicated that the mitochondria may possibly be affected. Increased levels of lactic acid, isocitric acid, 2-ketoglutaric acid, succinic acid, malic acid and citric acid were noted. However, several challenges similar to the limitations described by Kong et

al. (2001) presented themselves, which complicated the study. No sample clean-up was reported, indicating that the metabolites increased could be due to organic acidosis caused by excess citrate in the GNP solution. Complications with sample collection and biodistribution of GNPs were also faced. Therefore, a revised study design was necessary to address and avoid problems such as difficult sample collection, false positive/negative results due to the lack of sample clean-up, and complications of the metabolomics analysis due to bio-distribution of GNPs.

2.9 Metabolomics

Considering the flow of genetic information, the genome consists of DNA-molecules which is transcribed to RNA and translated into proteins. The final downstream product of the genome is the metabolome. Metabolites are the biochemical representatives of the functional phenotype of the cell and can therefore provide information downstream from the proteome and transcriptome. Also, occasionally, metabolic variation is observed when variation regarding transcripts and proteins are not detectable. Metabolomics can be described as “the quantitative analysis of all the small-molecular weight metabolites present inside a cell or other sample” (Cammack et al., 2006). The aim of a metabolomics approach is to comprehensively quantify metabolic changes in a biological system or sample to deduce the biological functions and provide information regarding the biochemical responses of cells. According to Čuperlović-Culf et al. (2010), cellular metabolomics analysis can be divided into five general steps, which include; the experimental design, cell culturing, metabolite quenching and extraction, metabolomics measurement, and data pre-processing and analysis (Čuperlović-Culf et al., 2010).

2.9.1 Applications, approaches, advantages and disadvantages

2.9.1.1 Applications

Metabolomics plays a significant role in linking the phenotype with the genome in terms of establishing a certain function (Hall, 2006). Possible applications for metabolomics analysis on cells are described by Čuperlović-Culf et al. (2010). These applications include bioreactor growth optimisation, phenotype classification, metabolic network determination, toxicity analysis and drug target biomarker discovery (Čuperlović-Culf et al., 2010).

2.9.1.2 Advantages and disadvantages

Metabolomics allows the comprehensive evaluation of systemic responses elicited by physiological changes towards specific stimuli. This property makes a metabolomics-based study suitable for detecting the cytotoxic effect on cellular systems (Robertson, 2005). Furthermore, the study of omics, which includes metabolomics, is useful in understanding and elucidating all aspects of biological systems (Goodacre et al., 2004). It is important to consider the endpoint of the study before establishing a metabolomics approach. A suitable approach would be to discover a new biomarker or to generate a hypothesis. In contrast, if a specific analyte or target organ is to be investigated, the metabolome may present some limitations (Robertson, 2005). Disadvantages also include an inability to measure, identify and quantify the whole metabolome at once. However, in combination with other metabolomics measurements, a large information pool can supply a good coverage of the metabolic processes in a biological system. Metabolomics analyses are cost-effective and sensitive; they present a rapid response in reaction to stimuli or physiological changes. Also, a characteristic of a normal individual's phenotype is associated with a lower degree of variation (Williams et al., 2012). This property allows the most recent monitoring of the state of an organism. However, the increased sensitivity can also be disadvantageous in the sense that it is more subject to noise, which tends to complicate the data interpretation. Also, complex statistical bioinformatics analysis is required to process the data and the setup costs are relatively expensive.

2.9.1.3 Metabolomics approaches

In metabolomics, there are mainly two pathways that can be considered, depending on the aim of the study.

An untargeted approach is hypothesis-generating and requires high-end instruments such as TOFs that will allow high coverage of metabolites which can be sorted via multivariate statistics. The metabolites of interest can then be used to follow a targeted analytical approach which is hypothesis-driven. For this approach, low-end instruments are sufficient, because only analysis of the metabolites of interest is required. However, extensive sample preparation is required, which is not necessary when following an untargeted approach.

Finally, a conclusive biological understanding is obtained or a specific biomarker is validated.

In the metabolome-analysis of cells, the exometabolome as well as the endometabolome can be analysed. The endometabolome is defined as the metabolic activity within a biological system, or the intracellular metabolome; where the exometabolome refers to the metabolic excretions on the external environment of the biological system or cell, which is similar to urine or blood.

2.9.1.4 Metabolite identification

Accurate metabolite identification is crucial in order to make unambiguous conclusions. Metabolite Identification levels are described by Schymanski et al. (2014). These different levels give an indication of the certainty of the identified compound based on evidence such as the structure, substance, formula or mass of the compound. The model consists of 5 levels: Levels 1 and 2 are based on the structure of the compound and have the highest certainty of the identified metabolites, which correlate with either a reference standard or matching spectral libraries. Levels 3, 4 and 5 are identification levels based on substance class, formula or the mass of interest. These identification levels are less certain and specific. Table 2-3 presents the identification levels and a brief description of how the compounds are identified (Schymanski et al., 2014).

Table 2-3: Identification levels of metabolites according to Schymanski et al., (2014).

Level	Description
Level 1: Confirmed structure	The proposed structure is confirmed according to the reference standard.
Level 2: Probable structure	The probable structure is identified based on evidence such as matching libraries and the % spectral match.
Level 3: Tentative candidate	There is evidence for a possible structure, however not sufficient information on one structure only (Isomers).
Level 4 Unequivocal molecular formula	Spectral information is used to propose possible structures, such as adducts, isotopes or fragment

	information.
Level 5 Exact mass (m/z)	No unequivocal information about the structure or formula exists. Is usually labelled as “unknown”

2.9.2 Analytical equipment

In order to obtain a comprehensive metabolic profile, a variety of analytical approaches are necessary. Combining untargeted GC-MS analysis with targeted amino acid and acyl-carnitine analysis will result in a wider spectrum of metabolites to be analysed. Goodacre et al. (2004) reported that extraction procedures in the literature are limited because only a portion of the metabolome is considered.

a) Gas chromatography–mass spectrometry (GC-MS)

Gas chromatography-mass spectrometry is an analytical technique used when analysing less polar, volatile compounds (Agilent Technologies, 2014). Non-volatile compounds such as amino acids require derivatisation prior to analysis (Agilent Technologies, 2014). The sample is injected and vaporised; it passes through the column where it is separated according to difference in boiling point and charge (Agilent Technologies, 2014). Thereafter, the molecules are ionised by EI (Electron Impact) ionisation and detected by the mass spectrometer. GC-MS is suitable for the high resolution separation of many compounds. This advantage enables effective separation of compounds that have similar structures. The method is more sensitive to fatty acids than it is to amino acids and is less expensive than LC-MS/MS (Agilent Technologies, 2014).

GC-MS as an analytical technique can also be used to analyse metabolic variation, and is a powerful tool that can be helpful in this study. Lu et al. (2011) investigated the effect of nanostructure size on biological systems by using GC-MS in combination with pattern recognition. They found that the metabolic profile of mice treated with three different silica nanoparticles changed significantly (Lu et al., 2011). The benefit of this method is that it is highly sensitive, meaning it can detect metabolic compounds very accurately. GC-MS can be used to evaluate the cell culture media (exometabolome) as well as the internal cellular

environment (endometabolome) (Section 2.9.1.3). However, it requires more intense sample preparation than NMR, which entails the analytical extraction of metabolites (mostly organic acids), and derivatisation.

b) Liquid chromatography–mass spectrometry (LC-MS)

In contrast with GC-MS, liquid chromatography-mass spectrometry (LC-MS) separates non-volatile compounds (Agilent Technologies, 2014). A greater range of chemical species can be analysed using this analytical technique. Large sugar species and amino acids are commonly analysed using LC-MS/MS. Derivatisation is often required to add unique retention and fragmentation properties to the amino acids (Agilent Technologies, 2014). Butylation is commonly used for this purpose, but other derivatisation methods are also available. The sample (in liquid form) passes through a column containing a specialised stationary phase such as C18 material, and is separated by retention between the stationary phase and the analyte of interest. After LC the compounds are ionised and enter the mass spectrometer to be detected. Soft ionisation techniques, such as electrospray ionisation (ESI) are commonly used. In the case of LC-MS/MS, the first mass spectrometer serves as a mass filter that can be set to detect a certain compound. The compounds then enter a collision cell and the fragmented ions are detected as product ions. This detection approach is also known as selected reaction monitoring (SRM). It enhances the sensitivity of the analytical equipment (Ho et al., 2003).

Beusen et al. (2014) evaluated the effects of nanomaterials such as SiO₂, ZrO₂, and BaSO₄ on rats after 28 days of oral exposure by using LC-MS in combination with GC-MS. They compared the nanomaterials with surface functionalised nanomaterials to study the effect on the plasma metabolome of the rats. The MetaMap®Tox database revealed no matches with specific patterns, however, further studies are required in this field (Buesen et al., 2014).

Combining GC-MS with LC-MS/MS analysis gives a more comprehensive indication of the effect that a treatment group has on the metabolome. For instance, LC-MS/MS can measure amine/nitrogen containing compounds such as acylcarnitines and amino acids much more accurately than GC-MS. A study done by Kankani et al. (2008) revealed that GC-MS derivatisation of class 3 compounds (NH₂) significantly distorts the final results. Therefore,

acylcarnitine and amino acid analysis can be done via LC-MS/MS instead, which is a semi-targeted approach.

c) Nuclear Magnetic Resonance (NMR)

Nuclear magnetic resonance (NMR) is a rapid technique with the capacity to detect hundreds of metabolites in tissue, serum or urine. The metabolomics analysis is reliable and quantitative because of the reproducible patterns and chemical shifts that occur within the protons of the molecules of interest. Although NMR is less sensitive than GC-MS and LC-MS, it requires much less intensive sample preparation. Moreover, there is an overlap in the chemical shifts of various metabolites, which complicates the detection of metabolites (Schnackenberg et al., 2012).

Each method used in the literature has benefits as well as limitations. To ensure a more comprehensive analysis of metabolites, a combination of techniques can be used.

d) Seahorse XF⁹⁶ analyser

The oxygen consumption rate (OCR) of cells can be measured using the Seahorse XF⁹⁶ analyser. The injection of different compounds allows for the measurement of different parameters in the mitochondrial function of cells. These parameters include the basal respiration, ATP production and maximal respiration from which the proton leak and spare respiratory capacity can be calculated. The three compounds which are injected serially include the following; oligomycin, FCCP and a combination of rotenone and antimycin A. The basal respiration is where the cells are in a natural respiration state. With the addition of oligomycin, ATP synthase is inhibited and ATP production decreases. Thereafter, FCCP is injected, which is an uncoupler. Adding this compound accelerates the electron transport chain (ETC), allowing maximal respiration. Finally, a combination of rotenone and antimycin A is injected, which immediately ceases mitochondrial respiration. Figure 2-9 illustrates the injected compounds and the changing parameters while OCR is measured.

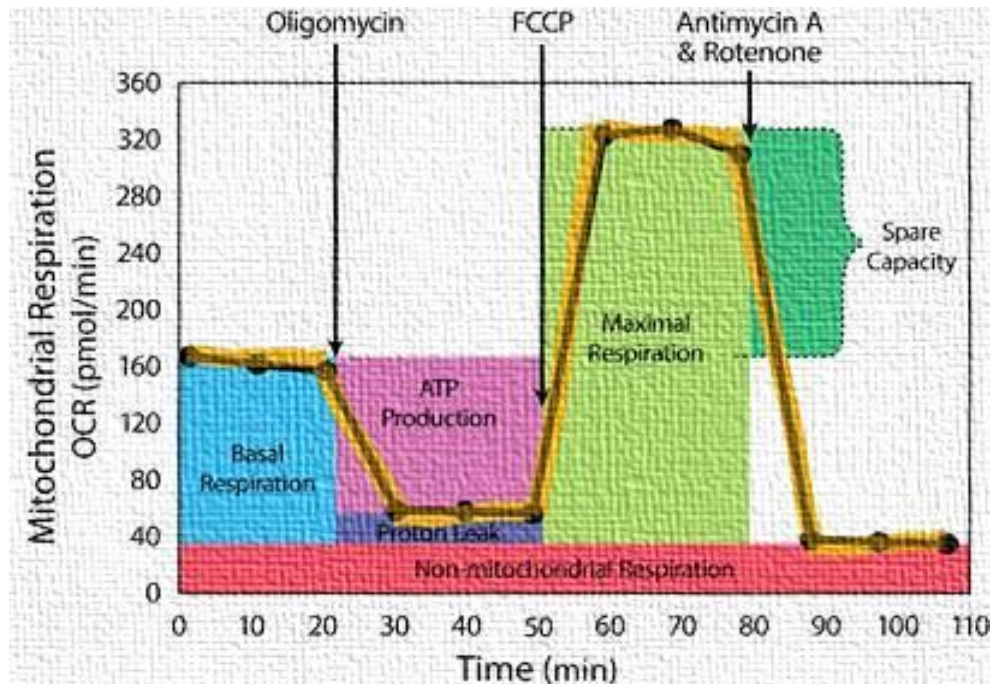


Figure 2-9: Mitochondrial respiration and the parameters measured using the Seahorse XF96 analyser.

The basal respiration is where the cells use energy during a state of rest to maintain vital cellular functions. An ATP coupler, oligomycin is added to the cells. ATP production is reduced significantly due to the inhibition of the enzyme ATP synthase. With addition of FCCP, the ETC is accelerated and the cells undergo maximal respiration. The final injection is a combination of rotenone and antimycin A, which ceases all mitochondrial respiration.

2.10 Problem statement

Due to the characteristics of GNPs, their use in research and pharmaceutical applications presents advantages in drug delivery regarding targeted treatment of various diseases such as rheumatoid arthritis and cancer therapy (Pillai, 2014). However, possible negative effects have been a concern which may affect the genome, transcriptome and proteome in various animal- and tissue-culture models; whereas other studies reported no significant change as a result of GNP treatment (Alkilany & Murphy, 2010). Hence, the results discussed in the literature are either contradictory or inconclusive, mostly due to inherent limitations in the protocols used (Kong et al., 2011). More importantly, literature on the effect of GNPs on the metabolome level of cells and organisms is scant. There is very limited published information on the subject, with a few papers mostly focusing on target compounds only. Because of this lack of research, a study was previously done at the North-West University (NWU) to determine the effect of GNPs on the organic acid profile of Sprague Dawley rats. However, due to limitations in the study design (similar to those reported by Kong et al., 2011), it was decided to design a new study where issues such as bio-distribution, vehicles used for intravenous administration (which caused organic acidemia), and urine sample collection for metabolomics analyses could be addressed and avoided. The possible effects of GNPs on the energy metabolism and mitochondria observed in this study as well as in the literature (Leite et al., 2015) can be further elucidated at the NWU by using the Seahorse XF⁹⁶ analyser. Lastly, the effect of differentially coated particles on the metabolome has not yet been studied. Recent studies have shown that performing ligand exchange seems to increase the biocompatibility of GNPs (Fraga et al., 2013) which could complement the research of standard coated GNPs.

2.11 Aim and objectives

The aim of this study is to investigate the metabolic changes in cultured cells treated with differentially functionalised GNPs.

The following objectives were put forth to reach the aim. These objectives are described as synthesis, cell culturing, a pilot study and a main study.

a) Synthesis

- Standardisation of GNP synthesis and coating methodology.
- Synthesis and coating of GNPs for use in this study.
- Characterisation of the synthesised GNPs using adapted methods from published literature. Basic physicochemical techniques such as TEM, DLS and UV-Vis spectroscopy will be used to characterise the GNPs.
- Stability evaluation of GNPs in a physiological environment.

b) Cell culturing

- Culturing of HepG2 cells using basic, standardised culturing techniques until a sufficient number of biological repeats is obtained.

c) Pilot study

- Conducting a dose-response pilot study to find an adequate treatment dose where most cells are still viable for metabolomics analysis. The intention is to put the cells under stress and evaluate the cellular response without inducing severe cytotoxicity.
- Conducting a time-response pilot study to determine the appropriate treatment duration before sampling of cells and media for metabolomics analysis.

d) Main study

- Standardisation and evaluation of metabolomics methods for cell culture and media analysis. These methods include seeding density, quenching and extraction methods.

- Analysis of mitochondrial respiration using the Seahorse XF⁹⁶ analyser.
- Metabolomics analysis of the endometabolome of treated cells with GC-MS (to analyse mainly the organic acids) and LC-MS/MS (amino acids and acyl-carnitines).
- NMR analysis of the metabolised media which will represent the cellular exometabolome.
- Statistical analyses.

2.12 Study design

The study consists of two parts which include the pilot study and the main study. GNPs will be synthesised, functionalised and characterised. A stability evaluation will be performed to determine the most stable functionalised particles, and these particles will be selected for the rest of the study. Cells will be cultured and treated with the prepared GNPs for each analysis; including standardisation.

For the pilot study, the most suitable dosage and time points for the treatment of each functionalised gold nanoparticle (GNP) sample will be standardised. These specific dosages and time points will be used for the main study. The Seahorse XF⁹⁶ analyser will be used to measure cellular mitochondrial respiration after treatment with each functionalised GNP with the selected dosages and time points. Metabolomic analysis will be done on cells and metabolised media treated with three differentially functionalised GNPs. The extracted metabolites will be analysed, firstly with GC-MS and LC-MS/MS to study the effect of these particles on the primary metabolism and amino acid and acylcarnitine profiles, respectively. Secondly, NMR analysis will be done on the metabolised media to study the effect of these particles on the exometabolome. A vehicle control group will be incorporated with every study which will receive the same amount of vehicle in which the GNPs are suspended. Figure 2-10 presents an accompanying explanation of the study design.

Study design

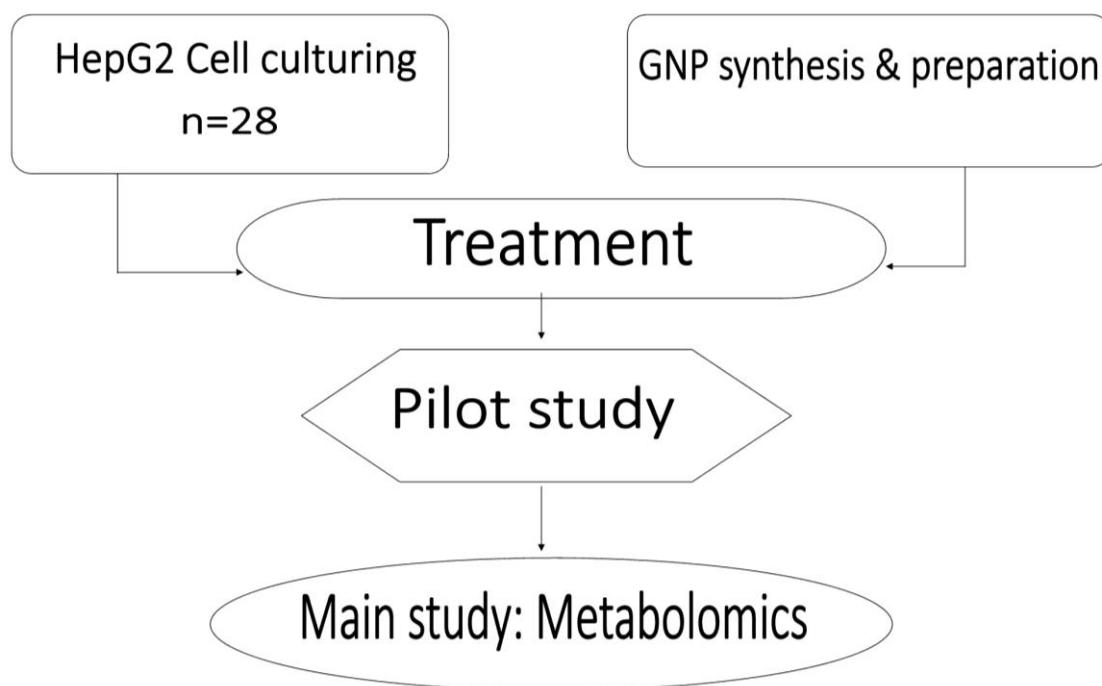


Figure 2-10: The study design. GNPs will be synthesised, functionalised and characterised. HepG2 cells will be cultured and treated with the prepared GNPs for each analysis. The pilot study will include standardising the dosage and time point for treatment. The main study will include treatment with functionalised GNPs with the selected dosages and time points and the metabolomics analysis. Cellular mitochondrial respiration will be measured using the Seahorse XF analyser. Endometabolome analysis will include GC-MS analysis to obtain an organic acid profile and LC-MS/MS analysis of acyl-carnitines and amino acids. Exometabolome analysis will include assessment of metabolised cRPMI media using NMR.

Chapter 3: Nanochemistry

3.1 Introduction

This chapter will focus on the synthesis of gold nanoparticles (GNPs), including surface functionalisation, physicochemical characterisation, and differential aqueous stability (i.e. pH, bio-molecules and ionic strength) of the GNPs.

The chapter commences with a section on materials and methods, and is followed by the results and discussion of the nanochemistry work. The work done in this section will lead to Chapter 4 (Cell biology) where the overall effect on the cell biology of hepatocellular carcinoma cells (HepG2) after treatment with GNPs will be elucidated. Thereafter, the effect on the metabolome will be assessed (Chapter 5).

3.2 Methods

3.2.1 GNP synthesis

All glassware were treated with Aqua Regia ($\text{HNO}_3:\text{HCl} = 1:3$) and rinsed thoroughly with ultrapure water (ddH_2O ; $18.2 \text{ M}\Omega\cdot\text{cm}$) prior to the synthesis. An aqueous solution containing 1 mM HAuCl_4 was stirred at moderate speed and heated to 90°C on a hotplate-stirrer (Stuart). Trisodium citrate (Sigma Aldrich S4641-500G, 1% stock solution) was added to the heated solution to a final concentration of 0.87 mM citrate (Ghosh et al., 2011). The solution underwent a colour change within 30 seconds: golden yellow \rightarrow light yellow \rightarrow colourless \rightarrow grey \rightarrow black \rightarrow purple \rightarrow rose red. The colour change is indicative of the reduction of the aurate salt, followed by nucleation of gold atom clusters and the subsequent maturation to GNPs. The red hue of the solution was indicative of GNPs. The GNP solution was removed from the heat source after 15 minutes and left overnight in the dark at ambient room temperature (25°C). The GNPs were filtered using a $0.2 \mu\text{m}$ filter (GVS, L1133912) and stored at 4°C prior to use (Ghosh et al., 2011).

3.2.2 Sample clean-up

Ten ml GNPs were aliquoted in 15 ml Falcon tubes and centrifuged at $800 \times g$ for two hours (Lasec Z 206 A, fixed angle rotor). The supernatant was carefully removed and the pellet suspended in $5 \text{ ml ddH}_2\text{O}$ (ddH_2O will serve as a vehicle for this study).

3.2.3 GNP characterisation

The GNPs were characterised for morphology, size distribution and net surface charge using UV-Vis spectrometry, agarose gel electrophoresis, dynamic light scattering (DLS) and transmission electron microscopy (TEM).

3.2.3.1 UV-Vis spectrometry

One hundred μl GNP solution was pipetted into a 96 well plate (Cellstar, 655180) to determine the UV-Vis spectra for $300\text{-}700 \text{ nm}$ by using the Synergy HT UV-Vis plate reader

from Biotek and Gen 5.1 software. The estimated concentration and average diameter were calculated according to Haiss et al. (2007).

Concentration and size calculations

An example of the calculations used to determine the average diameter and concentration of the GNPs can be seen in Equation 3-1 and Equation 3-2, as well as Table 3-1 and 3-2. Cit-GNPs were used for these calculations due to the observance that surface functionalisation of the GNPs alter the local surface plasmon, causing the direct calculations using UV-Vis spectrometry to be inaccurate, except for when the reference wavelength used is 450 nm, which is a constant value for all GNPs regardless of surface modifications (Haiss et al., 2007). The maximal absorbance peak (λ_{max}) which is usually at OD₅₂₀, shifts between different sizes of GNPs (Chanana & Liz-Marzán, 2012); this phenomenon occurs due to an increase in electrons which cause absorption. The same concept also applies to an increase in electrons due to ligands attached to the GNP surface. The corresponding dosages used to treat the cells were then adapted mathematically so that the concentration for each dosage could be calculated (Haiss et al., 2007). Cit-GNPs were used as the reference value to use in correlation with the rest of the GNPs.

Equation 3-1: Calculation of Cit-GNP size using the OD obtained from UV-Vis spectrometry.

$$Size = \frac{OD_{520} (\lambda_{max})}{OD_{450}}$$

Where $OD_{520} (\lambda_{max})$ is the maximum absorbance at 520 nm and OD_{450} is the absorbance at 450 nm.

Firstly, a blank subtraction of the OD_{450} is determined.

A Average OD_{450} Citrate GNPs – Average Blank OD_{450}

$$(15.33 \times 10^{-2}) - (4.43 \times 10^{-2}) = (10.9 \times 10^{-2})$$

A blank subtraction of the OD_{520} is determined

B Average OD_{520} Citrate GNPs – Average Blank OD_{520}

$$(22.80 \times 10^{-2}) - (4.43 \times 10^{-2}) = (18.30 \times 10^{-2})$$

Thus,

$$Size = \frac{OD_{520} (Max)}{OD_{450}}$$

$$Size = \frac{(18.30 \times 10^{-2})}{(10.9 \times 10^{-2})}$$

$$= 1.68$$

The resulting value can be used to correlate the diameter of the GNP in nm (Haiss et al., 2007). The A_{Spr}/A_{450} was 1.68. The value obtained was used to determine the diameter (d) in nm of the particles using Table 3-1 from Haiss et al. (2007). Therefore, the Citrate-GNPs have an average diameter of ± 17 nm.

Table 3-1: The absorbance values determined using UV-Vis spectrometry and the correlating diameter (d) of GNPs (in nm; adapted from Haiss et al., (2007)).

$OD_{520} (\lambda_{Max}) / OD_{450}$	d(nm)
1.10	3
1.33	6
1.65	16
1.69	18
1.92	35
2.17	75

The particle concentration was then calculated using the molar decadic extinction coefficient (ϵ) at $\lambda = 450$ nm according to the formula and table supplied by Haiss et al. (2007).

Equation 3-2: Determination of GNP concentration.

$$c = OD_{450} / \epsilon_{450}$$

Where c is the concentration of Cit-GNPs and ϵ_{450} is the molar decadic extinction coefficient (ϵ) at $\lambda = 450$ nm.

Table 3-2 shows the decadic extinction coefficient values at 540 nm according to size which was supplied by Haiss et al. (2007).

Table 3-2: The size dependent decadic extinction coefficient values at 540 nm.

d/nm	$\epsilon_{450} / M^{-1} cm^{-1}$ ($\times 10^5$)
2	4.25
5	72
10	615
15	2180
18	3870
20	5410

Preparing a serial dilution and plotting a graph from the calculated concentrations will allow an approximate indication of GNP concentration (Addendum B).

3.2.3.2 Agarose gel electrophoresis

The surface charge of GNPs could possibly influence the effects on biological systems (Fraga et al., 2013, Goodman et al., 2004). Therefore, GNPs were evaluated for charge and size difference by agarose gel electrophoresis. A 0.25 % agarose gel (Merck, 1.01236.0100) was prepared using 200 ml 1× TBE buffer (pH 8). The analysis was repeated for certain groups of particles, after ligand exchange (Section 3.2.4) using TAE buffer (pH 8). The GNP sample was mixed with 80 % glycerol (Merck, 1.04092.1000) in an equal volume, which was followed by loading 20 µl in the wells of the gel. The samples were electrophoresed for 55 minutes at 40 V using a gel box (Vacutech) and power supply (Baygene, BG power 300). The agarose gel was visualised and photographed using a Canon SX130 IS HD camera.

3.2.3.3 Transmission electron microscopy (TEM)

GNP sample preparation was done as reported earlier (Section 3.2.2); however, suspension of the sedimented GNPs was done in 1 ml ddH₂O. TEM was done with a Tecnai F20 high resolution field emission transmission electron Microscope at the Electron Microscopy Unit of the North-West University (Potchefstroom Campus). Micrographs were analysed using ImageJ software (V1.XXX).

3.2.3.4 Dynamic light scattering (DLS)

The hydrodynamic diameters of the GNPs were measured using the Zetasizer Nano ZS90 (Malvern). Polystyrene cuvettes (Malvern, DT50012) were rinsed three times with ddH₂O, dried and closed with a cap. Serial dilutions of the GNPs in ultrapure water (ddH₂O) were used for DLS measurement.

3.2.4 Ligand exchange

3.2.4.1 Ligand exchange standardisation

GNPs were used for ligand exchange using different ligands to confer different surface chemistry charges. The pH of the GNP solution was adjusted between $5 < \text{pH} < 8$, using hydrochloric acid (HCl, Merck, 1.00313.2500) and sodium hydroxide (NaOH, Merck, 1.06462.1000).

Two ml of the GNP stock solution (4.36×10^{-12} mol) was aliquoted into each of 60 falcon tubes (CellStar) and the pH was adjusted to pH 5, 6, 7 and 8, respectively, using HCl and NaOH. A dilution series of ligand was prepared for each ligand group and added to each pH sample. Table 3-3 represents the ligand: GNP ratio added to each pH group. The calculations are shown in Addendum E.

Table 3-3: The Ligand:GNP ratio that was added to each pH group (5, 6, 7 and 8, respectively) of GNPs (4.36×10^{-12} mol) to differentially functionalise the GNPs.

Ligand (in ppm) added to each pH group.	GSH, PVP and PEG	MUA ($\times 10^{-2}$)	BSA & PSSNa ($\times 10^2$)	Citrate ($\times 10^{-1}$)
	0.60	0.23	0.22	0.20
	0.70	0.27	0.28	0.24
	0.80	0.32	0.32	0.28
	0.90	0.36	0.37	0.32
	1.00	0.41	0.41	0.36
	1.10	0.45	0.46	0.40

The most favourable pH as well as ideal ligand:GNP ratio was determined by visually evaluating the most narrow, well defined UV-Vis peak. Table 3-4 lists the ligands used for this study, as well as the pH and final concentrations that were standardised.

Table 3-4: Ligands with their stock solutions, favourable pH for ligand exchange, and final concentration in GNP-solution.

Ligand	Stock Concentration	pH	Final	
			Concentration	ppm:GNP
Trisodium citrate	38.8 mM	pH 5	0.87 mM	0.20×10^{-1}
Poly-(sodium styrene-sulfonate) (PSSNa)	1 %	pH 6	0.048 %	0.22×10^{-2}
Polyvinylpyrrolidone (PVP)	2.5 mM	pH 5	0.23 mM	3.01×10^{-29}
Bovine serum albumin (BSA)	1 mg/ml	pH 7	0.048 mg/ml	0.22×10^{-2}
11-Mercaptoundecanoic acid (MUA)	1 mM	pH 6	0.057 mM	7.22×10^{-28}
Polyethylene glycol (PEG)	25 mM	pH 7	1.64 mM	2.11×10^{-30}
Glutathione (GSH)	25 mM	pH 8	1.19 mM	1.51×10^{-30}

Each tube was mixed briefly by inversion for 10 seconds and then left to stand at room temperature overnight. Ligand exchange was assumed to be complete after 24 hours, where the tubes were centrifuged at $800 \times g$ for two hours to remove excess ligand, and the pellet suspended in ddH₂O. The ligand exchanged GNPs or differentially functionalised GNPs will henceforth be referred to as Lig-GNPs.

Further analysis was done to evaluate whether the surface modifications are stable under physiological circumstances over time.

3.2.4.2 Ligand exchange stability evaluation

The stability of the Lig-GNPs was evaluated for aqueous solutions at different pH ranges, ionic strength of various salts and other (bio)molecules. Changes in the GNP microenvironment alter the solubility of the GNPs, whether it is by electrostatic attraction/repulsion, or displacement of the ligands from the GNP surface. Evaluation of the

GNPs in complete cell culture media (RPMI 1640 culture media; 10 % FBS, and 1× Pen-Strep) which will be referred to as cRPMI, assists in determining any potential non-cellular GNP interactions during cell culture. Table 3-5 shows the compounds used to test stability. On addition of the compound, a change in colour from red to purple, blue or grey is indicative that the particles are unstable. The particles were analysed with UV-Vis spectrometry to identify if the absorbance peak remains normal when compared to the UV-Vis spectrum of untreated Lig-GNPs.

Table 3-5: A summary of the compounds and concentrations/pH values used to determine the stability of GNPs in a physiological environment.

Compound group evaluated for stability	Specifications	
	Compound used	Concentration / pH ranges
Salt titration	NaCl	1 mM, 10 mM, 50 mM and 100 mM
Buffers	EDTA	(0.5 ×, 1 ×, 2.5 ×, 5 ×)
	10 mM MOPS	(pH 9 and pH 10),
	100 mM HEPES	(pH 7 and pH 8)
	PBS	(0.5 ×, 1 ×, 2.5 ×, 5 ×)
Culture media	Complete media	1 ×
	Clean media	1 ×
Organic molecules	Citrate (38.8 mM)	pH 4, 5 and 6
	Glycine (100 mM)	pH 2, 3, 9 and 10
Thiols	β-Mercaptoethanol	20 μl
pH	HCl, NaOH	pH 3, 4, 5, 6, 7, 8, 9 and 10

3.3 Results and discussion

3.3.1 GNP synthesis and characterisation

Citrate gold nanoparticles (Cit-GNPs) were successfully synthesised using the Turkevich method and cleaned up with centrifugation. The Turkevich method is the most commonly used method in literature for the particle size of interest and will be suitable to compare with other results found in the literature (Wang & Ma, 2009). UV-Vis spectrometry, TEM and DLS were used to characterise the GNPs.

3.3.1.1 UV-Vis spectrometry results

Figure 3-1 presents a graph showing the UV-Vis results of Cit-GNPs. The optical density (OD) was measured using UV-Vis spectrometry. The spectrum obtained is an indication of GNP stability, morphology and size. Figure 3-1 illustrates the particles starting to absorb light at 450 nm, and a maximum absorbance peak is reached at 520 nm, which is a known trait for spherical GNPs (Fraga et al., 2013, Haiss et al., 2007). The half width is used as an indication of GNP size (Berciaud et al., 2005, Gomes Silva et al., 2010, Khlebtsov and Khlebtsov, 2011)

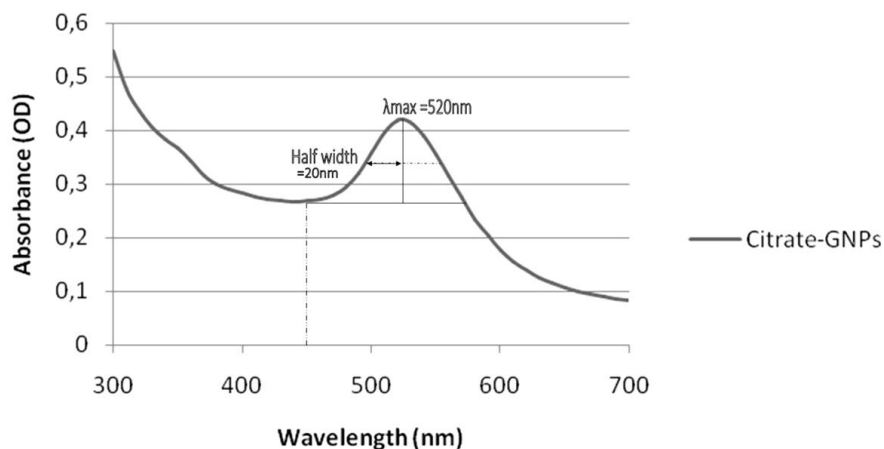


Figure 3-1: The absorbance spectrum of citrate capped GNP measured in the 300-700 nm wavelength range. The particles start to absorb light at 450 nm; a maximum absorbance peak (λ_{max}) is reached at 520 nm. The narrow, well-defined peak indicates that the GNP are stable. The half width is used to indicate the average GNP diameter.

This absorbance spectrum was used to further calculate the diameter and finally the concentration of the Citrate-GNPs (Haiss et al., 2007).

As mentioned in the methods (Section 3.2.3.1), the equation from Haiss et al. (2007) was used to determine the size of Cit-GNPs from the absorbance by using the optical density at 450 nm and 520 nm (OD_{450} & OD_{520}). The diameter and concentration of the Cit-GNPs were calculated as 18 nm (Tables 3-1 & 3-2) and 2.18 nM, respectively. A serial dilution was prepared and the OD of the sample range was measured, following the plot of the correlating concentration graph, which is shown in Addendum B.

Table 3-6: Summary of the calculated size and concentration of GNPs based on the OD of the particles and calculations (Haiss et al., 2007)

Sample number	GNPs (μl)	ddH ₂ O (μl)	OD ₄₅₀ ($\times 10^{-2}$)	Concentration (nM)	GNPs (ppm)
1	100	0	5.45	2.18	1.31×10^{17}
2	50	50	2.73	1.09	6.56×10^{16}
3	25	75	1.36	0.54	3.25×10^{16}
4	12.5	87.5	0.68	0.27	1.63×10^{16}
5	6	94	0.34	0.14	8.43×10^{15}
6	3	97	0.17	0.07	4.21×10^{15}

The results were confirmed with other techniques, which include TEM and DLS.

3.3.1.2 TEM Results

GNPs were characterised using TEM and analysed with ImageJ software. A particle distribution was obtained with the majority of the GNPs having an average size of 18 nm. Figure 3-2 is a TEM micrograph showing the cores of Cit-GNPs.

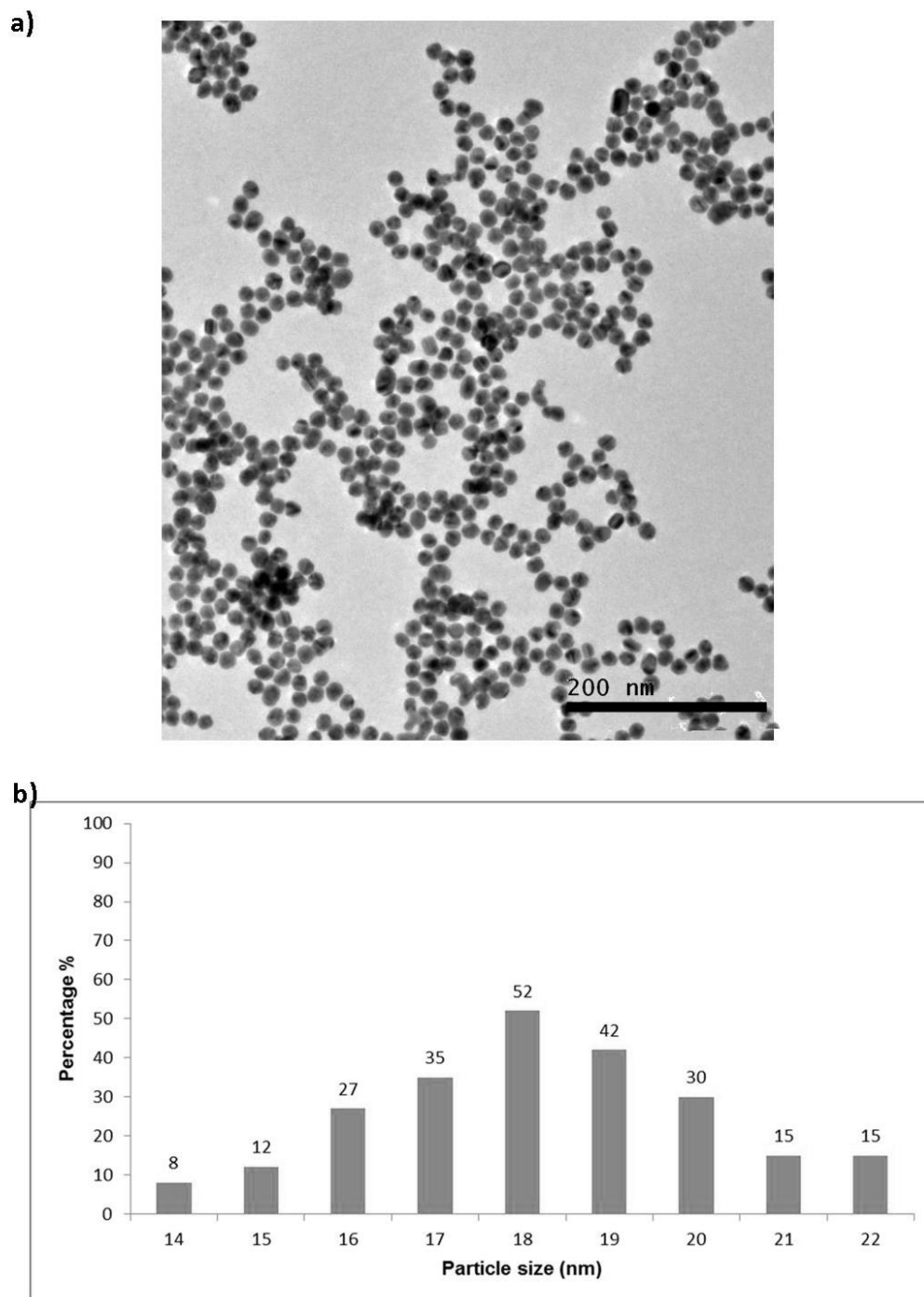


Figure 3-2: TEM results showing the morphology and diameter of citrate capped GNPs (a). The TEM images showing the majority of the Cit-GNPs had a diameter of 18 nm, as determined via ImageJ software and shown in (b) as particle distribution percentage.

TEM allows visual presentation of the GNP core in a dry environment which confirms that the particles are spherical. With both methods used (TEM and UV-Vis), the GNP size range corresponds (± 18 nm). However, TEM is limited to visualisation of the GNP core and does not take the hydrodynamic diameter or the effect of the ligand on the GNP surface into account. It also does not give an indication of the interaction with surrounding molecules. Therefore, characterisation of GNPs via DLS was also performed to include the interaction and effects of salts, pH, and temperature of Lig-GNPs in solution.

3.3.1.3 DLS results

The average hydrodynamic diameter of the synthesised Citrate-GNPs was 17 nm, as measured by DLS. Figure 3-3 shows the size distribution of Citrate-GNPs measured by the Zetasizer nanoZS90.

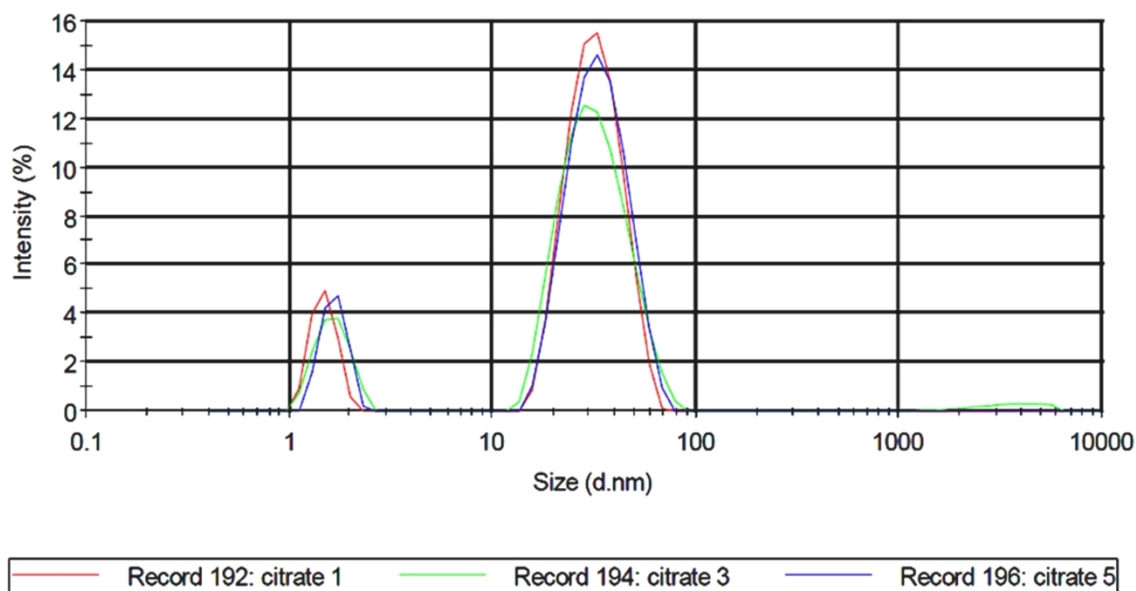


Figure 3-3: The size distribution graph indicating the % signal intensity measured by DLS.

The average hydrodynamic diameter of citrate capped GNPs was 17 nm. Combining the results obtained from UV-Vis spectrometry, TEM, and DLS, the average size of the synthesised GNPs are approximately 17-18 nm, with a narrow size distribution. These values all correlate with each other. The intensity peak noted at 1 d (nm) is present possibly due to unreacted GNP seeds from the synthesis that was carried over during sample clean-up (Zhao et al., 2013).

3.3.2 Ligand exchange standardisation & characterisation

Ligand exchange was successfully performed (Section 3.2.4). The Lig-GNPs were characterised similarly to Cit-GNPs, including UV-Vis spectrometry and DLS. Agarose gel electrophoresis (which includes Cit-GNPs as the reference nanoparticle) was also done. For the agarose gel electrophoresis, the citrate particles and GSH particles which were loaded with sucrose instead (the particles were unstable in glycerol).

3.3.2.1 UV-Vis spectrometry results

A UV-Vis spectrum was obtained for each Lig-GNP within the range of 300-700 nm. The absorbance spectra were compared to indicate the slight shift in maximum absorbance values (OD_{520}) as an indicator that ligand exchange has taken place successfully. Figure 3-4 shows the absorbance spectra of the Lig-GNPs and the shifts in absorbance due to changes of the surface chemistry of each Lig-GNP group. Table 3-7 shows the OD_{450} and maximum absorbance values (OD_{520}) for each Lig-GNP sample.

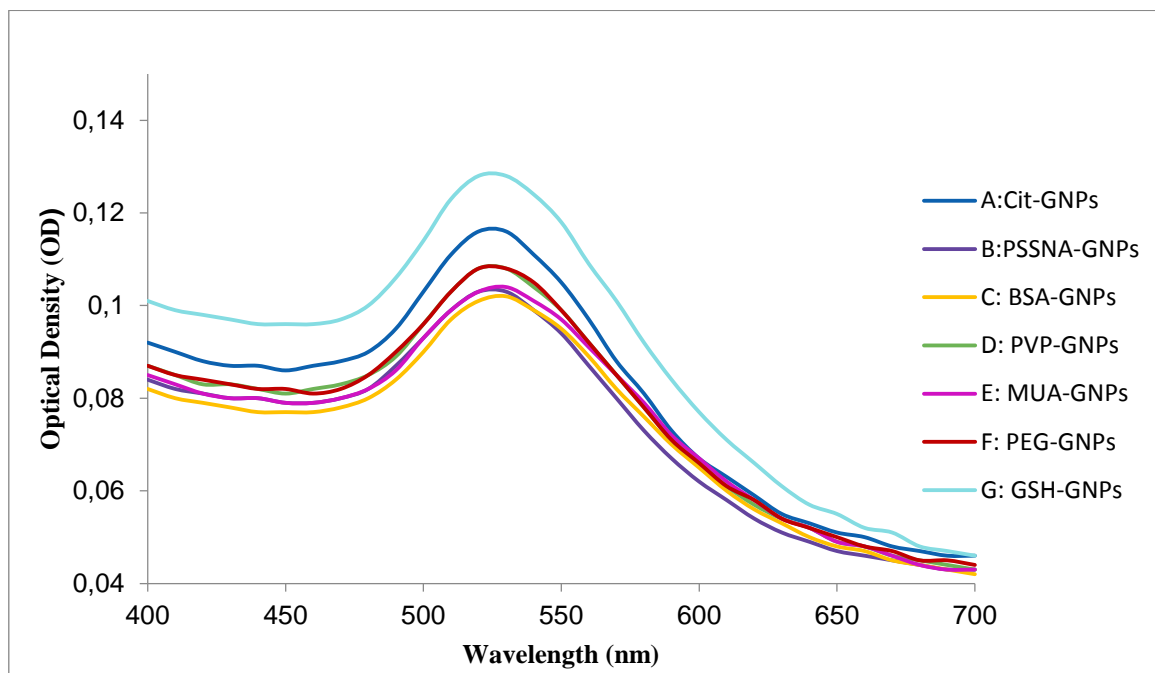


Figure 3-4: Absorbance spectra of the differentially functionalised GNPs used in this study. A) Citrate-GNPs are used as reference point, B) PSSNa-GNPs, C) BSA-GNPs, D) PVP-GNPs, E) MUA-GNPs, F) PEG-GNPs, and G) GSH-GNPs.

Table 3-7: The OD_{450} and maximum absorbance values (OD_{520}) of the Lig-GNPs.

	A	B	C	D	E	F	G
	Cit-GNPs	PSSNa-GNPs	BSA-GNPs	PVP-GNPs	MUA-GNPs	PEG-GNPs	GSH-GNPs
$OD_{450} (\times 10^{-2})$	8.60	7.90	7.70	8.10	7.90	8.20	9.60
$OD_{520} (\times 10^{-2})$	11.60	10.30	10.10	10.80	10.30	10.80	12.80

The UV-Vis spectra for all the Lig-GNPs correlate with the Cit-GNPs spectrum, indicating that all the Lig-GNPs are spherical and similar in size. A slight change in absorbance as well as a shift in wavelength is noted between the rest of the Lig-GNPs. These changes indicate that the surface characteristics of the GNPs were altered; however the changes are very subtle. The GSH-GNPs are above the reference, indicating that possible inter-particle coupling takes place where the particles interact with each other due to instability

Further stability evaluation (Section 3.3.3) reveals that GSH-GNPs are unstable, especially in cRPMI culture media, which contributes to why interparticle coupling possibly occurs (Ghosh and Pal, 2007). The OD_{520}/λ_{max} indicates that the particles are stable and the defined peak indicates a narrow size distribution (Berciaud et al., 2005).

3.3.2.2 Agarose gel electrophoresis results

To further investigate the differentially functionalised GNPs, the size and charge differences were evaluated by agarose gel electrophoresis. The results are shown in Figure 3-5. Figure 3-5a: A-G in TBE Buffer, pH 8 and Figure 3-5b A-D in TAE buffer pH 8. The Cit-GNPs and GSH-GNPs were loaded with sucrose instead due to instability with glycerol.

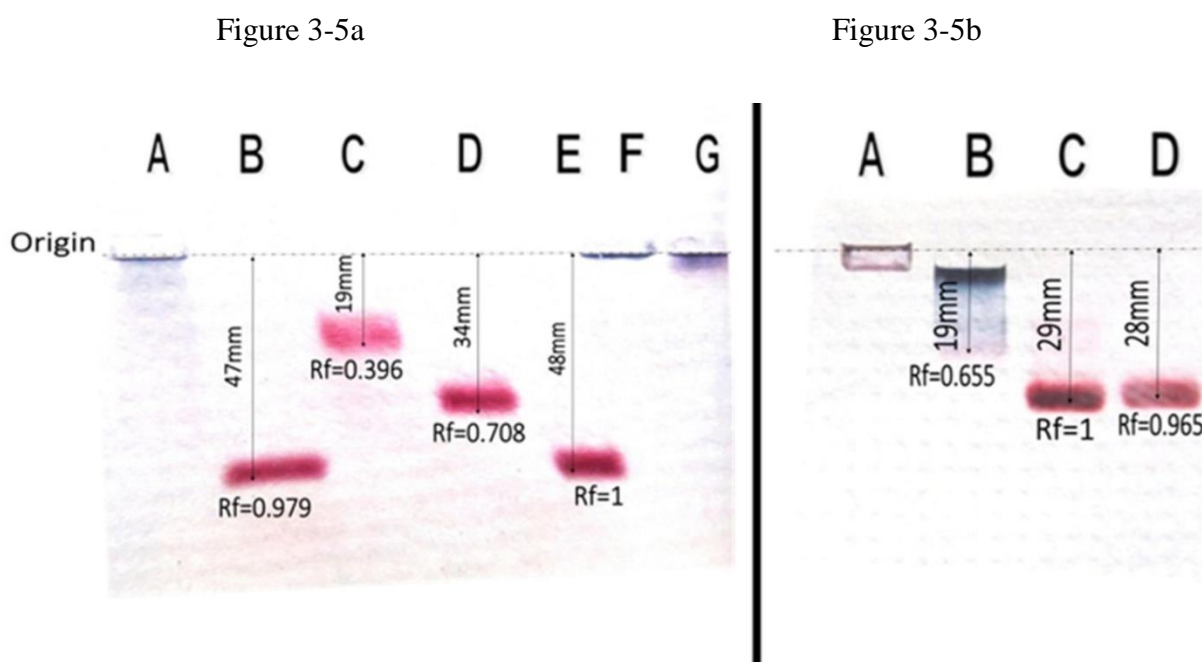


Figure 3-5: Agarose gel electrophoresis of Lig-GNPs at pH8, 50 V for 45 minutes. Figure 3-5a in TBE Buffer (A) Cit-GNPs (B) GSH-GNPs (C) BSA-GNPs (D) PVP-GNPs (E) PSSNa-GNPs (F) PEG-GNPs (G) MUA-GNPs. Figure 3-5b the Lig-GNPs in TAE Buffer (A) Cit-GNPs, (B) PEG-GNPs, (C) GSH-GNPs and (D) MUA-GNPs.

The figure reveals that (A) Cit-GNPs, (F) PEG-GNPs and (G) MUA-GNPs are not stable in TBE Buffer (3.5a). Hence, the agarose gel electrophoresis was repeated using TAE buffer. Certain Lig-GNPs such as (D) MUA-GNPs seems to be more stable in this buffer, however (A) Cit-GNPs and (B) PEG-GNPs are still unstable. The RF-values were calculated for each sample.

From the agarose gel electrophoresis results shown in Figure 3-5, the RF-values (which are usually used in chromatography quantification) were calculated to quantify the migration of each Lig-GNP sample. These values are listed in Table 3-8.

Table 3-8: RF values of Lig-GNPs which migrated through the agarose gel.

Lig-GNP	RF-Value	Surface charge
Cit-GNPs	-	Negative*
PSSNa-GNPs	1.00	Negative
GSH-GNPs	0.98	Negative
MUA-GNPs	0.97	Negative
PVP-GNPs	0.71	Negative*
PEG-GNPs	-	Neutral*
BSA-GNPs	0.40	Negative

*PVP-GNPs appear to be negatively charged, however these particles will undergo protonation at a physiological pH and will therefore be positively charged. The results for Cit-GNPs and PEG-GNPs were unclear.

Cit-GNPs and PEG-GNPs were unstable in both gels, the purple and grey colour changes indicate that the particles agglomerated and did not migrate through the gel due to complex structures that were formed, and therefore it was not possible to determine the RF values for these Lig-GNPs. According to the literature, Cit-GNPs are negatively charged (citrate

$\text{C}_6\text{H}_5\text{O}_7^{3-}$) and PEG-GNPs are neutral at physiological pH (Laskar et al., 2016). The more negatively charged molecules such as PSSNa-GNPs migrated faster through the gel towards the cathode. Even though PSSNa is a large molecule, it migrates rapidly through the gel due to its spherical orientation on the GNP surface (Figure 3-6). The same pattern is noticed in small, negatively charged particles such as MUA in Figure 3-5b; whereas larger molecules such as PVP and BSA migrate slower through the gel pores. All the Lig-GNPs that were stable migrated towards the cathode, indicating that all the samples are negatively charged at pH 8. However, PVP is a molecule that will be positive at a lower, physiological pH (pH6-pH7) due to protonation, as it has a pKa value of 5 (Mahltig et al., 2002).

Compared to the UV-Vis spectrometry results, agarose gel electrophoresis provides more information with regards to the estimate GNP size and net surface charge, but no information on morphology. TEM results have already confirmed that the GNP core is spherical. DLS analysis gives a more accurate indication of the orientation and sizes of the Lig-GNPs in a wet medium, where the pH, salts and interaction with each other can be taken into account.

3.3.2.3 DLS results

The hydrodynamic diameters of the Lig-GNPs were measured using DLS. The different hydrodynamic diameters are reported in Table 3-9.

Table 3-9: The hydrodynamic diameter of Lig-GNPs measured by DLS.

Ligand-GNPs	Average hydrodynamic size
Cit-GNPs	17 nm
PSSNa-GNPs	17 nm
PVP-GNPs	19 nm
BSA-GNPs	21 nm
MUA-GNPs	17 nm
PEG-GNPs	19 nm
GSH-GNPs	17 nm

From the results shown in Table 3-9, it is clear that the functionalised surface coating changes the hydrodynamic size of the GNP. Larger molecules such as PVP and BSA cause a size increase of 2-4 nm on the GNP surface, whereas ligand exchange with smaller molecules such as MUA and GSH cause the hydrodynamic diameter to remain 17 nm. Interestingly, large polymers attached to a GNP surface such as PSSNa-GNPs, results in a relatively small particle. This is due to the binding orientation on the surface of the particle. Figure 3-6 shows the difference in surface binding orientation between PSSNa and BSA, which are both large molecules; however, PSSNa has multiple attachment points, allowing a single molecule to wrap around the surface of the particle.

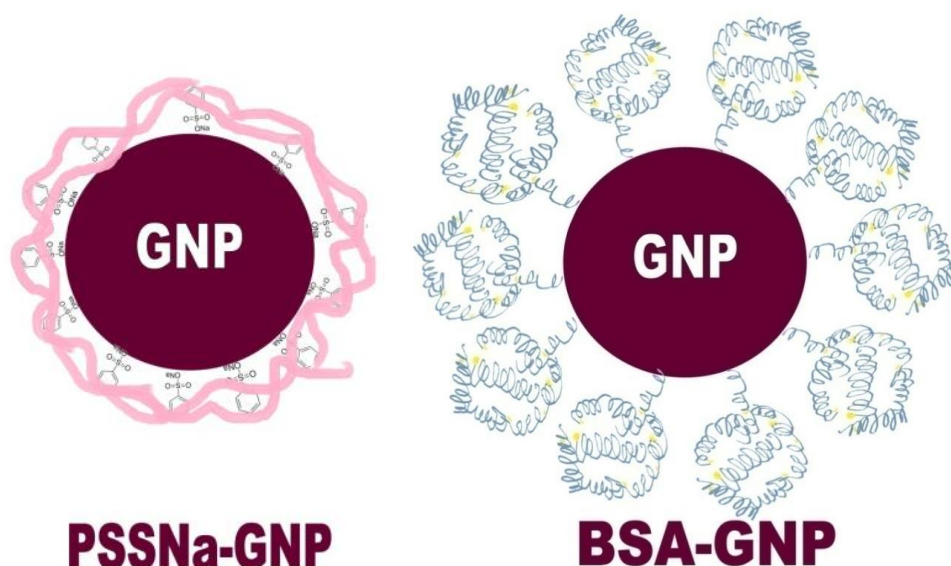


Figure 3-6: The size and orientation differences between a PSSNa-GNP and a BSA-GNP (not to scale). BSA is a large coiled protein molecule of approximately 66 kDa, where PSSNa is much larger at 70.000 kDa. However, PSSNa is a very long molecule with multiple attachment points which wrap around the GNP core, where BSA only has a single attachment point for one entire molecule.

The rest of the Lig-GNP structure illustrations are shown and described in Addendum C.

In conclusion, the synthesis and characterisation of GNPs were successful. The sizes correspond between UV-Vis spectrometry, TEM, agarose gel electrophoresis and DLS (17-18 nm GNPs). The characteristics of the surface coatings determine the charge, morphology and size of the GNPs. The slight differences in the results between DLS and the other

characterising methods are possibly due to the different microenvironments of each analysis. For instance, TEM could give a visual indication of the Cit-GNP core size, but is limited to a visual representation of the reference particle and does not include interaction with surrounding molecules and other aspects (such as pH) when in solution. DLS measurement would take other parameters into consideration such as the pH, interaction of salts or other molecules as well as the temperature of the GNP solution. A combination of the different techniques used for the characterisation of Lig-GNPs give a holistic indication of the characteristics of GNPs.

Further analysis was done to evaluate whether the surface modifications are stable under physiological circumstances over time, which will be indicative of whether the Lig-GNPs are more biocompatible compared to Cit-GNPs (Fraga et al., 2013).

3.3.3 Ligand exchange stability evaluation

The stability of Lig-GNPs was evaluated to predict their behaviour within the cellular environment. The pH, salt concentration, and stability with cRPMI were the most important aspects to consider and will therefore be discussed in this section. The rest of the stability data is discussed in more detail in Addendum D. Table 3-10 shows a summary of the stability of each Lig-GNP under these circumstances.

The data reveals that all the particles were stable under physiological pH values. Most Lig-GNPs were stable up to 50 mM NaCl. Other Lig-GNPs remained stable with 100 mM NaCl such as BSA-GNPs and MUA-GNPs. All of the Lig-GNPs had a wider range of pH stability compared to Cit-GNPs because of their uniquely modified surface-chemistries.

During evaluation of stability with PBS, the results have shown that almost all Lig-GNPs were unstable in $1 \times$ PBS. The reason for instability is possibly due to interactions between the Lig-GNPs and molecules present in the buffer (phosphates, sodium, potassium and chlorine ions). Therefore, PBS could not have been used as a vehicle; ddH₂O was used instead. The cRPMI culture media did not cause instability with most of the Lig-GNPs, with the exception of GSH-GNPs. Therefore, it was decided to exclude the evaluation of the effects of GSH-GNPs on cells during the main study (Chapter 5: Metabolomics). The

addition of β -Mercaptoethanol to the Lig-GNPs represented stability of the GNPs with thiol-containing substances, which are present within the cells and could have an effect on the cellular function or elicit a cellular response. All of the Lig-GNPs were stable for up to one hour, which is more stable when compared to the reference Cit-GNPs.

Table 3-10: A summary of the aqueous stability ranges of the Lig-GNPs.

	Citrate-GNPs	PSSNa-GNPs	PVP-GNPs	BSA-GNPs	MUA-GNPs	PEG-GNPs	GSH-GNPs
*pH	6<pH<10	4<pH<10	4<pH<10	5<pH<10	4<pH<10	5<pH<10	5<pH<10
*[NaCl] (mM)	1-10	1-50	1-50	1-100	1-100	1-50	1-50
*PBS	Not stable	Not stable	Not stable	Stable	Not stable	Not stable	Not stable
*Media (cRPMI)	Stable	Stable	Stable	Stable	Stable	Stable	Not Stable
*B-Mercaptoethanol	Not stable	>1h	>1h	>1h	>1h	>1h	>1h
10mMMOPS	9<pH<10	9<pH<10	9<pH<10	9<pH<10	9<pH<10	9<pH<10	9<pH<10
100mMHEPES	7<pH<8	7<pH<8	7<pH<8	7<pH<8	7<pH<8	7<pH<8	7<pH<8
EDTA	>0.01 M	>0.01 M	>0.05 M *	>0.05 M	>0.01 M	>0.01 M *	>0.01 M
Glycine	3<pH<10	2<pH<10	2<pH<10	9<pH<10	3<pH<10	2<pH<10	9<pH<10
Citrate	4<pH<6	4<pH<6	4<pH<6	4<pH<6	4<pH<6	4<pH<6	pH 6

*Most relevant and important stability conditions which are discussed.

These results indicate that the functionalisation of GNPs does, in fact, increase the biocompatibility of GNPs, as described by Fraga et al. (2013).

3.4 Summary

GNPs were successfully synthesised using the Turkevich method and cleaned up to avoid cellular responses due to unreacted reagents from the synthesis procedure (Alkilany & Murphy, 2010). The citrate GNPs were characterised via UV-Vis spectroscopy, agarose gel electrophoresis, TEM and DLS. GNPs were functionalised using six various ligands, the Lig-GNPs were characterised, and the stability of each Lig-GNP was evaluated. Each Lig-GNP had unique properties in terms of size, charge and morphology. These characteristics influenced the stability and surface chemistry of the Lig-GNPs when environmental changes occurred or interaction with molecules such as salts or physiological materials took place. In most cases, the functionalised Lig-GNPs were more stable than citrate GNPs. This ability of GNPs to bind to various ligands increases its benefits of being more stable, depending on the ligand on the surface of the particle. As Fraga et al. (2013) reported, ligands attached to the surface of GNPs improve their overall biocompatibility and safety which is a promising feature for drug delivery when the drug can be used to cap the particle.

Chapter 4: Cell Biology – Pilot study

4.1 Introduction

This section will describe general culturing procedures of HepG2 cells. This cell line was chosen based on the ability that liver cells allow GNPs to internalise well. Moreover, HepG2 cells are easily cultured. The GNPs are also evaluated to determine cellular viability (WST-1 viability assay and APOPercentage apoptosis assay) related to the internalisation of GNPs into the cells by using inductively coupled plasma mass spectrometry (ICP-MS) performed by Mr. Johan Hendricks. Dosages and sampling time points for evaluating the effect of the particles on the metabolome were also determined in this section. All procedures were done under sterile conditions, unless otherwise stated. All assays were performed on cells that were at passage 28.

4.2 Methods

4.2.1 General culturing

HepG2 cells were retrieved from cryopreservation. The cells were thawed on ice, placed in preheated (37 °C) complete media (RPMI 1640 culture media, Hyclone SH30027.01; 10 % FBS, Biochrom BC/S0615 and 1 × Pen-Strep, Lonza DE17-602E), and seeded in a T25 (25 cm³) cell culture flask (NUNC, 156367). The cells were incubated in a humidified incubator with 5 % CO₂ at 37 °C (HeraCELL, Heraeus). The cells were allowed 16-24 hours for attachment. The spent media was replenished with fresh cRPMI as required. The cells were sub-cultured and passaged to new culture vessels upon attaining ~80 % confluency.

4.2.2 Trypsinisation, cell counting and cell seeding

Once the HepG2 cells reached 80 % confluency, the spent media were removed and the cells were washed gently with 37 °C sterile PBS (Sigma Aldrich P4417-100TAB). The PBS was removed and 2 ml of 1 × trypsin (Lonza, BE02-007E) was added to the cells, followed by incubation at 37 °C for 5 minutes. The culture flask was gently agitated to dislodge all the cells. The cells were centrifuge sedimented by centrifugation (Multifuge 1L-R, Heraeus swinging bucket rotor) in a 15 ml falcon tube (Cellstar, 188261) at 1000 rpm for 5 minutes. The supernatant was discarded and the cell pellet was suspended in 10 ml cRPMI.

Cell counting was done using the Sceptor 2.0 automated handheld cell counter (Merck, PHCC20060) according to the manufacturer's guidelines. Sterile PBS (900 μ l) and 100 μ l cells were pipetted into a sterile 1.5 ml micro-centrifuge tube and was gently mixed by inversion. The Sceptor 2.0 was switched on and the cell counter sensor was attached. The sample was submerged in the sensor, the plunger was released and the amount of cells per ml was automatically calculated. The amount of cells was multiplied by 10 to compensate for the dilution factor and the amount of cells and media was calculated for the cell seeding density required per well for the analysis. The seeding density and amounts of reagents used differ according to the flask/plate being used. The cells were subsequently seeded according to Table 4-1 (adapted from Corning, 2015) which lists the recommended amounts of PBS, trypsin, cells and media for each culturing container.

Table 4-1: The quantities of PBS, trypsin, cells and media used for each container. (Adapted from Corning, 2015).

	PBS Wash	Amount of trypsin used	Cells seeded	cRPMI media added	Final volume
75cm² Cell culture flask	2 × 5 ml	2 ml Trypsin	500 cells/ μ l	13 ml media	Final Volume 15 ml
25cm² Cell culture flask	2 × 2 ml	1 ml Trypsin	100 cells/ μ l	9 ml media	Final volume 10 ml
6 well plate (NUNC)	-	-	400 000 cells per well	2 ml media	3 ml *
96 well plate	2 × 200 μ l	-	7500 cells per well	120 μ l Media	220 μ l *
Seahorse 96 well plate (Flux pack)	-	-	7500 cells per well	120 μ l Media	220 μ l*

*After treatment

4.2.3 Treatment of HepG2 cells with Lig-GNPs

After sub-culturing and seeding of the cells, each well was treated with Lig-GNPs accordingly. Table 4-2 shows the treatment values adapted from concentration to ppm (parts per million) cells which were used for the WST-1 cell viability assay as well as the dosage that was selected for each Lig-GNP for the rest of the assays performed during the study.

Table 4-2: Treatment conversion from nM to ppm.

Dosage	Concentration (nM)	Amount in ppm	Lig-GNPs for which the dosage was used
1	1.10	1.33×10^{17}	N/A*
2	0.50	6.63×10^{16}	Cit-GNPs
3	0.25	3.31×10^{16}	PVP-GNPs, PSSNa-GNPs, BSA-GNPs & PEG-GNPs
4	0.13	1.72×10^{16}	MUA & GSH
5	0.07	9.72×10^{15}	N/A*

*Not applicable (N/A) or suitable dosage (either too high or low)

4.2.4 Cell viability assays

The WST-1 Cytotoxicity assay is a quantitative method, which can be used to measure the effect of Lig-GNPs in different dosages. Based on these findings, the IC₃₀ (4.2.4.1) for each Lig-GNP group was selected as the dosage with which the study continued.

The APOPercentage apoptosis assay was also performed, to determine whether the cells undergo apoptosis or necrosis upon treatment with GNPs as well as to determine at which time point apoptosis occurs after treatment with the Lig-GNPs.

4.2.4.1 WST-1 cytotoxicity assay

The 30 % Inhibition Concentration (IC₃₀) of GNPs on cells was standardised using the WST-1 viability assay kit. The 50 % inhibition concentration (IC₅₀) value is the concentration of a substance that causes inhibition of 50 % of the biological activity or enzyme activity of a biological system (Yung-Chi & Prusoff, 1973). The IC₃₀ will allow the cells to be 70 % viable so that changes in the metabolic profile can be detected without eliciting an excessive cellular stress response. Part of the analysis included performing the analysis on the unbound

ligands (i.e. ligands without the GNP). The ligand exchange stability evaluation results (Section 3.3.3) showed that displacement of the ligand could occur in the presence of thiols. Therefore, the highest dosage of ligand was investigated to get an indication of the overall effect of unbound ligands on HepG2 cells. The assay was performed to give a quantitative indication of the differences in trends between the Lig-GNP treatment groups.

Cells were cultured, harvested and seeded in a 96 well plate with 100 μ l media, and incubated to attach to the culture plate surface and reach 60 % confluence ~16 hours (Section 4.2.1-4.2.2). The cells were treated in triplicate ($n = 6$ wells) with 6 different dosages of each Lig-GNP, which were prepared in ddH₂O to a final volume of 100 μ l Lig-GNP solution (Table 4-2). The plate was incubated and, after 24 hours, the total mixture volume (spent cRPMI and Lig-GNP) on the cells were removed, followed by a gentle wash with sterile PBS. The spent cRPMI / Lig-GNP mixture as well as the PBS were kept and preserved at -20 °C for ICP-MS analysis. Next, 100 μ l fresh cRPMI was added to the appropriate wells followed by the addition of 10 μ l WST-1 reagent to each well. The plate was gently agitated to ensure proper mixing of the cRPMI and WST-1 reagent. Table 4-3 presents a list of controls included for the WST-1 analysis.

Table 4-3: Controls included for the WST-1 cell viability assay.

	Control	Specifications
1	Ligand only	Cells treated with ligand only, correlating with dose 1, the highest dosage used.
2	cRPMI media blank	100 μ l media only, no cells.
3	WST-1 blank	100 μ l media and 10 μ l WST-1 reagent, no cells.
4	Vehicle Control (VC)	Cells treated with 100 μ l ddH ₂ O, media and 10 μ l WST-1 reagent.
5	Negative control	Cells treated with 100 μ l H ₂ O ₂ , media and 10 μ l WST-1 reagent.

The 96 well micro plate was incubated in the UV-Vis spectrometer (HT synergy, Biotek and Gen 5.1 software) at 37 °C and a reading was obtained for selected wavelengths (440 nm, 450 nm, 460 nm, 470 nm, 480 nm and a reference value of 660 nm) in 30-minute intervals.

The percentage cytotoxicity was calculated as follows:

Equation 4-1: Calculation of % cytotoxicity from WST-1 data.

$$\% \text{ Cytotoxicity} = \frac{\text{VC} - \text{treated}}{\text{VC}} \times 100$$

Where the Vehicle Control (VC) consists of HepG2 cells, cRPMI media and ddH₂O and the treated value consists of the experimental GNP treated HepG2 cells in cRPMI.

4.2.4.2 APOPercentage (Apo %) apoptosis assay

After the dosages of Lig-GNPs were standardised (4.2.1), the APOPercentage apoptosis assay was performed to firstly establish whether apoptosis or necrosis (if any) occurs after treatment. Gioria et al. (2015) established a link between apoptosis and the metabolism of Cit-GNP treated cells. Therefore, the effect on the metabolism of Lig-GNP treated cells undergoing apoptosis is of interest in this study. Secondly, the apoptosis induction time point (Sundquist et al., 2006) is useful to determine whether a time-dependent cellular reaction occurs during treatment with Lig-GNPs. A study done at this institution by Mulder (2016) observed that the apoptosis induction time points correlated with cellular DNA damage of Lig-GNP treated HepG2 cells.

Cells were cultured, harvested, seeded in a 96 well plate and incubated. Cells were treated (Section 4.1.3) and apoptosis was monitored after treatment at specific time points; 0 hours, 3 hours, 6 hours, 12 hours and 24 hours, respectively. After each time point, the culture media-Lig-GNP mixture was removed and substituted with the prescribed dye-reagent and incubated for 30 minutes. Each sample was analysed in duplicate.

After 30 minutes, the dye was removed and the wells were rinsed with PBS as described in Table 4-1 (Section 4.2.2). Then, 50 μ l PBS was added to the wells and the cells were photographed under a light microscope (Leica). After the cells were micrographed, 100 μ l of dye release reagent was added to each well. The plate was shaken for 5 minutes and the OD was measured at 550 nm (OD_{550}) using the HT synergy UV-Vis plate reader (Biotek).

The samples were normalised to compensate for baseline apoptosis by using the absorbance values at 550 nm after adding the dye release reagent. The formula is given as Equation 4-2.

Equation 4-2: Normalisation of baseline apoptosis.

$$(N) = \frac{OD_{550} \text{ sample}}{OD_{550} VC}$$

Where N is the normalised value, OD_{550} is the optical density at a wavelength of 550 nm, the sample is the respective Lig-GNP treated cell groups, and VC is the vehicle control.

4.2.5 Internalisation analysis using inductively coupled plasma mass spectrometry (ICP-MS)

ICP-MS was performed to determine the percentage of GNPs that was taken up (internalised) by the cells. The HepG2 cells, culture media and PBS-wash triplicate samples (obtained from the WST-1 assay, after analysis) were combined and digested respectively with concentrated nitric acid (HNO_3 , Merck, 100456) overnight. After digestion, the samples were diluted to 10 ml H_2O with a final HNO_3 concentration of 1 %. The gold-content was determined by using an Agilent Technologies 7500CE series inductively coupled plasma mass spectrometer with a MicroMist Nebuliser and spray chamber temperature of 2 °C. The sample depth was 8 mm, an RF Power of 1550 W was used, and argon was used as carrier gas at 0.92 L/min, and makeup gas (argon) at 0.25 L/min with an integration time of 100 ms.

4.3 Results and discussion

4.3.1 WST-1 cell viability/cytotoxicity assay results

The effect of Lig-GNPs on the HepG2 cells was determined by using the WST-1 cell viability/cytotoxicity assay (Section 4.2.1). Tetrazolium assays are based on the principle that tetrazolium salts cleave to formazan by cellular enzymes, which is directly proportional to the cellular viability expressed as mitochondrial activity. This assay was preferred over the MTT assay because it yields water soluble products which do not require additional solubilisation. The WST-1 assay is more stable and ready to use when compared to XTT and MTS assays. It also has a wider range and better colour development than the XTT assay (Berridge et al., 1996).

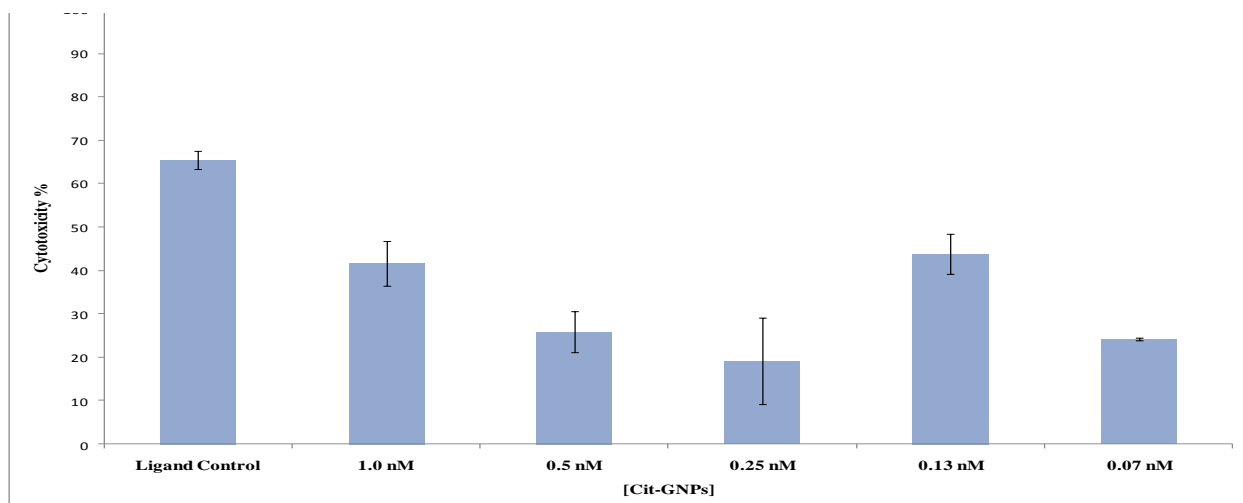
By using the WST-1 assay, cellular viability was quantitatively measured to give an accurate indication of the IC_{30} dosage, which is selected for the main study. The cellular cytotoxicity was measured after treatment with Citrate-GNPs, PSSNa-GNPs and PVP-GNPs, respectively. These were selected as examples to show the various cytotoxicity trends observed. It is also worth mentioning that the VC is not included in the graphs, as the VC is used as the baseline according to Equation 4-1, and thus zero. Table 4-4 presents a summary of the selected dosages based on these results for the rest of the Lig-GNPs used in the study.

Table 4-4: Lig-GNPs dosages selected for the main study based on the IC₃₀ values obtained by the WST-1 cytotoxicity assay.

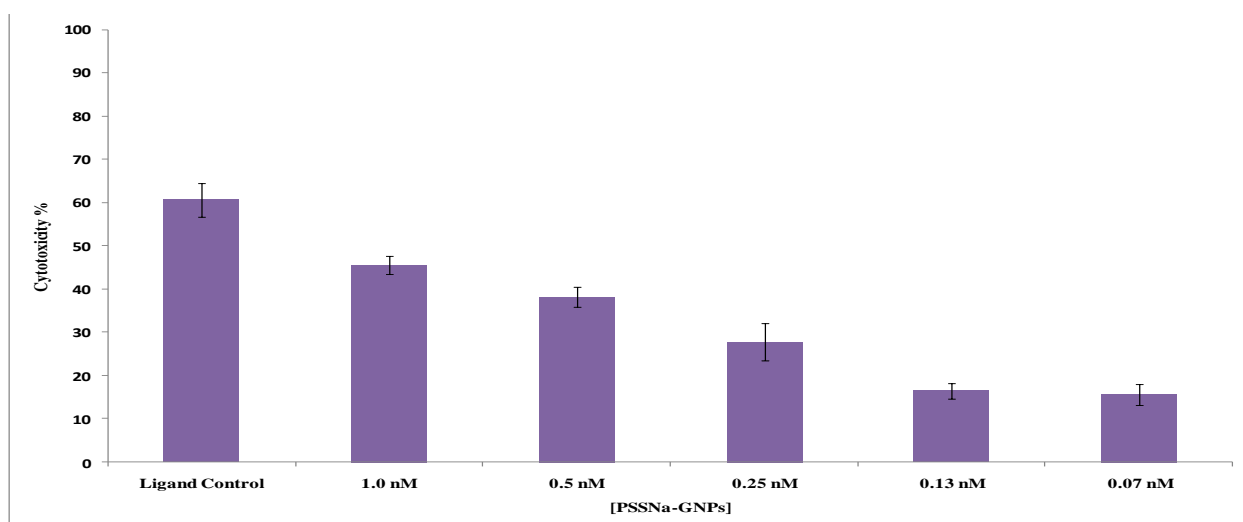
Ligand-GNPs	IC ₃₀ Dosage selected	
	Concentration (nM)	Amount (ppm)
Cit-GNPs	0.50	6.63×10^{16}
PSSNa-GNPs	0.25	3.31×10^{16}
PVP-GNPs	0.25	3.31×10^{16}
BSA-GNPs	0.25	3.31×10^{16}
MUA-GNPs	0.13	1.72×10^{16}
PEG-GNPs	0.25	3.31×10^{16}
GSH-GNPs	0.13	1.72×10^{16}

Figure 4-1a-c presents a graph of the cellular cytotoxicity after treatment with Citrate-GNPs, PSSNa-GNPs, and PVP-GNPs, respectively.

a)



b)



c)

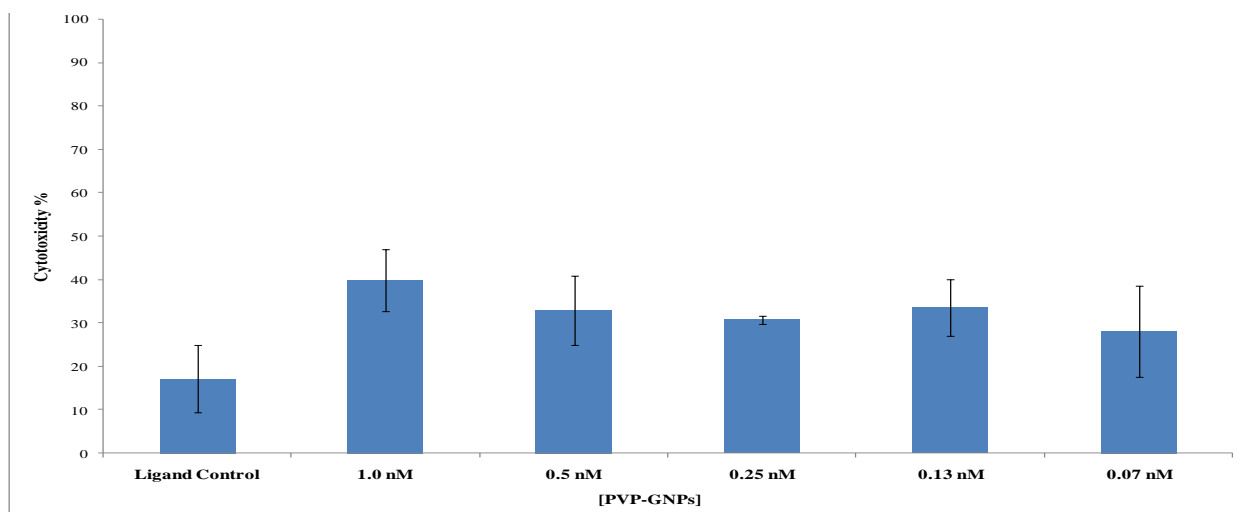


Figure 4.1: The % cytotoxicity after treatment with a range of different concentrations of a) Citrate-GNPs, b) PSSNa-GNPs and c) PVP-GNPs. The error bars show the standard deviation of the triplicate samples.

The results give an indication of the level of cytotoxicity caused by different Lig-GNPs. For all three Lig-GNPs, the cytotoxicity is directly proportional to an increase in dosage. The highest dosage where the Lig-GNPs are 30 % cytotoxic was chosen as the dosage with which to continue for the main study.

This trend is observed with all the Lig-GNPs; with the exception of PVP-GNPs, which had a horizontal trend, and GSH-GNPs, which showed a reverse trend (results not shown). The cytotoxicity of GSH is possibly due to oxidation [$2 \text{ GSH} + \text{RO-OH} \leftrightarrow \text{GSSG} + \text{H}_2\text{O} + \text{ROH}$] due to instability (Section 3.3.3), and therefore the cells react by reducing the oxidised form of the molecule. The reason why GSH-GNPs may have a reverse trend in cytotoxicity is possibly due to a phenomenon known as hormesis. Hormesis is a term used to describe the cellular response observed when a low dosage of toxin elicits metabolic alterations, but the response is inhibited at higher dosages of the toxin. Zhang et al. (2008) describe hormesis as a counteracting homeostatic control mechanism, however the exact mechanism explaining how GSH-GNPs are counteracted is not yet fully understood.

The ligand only controls were incorporated in the study to get an indication of the effects of unbound ligands on the viability of HepG2 cells, because the stability results (Section 3.3.3) revealed that displacement of the ligands on the GNP surface may occur due to the presence of thiols within the cells. The ligands have very different chemical properties when bound to the GNP surface compared to when unbound. Therefore, evaluating the behaviour of the unbound Lig-GNP will allow more reliable conclusions to be made. The results revealed that some of the unbound ligands such as Citrate (68 % cytotoxic) and PSSNa (60 % cytotoxic) are highly disadvantageous to the cells, where other compounds such as PVP is significantly less toxic than the correlating PVP-GNPs dosage. The reason for these observations is based on the chemical structure and spherical orientation of the ligands on the surface of the GNPs. An increase in citrate could most probably induce organic acidosis by altering the Krebs cycle, and could therefore finally affect cellular energy production. PSSNa is an exceedingly large polymer; when bound to a GNP core, the molecule is structured in such a way that it wraps around the GNP and cross links with itself (Figure 3-6). Unbound PSSNa is much larger and can influence the normal cellular environment. PSSNa is used as a non-cytotoxic antimicrobial contraceptive (Anderson et al., 2000); however, some studies have shown that

the polymer may have negative effects in the presence of certain compounds such as sorbitol (Sterns et al., 2010). PVP is a derivative of the amino acid proline and has a very similar structure, which is possibly why the cells do not have a very negative reaction towards the molecule.

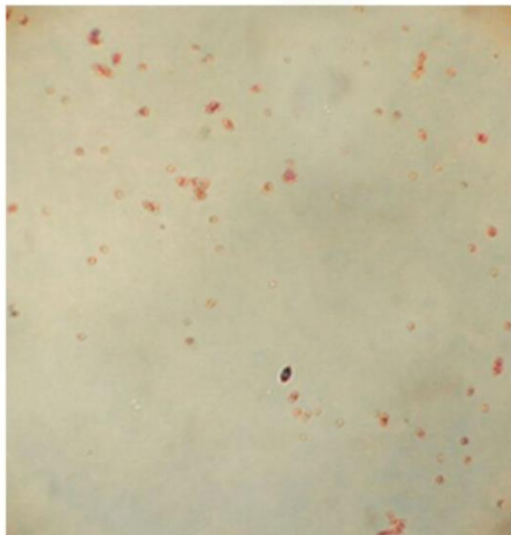
The rest of the WST-1 data results are reported in Addendum E as part of the cell viability assay results.

4.3.2 APOPercentage (Apo %) apoptosis assay results

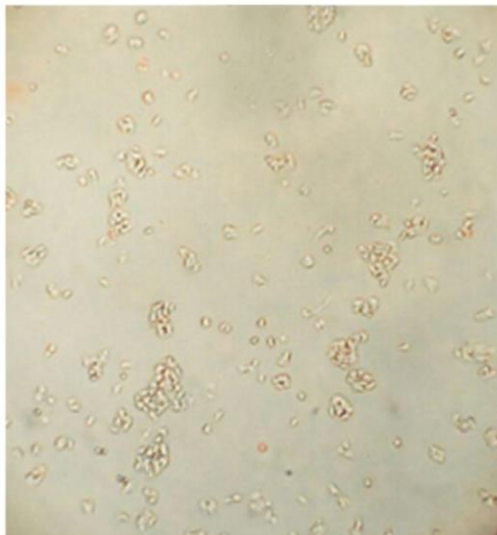
The APOPercentage apoptosis assay kit was used firstly to determine whether the Lig-GNP treatment causes the cells to undergo necrosis or apoptosis. A correlation was observed in the literature between metabolism and apoptosis in cells treated with GNPs (Gioria et al., 2015). Secondly, the assay was to give a qualitative indication of the apoptotic induction time points of each treatment group after normalisation (Sundquist et al., 2006). Mulder et al. (2016) observed DNA damage after 3 hours of treatment with GNPs, which correlated with the apoptotic induction time points observed.

Five different time points were evaluated for each Lig-GNP treatment: 0 hours, 3 hours, 6 hours, 12 hours, and 24 hours after treatment (results not shown). The cells that underwent apoptosis were stained pink with the prescribed Apo % apoptosis dye. Figure 4-2 shows micrograph photos of the cells treated with the Apo % dye 24 hours after treatment. a) Positive control (10 mM H₂O₂ treated cells); b) Vehicle Control/ VC (sterilised ddH₂O treated cells); c) PVP-GNP treated cells; and d) PSSNa-GNP treated cells.

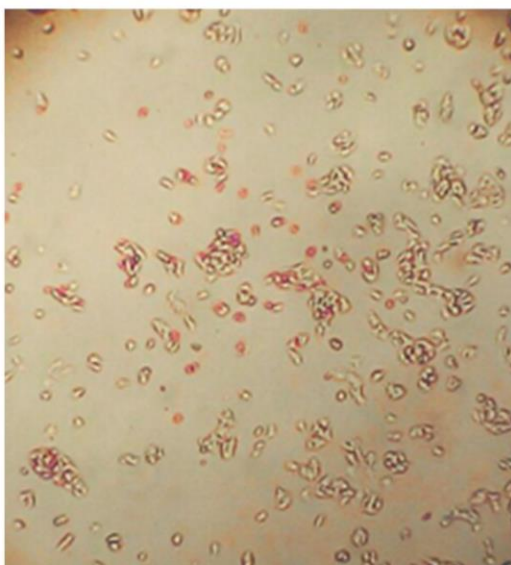
a) Positive control



b) Vehicle control (VC)



c) PVP-GNPs



d) PSSNa-GNPs

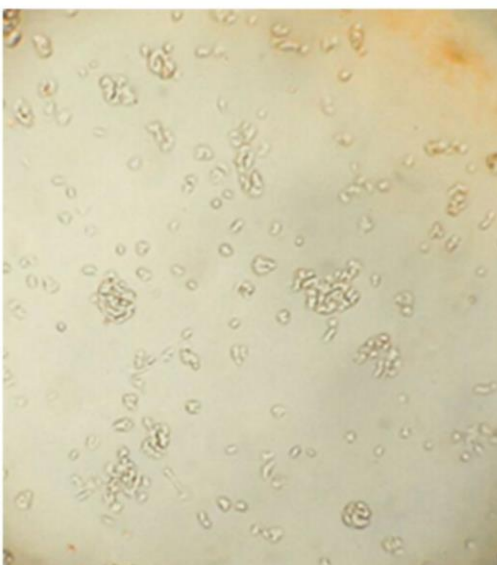


Figure 4-2 HepG2 cells analysed with the APOPercentage apoptosis dye reagent 24 hours after treatment. The cells were treated a) with 10 mM H₂O₂ (Positive control), b) sterilised ddH₂O (VC), c) PVP-GNPs and d) PSSNa-GNPs.

When evaluating the micrographs in Figure 4-2, the positive control (a), showed the cells were smaller, less in number as they detached and were washed away. The cells were stained pink, which indicates that the cells are undergoing apoptosis. Cells treated with the VC (b) underwent no significant visible apoptosis. The cells are more confluent and unstained, indicating that the cells are viable. (c) HepG2 cells treated with PVP-GNPs. 30 % of the cells are stained pink, indicating that there is an increase in apoptosis when compared to the VC (b). HepG2 cells treated with PSSNa-GNPs (d) resembled results that correlate with the VC. A small amount of cells were stained pink, the majority of cells were clear, indicating that very little apoptosis occurred.

After the micrographs were taken, a dye release reagent was added to each sample and the OD of the plates was measured and the samples were normalised. The normalised values of each time point of PVP-GNPs and PSSNa-GNPs as representative data is illustrated in Figure 4-3, respectively. The rest of the values for the other Lig-GNPs are reported in Table 4-5.

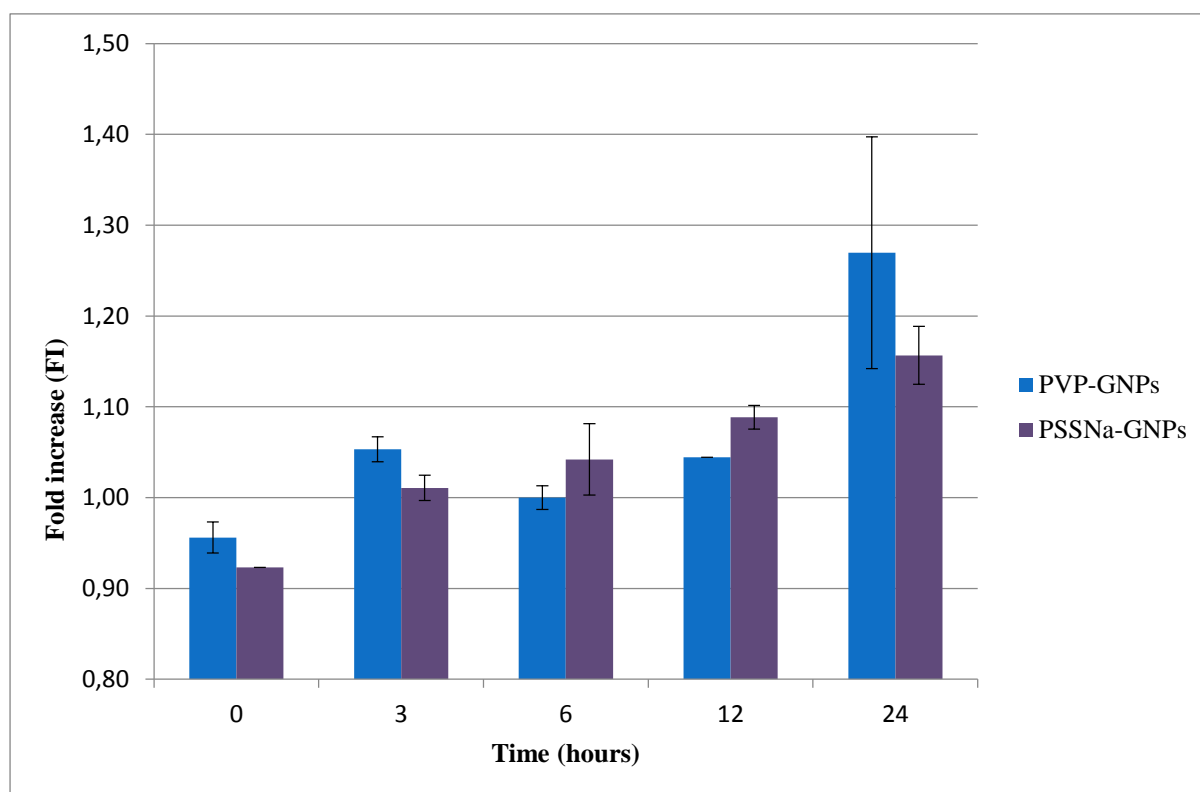


Figure 4-3: The FI values of PVP-GNP and PSSNa-GNP treated cells over 24hours. The error bars show the standard deviation of the duplicate samples.

The values of all the Lig-GNP treated cells are presented as a summative table in Table 4-5.

Table 4-5: The FI values of the Lig-GNPs at the selected time points.

	0h	3h	6h	12h	24h	Induction time point
Cit-GNPs	0.96	1.06	1.09	1.10	1.31	Stepwise
PVP-GNPs	0.96	1.05	1.00	1.04	1.27	3h
PSSNa-GNPs	0.92	1.01	1.04	1.09	1.16	3h
BSA-GNPs	0.97	0.99	1.06	1.09	1.23	Stepwise
GSH-GNPs	0.91	1.12	1.00	1.07	1.12	3h
MUA-GNPs	0.93	1.01	1.05	0.97	1.04	6h
PEG-GNPs	0.98	1.13	1.04	1.05	1.17	3h

Stepwise = indicates a stepwise increase in apoptosis over time with no obvious induction time point.

The APOPercentage apoptosis assay was done to establish whether the Lig-GNP treatment causes apoptosis, and if so, at which induction time points. Sundquist et al. (2006) described the induction time points at which apoptosis occur depending on the treatment and cell type. The results show an overall stepwise increase in apoptosis in all the Lig-GNPs. The majority of induction time points were at 3 hours. Mulder et al. (2016) observed DNA damage at the 3 hour time point, therefore this time point was selected for metabolomics analysis.

4.3.3 Internalisation Results

ICP-MS was performed to give a qualitative indication of the percentage of GNPs that was internalised by the cells. The percentage of gold atoms in the cells, PBS and media are shown in Table 4-6.

Table 4-6: The gold atoms present in each Lig-GNP sample.

	Citrate	PSSNa	MUA	PEG	PVP	BSA	GSH
Cells %	16.81	22.91	10.15	21.90	31.86	2.04	91.99
PBS %	3.32	0.19	1.62	6.50	1.77	2.20	2.16
Media %	79.87	76.90	88.23	71.59	66.36	95.76	5.85

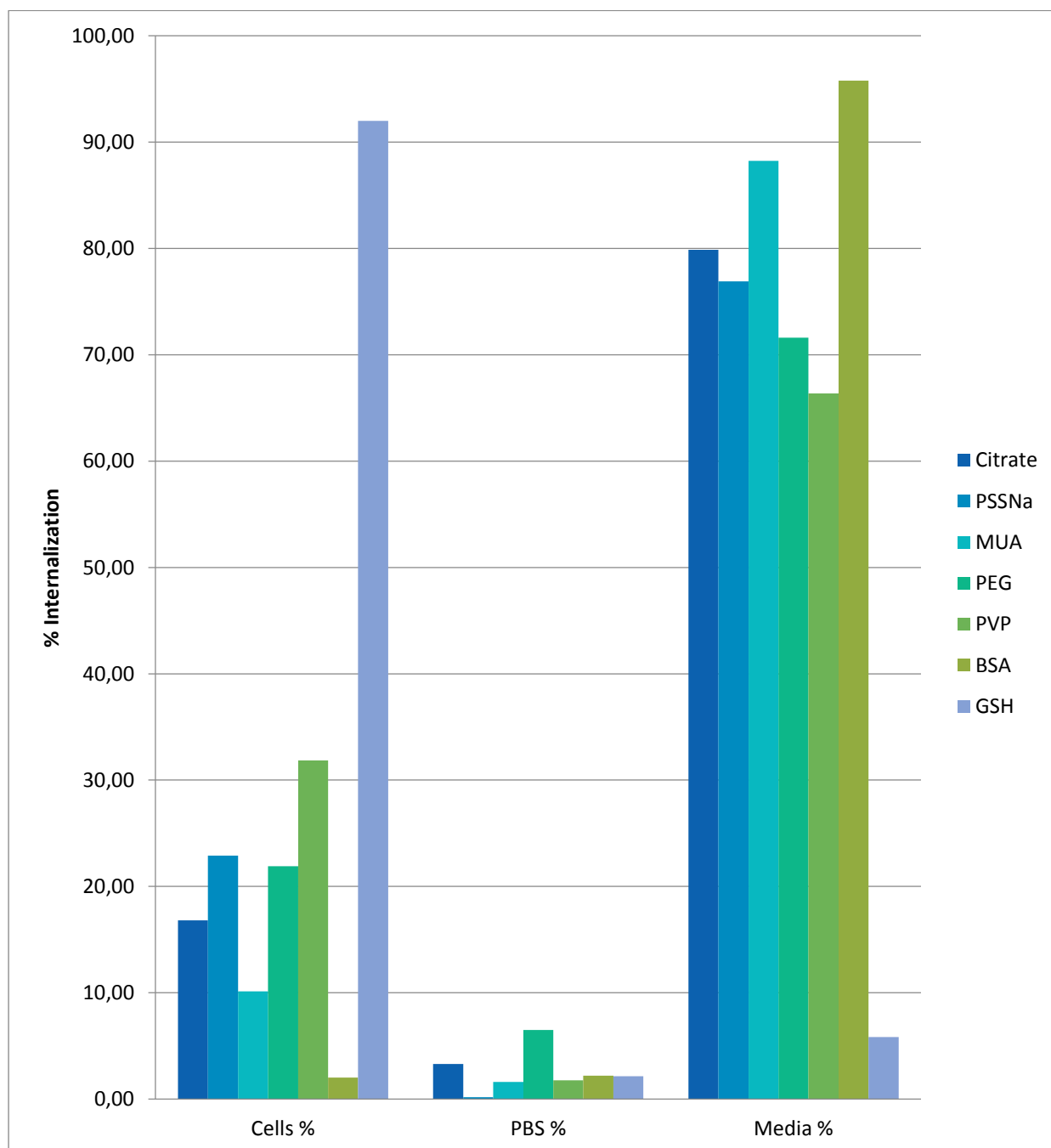


Figure 4-4: The percentages of Lig-GNPs in a) the cells, b) the PBS-wash and c) the media. There are no error bars because the triplicates were combined before ICP-MS analysis.

Most ligands only internalised up to 30 %, with the exception of GSH-GNPs. The difference between internalisation of the different Lig-GNPs is due to changes in chemical properties of the surface chemistry. Large structures such as BSA-GNPs and extremely anionic structures such as MUA-GNPs did not internalise well; whereas smaller, cationic molecules such as PVP moved into the cells more effectively. GSH-GNPs showed significantly increased internalisation (92 %) when compared to the other Lig-GNPs. GSH is a natural antioxidant within cells, therefore the molecules can use cellular machinery to freely move across the membrane.

From Figure 4-4 the conclusion can be made that the unique surface chemistry of each Lig-GNP causes different internalisation patterns. Surface charge plays a noteworthy role as described by Goodman et al., (2004). Anionic particles do not interact with the negatively charged cell membrane due to repulsion forces, explaining why negatively charged particles such as MUA-GNPs did not internalise well, even though the ligand on the surface is a small molecule. Moreover, PVP-GNPs, which are larger, cationic molecules, have a strong electrostatic affinitive interaction towards the negatively charged cellular membrane and are therefore taken up by the cell with ease. GSH-GNPs have the ability to enter through GSH cellular transport mechanisms, because GSH occurs naturally in the cellular environment and plays the role of an antioxidant, therefore allowing successful transport of GSH-GNPs across the cell membrane and a significant internalisation rate of 92 %.

In conclusion, the surface charge and the nature of the molecule on the surface of a GNP is an important aspect of the particles, which will determine how well internalisation takes place.

The Lig-GNPs, which had the highest internalisation pattern, were selected for metabolomics analysis. GSH-GNPs were excluded, because even though the GSH-GNPs internalised exceptionally well, they are unstable in cRPMI media and follow an unusual cytotoxic pattern known as hormesis in the WST-1 assay, which will require further research. Therefore, PVP-GNPs and PSSNa-GNPs, which had the second and third most successful internalisation rate, were selected for metabolomics analysis.

4.4 Conclusive summary

HepG2 cells were successfully cultured, treated and analysed to determine the cytotoxicity caused by the Lig-GNPs. Two independent cell viability analyses were done to ensure the reliability of the results and avoid false positive/negative results as suggested by Kong et al. (2011). These two independent cell viability analyses included the WST-1 cell viability/cytotoxicity and the APOPercentage apoptosis assay.

The WST-1 cell viability/cytotoxicity assay revealed the IC_{30} values, which were used as dosages for treatment for each Lig-GNP. These dosages allow the cells to be 70 % viable, not overwhelming the cells, while still triggering a cellular response. The APOPercentage apoptosis assay was performed in order to establish whether the Lig-GNP treatment induced apoptosis or necrosis, and secondly, to give an indication of the apoptosis induction time point. The overall trend in apoptosis was a stepwise increase with the majority of treatment groups inducing apoptosis at the 3 hour time point; however, exceptions were noted, indicating that apoptosis varied depending on the ligand used. Therefore, the surface characteristics of the Lig-GNPs play a significant role in the percentage of apoptosis in HepG2 cells.

The 3 hour time point showed apoptotic induction for most of the treatment groups and was therefore selected for metabolomics analysis. Moreover, Mulder et al. (2016) reported DNA damage noted in Lig-GNP treated cells by comet assay analysis, which may link to the metabolome.

The ICP-MS results showed the percentage of Lig-GNPs that were taken up by the cells. The data showed an internalisation rate of 32 % in HepG2 cells treated with PVP-GNPs (Figure 4-4), and a moderate dosage of 0.25 nM was sufficient for an IC_{30} value (Table 4-6). PSSNa-GNPs internalised 21 % and seemed to be less cytotoxic than PVP-GNPs at the same dosage (0.25 nM). Small molecules such as MUA-GNPs did not internalise well (10.15 %), yet these MUA-GNPs still had a significantly lower dosage required to obtain an IC_{30} value, indicating that MUA-GNPs have a more negative cellular impact on HepG2 cells. In conclusion, each

Lig-GNP sample has its unique properties, which determines the internalisation rate and effects on a cellular system.

For the purpose of this study, the 2 Lig-GNPs which were the most stable under physiological circumstances (Section 3.3.3), with the highest internalisation rate (Section 4.4.3) and different visible effects on the cells (Section 4.4.2) at the same dosage (Section 4.4.1) were chosen to evaluate the effect in terms of metabolic variation that Lig-GNPs have on the metabolome of HepG2 cells. PSSNa-GNPs and PVP-GNPs were suitable candidates that complied with these requirements. Both molecules are polymers; however, each has a different surface net charge, which may affect the metabolome on different levels.

Chapter 5: Metabolomics

5.1 Introduction

In the previous chapters, the GNPs were synthesised, characterised and evaluated for stability. The methods used were standardised and biocompatibility was improved by functionalising the GNPs with selected ligands from the previous chapter. The dosage for Lig-GNP treatment on HepG2 cells was determined with the WST-1 cytotoxicity assay, and the APOPercentage apoptosis assay was used to determine whether the cells undergo apoptosis. The main component of the study was to use metabolomics techniques to determine whether the GNPs cause metabolic variation within the HepG2 cells. This chapter will include the cellular respiration and metabolomics components of the study. The Seahorse XF⁹⁶ analysis was done to measure the mitochondrial respiration of HepG2 cells treated with the prepared Lig-GNPs. Assessment of mitochondrial function was required due to previous studies in the literature, which revealed that there may be an effect on the mitochondria and that the energy metabolism of the cells was affected when treated with GNPs (Huang et al., 2015, Leite et al., 2015, Wang et al., 2012). Leite et al. (2015) found that PEG-GNPs did not affect cell viability; however, treatment with PEG-GNPs caused the cells' intracellular ATP levels and mitochondrial membrane potential to increase. Therefore, the analysis was performed on the entire range of Lig-GNPs and afterwards narrowed down to only 3 selected GNPs for metabolomics analysis. The 3 selected Lig-GNPs included PVP-GNPs, PSSNa-GNPs and Cit-GNPs, and were selected based on the WST-1, APOPercentage and ICP-MS analysis. PVP-GNPs treated cells will give an indication of whether a positively charged polymer causes variation within the metabolome of HepG2 cells. PSSNa-GNPs followed the same pattern as PVP-GNPs during the WST-1 analysis and ICP-MS analysis; however, their physicochemical properties such as net surface charge at a physiological pH differ, as observed with agarose gel electrophoresis separation and in the literature (Li et al., 2007), which possibly explains the different observances in apoptosis. Moreover, at a physiological pH, PSSNa-GNPs are negatively charged, therefore, PSSNa-GNP treated cells gives an indication of the effect of negatively charged GNPs, while PVP-GNPs represent positively

charged GNPs. These two Lig-GNPs also had a high percentage of internalisation when compared to the other Lig-GNPs (with the exception of GSH), and were therefore selected to evaluate the effect on the cellular metabolome. Cit-GNPs were kept as a baseline control and ddH₂O as Vehicle Control (VC).

According to a study done at this institution by Mulder et al. (2016), the apoptosis induction time points correlated with cellular DNA damage of Lig-GNP treated HepG2 cells, therefore, the 3-hour time point was selected for metabolomics analysis which included the following assays: Seahorse XF⁹⁶ analysis for measurement of mitochondrial respiration; NMR analysis to evaluate the metabolites excreted in the metabolised culture media which represents the exometabolome of the cells; and endometabolome analysis, which included acylcarnitine and amino acid analysis by using LC-MS/MS and untargeted GC-MS, respectively. The materials and methods for the Seahorse XF⁹⁶ and metabolomics extractions will be included in this chapter.

5.2 Materials and methods

5.2.1 Seahorse XF⁹⁶ analysis

The Seahorse XF⁹⁶ analyser measures the oxygen consumption rate (OCR) of cells, which serves as an indication of mitochondrial respiration. The detailed protocol is described in Addendum J.

5.2.1.1 Cell seeding, treatment and instrumentation

HepG2 cells were cultured, harvested and seeded (Section 4.1) in a Seahorse 96-well culture plate, which is part of the Seahorse XF⁹⁶ flux pack (Seahorse Bioscience, 102416-100). The cells were cultivated (Section 4.1.1) and allowed to reach 60 % confluence (~16 hours), and were treated 3 hours before the assay. The Sensor Cartridge was prepared 24 hours before the assay by adding 200 µl of Seahorse XF Calibrant into each well of the sensor cartridge utility plate. The plate was then covered with parafilm to prevent evaporation, and then placed in a non-CO₂ 37 °C incubator for 24 hours to ensure sufficient time for the cartridge to hydrate (Van Dyk, 2016).

5.2.1.2 Mito stress assay preparation

Assay medium was prepared by adding 1.5 ml sodium pyruvate (1 mM) and 1.35 ml glucose (5 mM) to 147.2 ml assay medium. The prepared-assay medium was pre-heated to 37 °C, and the pH was adjusted to pH 7.4 with 0.5 M NaOH. Ten ml of assay medium was then kept aside for the compounds applied during the assay. Using the Seahorse prep-station, the cell culture medium was removed and the cells were washed and incubated with 200 µl prepared-assay medium in a non-CO₂ incubator for 1 hour (Van Dyk, 2016). The compound solutions in the Seahorse XF⁹⁶ Cell Mito Stress Test Kit that are applied during the assay were prepared in assay medium with concentrations indicated in Table 5-1.

Table 5-1: Compounds applied during the analysis.

Solution	Compounds	Final Concentration
A	Oligomycin	1 μ M
B	FCCP	0.5 μ M
C	Rotenone & Antimycin A	1 μ M each

The loading guides supplied with the Seahorse cartridge kit were used to load 25 μ l of each compound solution into the respective wells. Three OCR readings were taken during each step of the respiratory assay. The cartridge and utility plate with calibration buffer were placed into the XF Analyser to calibrate the cartridge. Thereafter, the cell culture plate was loaded into the instrument and the assay was performed.

5.2.1.3 Data processing

The data were processed using Wave (Version 2.2) software and the XF Mito Stress Test Report Generator (Version 2). Blanking was done to compensate for baseline oxygen consumption. Normalisation was done with the Cyquant cell proliferation assay (Thermofisher). All OCR data points were visualised in Wave to get a qualitative view of the respiration of the cells during each step of the assay. In terms of statistics, the average of the three measurements during each step was exported to create a data matrix with four variables per sample; namely basal respiration, proton leak, maximal respiration and non-mitochondrial respiration. Spare capacity and ATP production were determined separately by subtracting the basal- from the maximal respiration, and proton leak from basal respiration, respectively. These two variables were added to the matrix.

5.2.1.4 Statistical analysis

Statistical analysis was performed by using Metaboanalyst 3.0 (www.metaboanalyst.ca). One-way ANOVA statistical analyses were performed with the focus of determining whether

any of the treated groups differed significantly from the VC (using Fisher's post-hoc results). The values were log transformed to assure a more normal distribution of variables.

5.2.2 Metabolomics analysis

The metabolomics analysis was divided into two sections; namely evaluation of the endometabolome and exometabolome, respectively (Section 2.9.1.3). Figure 5-1 visually illustrates the approach and techniques used.

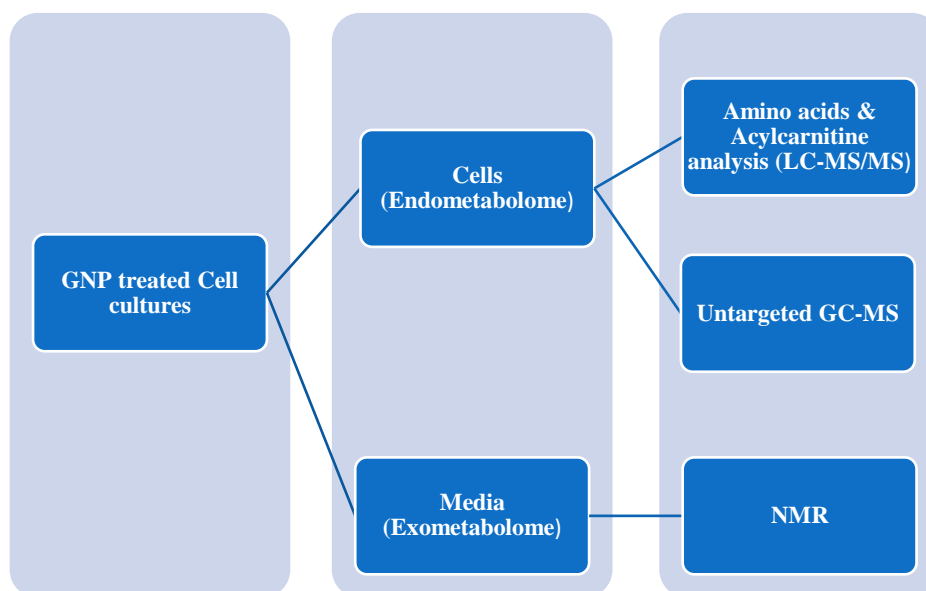


Figure 5-1 Schematic representation of the metabolomics analysis performed. Cells are seeded and treated with the differentially functionalised GNPs (Lig-GNPs). The intracellular content is extracted and analysed: firstly, with LC-MS/MS to evaluate the amino acid and acylcarnitine profile, and secondly, with untargeted GC-MS to consider metabolites present within the cells. Moreover, the metabolised culture media will be analysed using NMR to obtain a broad spectrum of metabolites.

5.2.2.1 Cell seeding and treatment

A sufficient number of cells was required for metabolomics to ensure that most metabolites were within the detection range of the respective instruments. Thus, the seeding and treatment dosages had to be adapted from 7500 cells per well in a 96 well plate to 400 000

cells per well in a 6 well plate (which is a 53-fold increase in cells). The GNP treatment solution was then adapted 53-fold to allow the same GNP per cell ratio for the metabolomics study.

HepG2 cells were cultured, harvested and seeded in four 6-well plates as described in Chapter 4 (Section 4.1). The cells were treated with Cit-GNPs, PVP-GNPs and PSSNa-GNPs. The VC cells were treated with ddH₂O, and H₂O₂ was used on the negative control cells (Seahorse XF⁹⁶ analysis). Each well was considered a biological replicate with each treatment group consisting of 6 replicates. The plates were incubated for 3 hours after treatment, after which metabolic quenching and metabolite extraction took place.

5.2.2.2 NMR analysis of exometabolome

The cells were seeded and treated (5.2.2.1). The GNP-culture media mixture was removed and kept for NMR analysis. The metabolised media samples were centrifuged at $10000 \times g$ for 5 minutes to remove cell debris or residual cells. 500 μ l of media was collected and 50 μ l potassium phosphate buffer solution (KH₂PO₄, trimethylsilyl-2,2,3,3-tetradeuteriopropionic acid, TSP – internal standard – dissolved in D₂O) was added to each sample (Dona et al., 2014). The samples were mixed under vortex and transferred to a 5 mm NMR tube. NMR was performed at 500 MHz on a Bruker Avance III HD NMR spectrometer equipped with a triple-resonance inverse (TXI) ¹H (¹⁵N, ¹³C) probe head and x, y, z gradient coils. ¹H spectra were acquired as 128 transients in 32 K data points with a spectral width of 6002 Hz. The sample temperature remained 27 °C and the H₂O resonance was pre-saturated by single-frequency irradiation during a relaxation delay of 4 seconds, with a 90 ° excitation pulse of 8 microseconds.

5.2.2.3 Analysis of cell cultures endometabolome

a) Metabolite extraction

Cellular metabolism was quenched with the addition of 1 ml -80 °C methanol. The cells in each well were scraped off using a Cell Scraper (99002, TTP) and transferred to a 2 ml microcentrifuge tube. One hundred and fifty μ l internal standard solution (3-phenylbutyric

acid, 150 ppm; L-Norleucine, 150 ppm and 2-Acetamid phenylalanine, 150 ppm) and 250 μ l stable isotope mixture (N13.02) were added to each tube, and a pellet size amount of glass beads (Restch) were added to the mixture. The tubes were shaken vigorously at 30 Hz for 5 minutes using a M400 vibration mill (Retsch), after which 660 μ l chloroform was added. The analyte samples were vortex mixed briefly and allowed to stand on ice for 20 minutes. The microcentrifuge tubes were centrifuged at $2930 \times g$ for 20 minutes. The entire top aqueous layer and bottom organic layer were aspirated into a clean GC-MS vial without disrupting the interphase consisting of cell debris and precipitated proteins. One third of each sample was then transferred to a separate vial for LC-MS/MS analysis of acyl-carnitines and amino acids. The samples were dried at 37 °C under nitrogen until visually confirmed as dry.

b) Oximation and silylation

The dried samples were derivatised for GC-MS analysis with the addition of 50 μ l methoxyamine hydrochloride (MOX). MOX solution was prepared by dissolving 20 mg MOX in 10 ml pyridine. After 1 hour incubation at 50 °C, the samples were allowed to cool down for 5 minutes before adding silylation reagent. One hundred μ l N,O-Bistrifluoroacetamide (BSTFA) and 2 μ l trimethylsilyl chloride (TMCS) were added to each sample and incubated as described above. All derivatisation reagents were transferred using an Agilent manual glass syringe. After derivatisation, the samples were allowed to cool down to room temperature and transferred into flat-bottom inserts before GC-MS analysis.

c) Butylation

For LC-MS/MS analysis, the dried samples were derivatised with the addition of 300 μ l butanolic-HCl (Obtained from PLIEM lab, Biochemistry Department, NWU Potchefstroom campus) using an Agilent manual glass syringe and incubated for 1 hour at 50 °C. Afterwards, the samples were allowed to cool down and were dried under nitrogen at 37 °C. The dried samples were re-dissolved in 100 μ l acetonitrile:water 50:50 and transferred into inserts before LC-MS/MS analysis.

d) GC-MS analysis

GC-MS analysis was performed on GC-TOF-MS system which consisted of an Agilent 7890A GC front-end system and a Leco Pegasus HT TOFMS with an Agilent 7693 autosampler. The samples were separated with an RTX-1 MS column (30 m \times 250 μ m \times 0.25 μ m) from Restek. Five μ l of the sample was injected splitless. Helium was used as a carrier gas with a constant flow rate of 1.5 ml/minute. The front inlet temperature remained 250 $^{\circ}$ C during injection. The GC oven initiated on a temperature of 70 $^{\circ}$ C for 1 minute, after which the temperature was increased stepwise to 120 $^{\circ}$ C at 7 $^{\circ}$ C /minute, then again increased to 230 $^{\circ}$ C at 10 $^{\circ}$ C /minute, and finally increased to 300 $^{\circ}$ C at 13 $^{\circ}$ C /minute. The GC oven remained 300 $^{\circ}$ C for 1 minute before cooling down and returning to its initial temperature. The transfer line remained at a constant temperature of 225 $^{\circ}$ C and the source remained 200 $^{\circ}$ C. Electron impact ionisation (EI) was performed at -70 V to fragment the compounds that eluted. A 450-second acquisition delay was allowed before the data was acquired at 20 spectra/second (50-950 m/z)

e) LC-MS/MS analysis

LC-MS/MS analysis was performed on an Agilent 6410 LC-MS/MS (QQQ) system with a 1200 series front-end. A C18 Zorbax SB-Aq column (150 mm \times 2.1 mm \times 3.5 μ m) from Agilent was used. The column temperature remained 30 $^{\circ}$ C throughout the analysis. One μ l of the sample was injected followed by the initiation of the programmed solvent gradient. The gradient for mobile phases A (0.1 % formic acid in water) and B (0.1 % formic acid in acetonitrile) is shown in Table 5-2, which ran over a period of 23 minutes. The column was equilibrated with a 10 min post run. The gas temperature for the ESI was kept at 300 $^{\circ}$ C at a flow rate of 7.5 l/minute. The capillary voltage was 3500 V and the nebuliser pressure remained 30 psi.

Table 5-2: Programmed mobile phase gradient used for separating butylated amino acids and acylcarnitines.

Time (min)	Mobile Phase A (%)	Mobile Phase B (%)	Flow rate (ml/min)
0	95	5	0.2
1	95	5	0.2
5	82	18	0.2
8	82	18	0.2
15	0	100	0.3
20	0	100	0.3
23	95	5	0.2

5.2.2.4 Data processing and normalisation.

5.2.2.4.1 NMR data

Bruker Topspin (V3.1) software (Ellinger et al., 2013) was used for pre-processing NMR spectral data. Automatic shimming of the sample was performed on the deuterium signal. The resonance line widths for TSP and metabolites were <1 Hz. Automatic Fourier transformation and phase and baseline correction were done. Each sample underwent 256 scans (each scan consisted of a 90 ° excitation pulse of 8 microseconds followed by a relaxation delay of 4 seconds) with a total run time of approximately 15 minutes per sample for one-dimensional (1D) ¹H-NMR analysis. In addition, two-dimensional (2D) J-resolved (JRES) and correlation (COSY) spectroscopy was done on one sample to aid in metabolite identification. Bruker AMIX (V3.9.12) software (Ellinger et al., 2013) was used to further process the NMR spectral data. Each NMR spectrum was divided into 0.02 spectral bins (buckets) between the interval of 0.5-10 ppm, excluding the region of the water peak – yielding a data matrix of 452 bins with spectral density data for statistical analysis. Following identification of important bins, metabolites were identified and confirmed using Bruker pH 7.0 spectral libraries of pure compounds, using both 1D and 2D information for level 1 identification.

5.2.2.4.2 GC-MS data

ChromaTOF software (Leco) was used to perform data extraction, which included a baseline offset of 1 (to avoid noise). The baseline was removed by using the “spanning” baseline tracking method. Automatic smoothing was performed by the software. An expected peak width of 3 seconds and signal-to noise ratio of 20 was used to detect the peaks with five apexing masses to confirm true peak detection. Spectral matching to the NIST11 commercial library and an in-house library was done to identify the compounds.

The compound could be identified when a match of 80 % similarity occurred between the library and compound (similar to 800 in ChromaTOF). The add-on package, Statistical Compare, was used to align the peaks and form a data matrix. All components were normalised with the internal standard to yield relative concentrations.

5.2.2.4.3 LC-MS data

MassHunter Quantitative Analysis was used for detection and integration of the peaks obtained from LC-QQQ data (Agilent). The software processed all samples in batch format. A compound aligned table or data matrix with integrated peak areas was created. Compounds, for which stable isotope internal standards were added, were normalised with these respective isotopes. Isotopes that were structurally very similar and eluted closest to the remaining compounds were used to normalise these compounds.

5.2.2.4.4 Statistical analysis

All samples were analysed in a single batch on all the analytical platforms. The data were still examined for within-batch effects/drifts during the analysis. Since no drifts were observed, the data was further processed with standard metabolomics procedures. A zero and QC filter was applied: components that were not present in all the samples of at least one experimental group were removed, followed by the removal of compounds that were not reliably measured (QC CV > 50 %). Log transformation was done to produce more normal distribution of the variables to allow the use of parametric statistical tests. Univariate statistical tests (one-way ANOVA and post-hoc tests) were done to find metabolites that differed significantly between

the groups (p -values ≤ 0.05). Multivariate statistics were done on the important metabolites to visualise their covariance which included evaluation by using principal component analysis (PCA). Statistical analyses were done with Metaboanalyst 3.0 (www.metaboanalyst.ca) and MS Excel.

5.3 Results and discussion

5.3.1 Seahorse XF⁹⁶ analysis

The Seahorse XF⁹⁶ analysis was used to measure the mitochondrial respiration of HepG2 cells treated with the Lig-GNPs at the time points discussed in Chapter 4. Initially, all the Lig-GNPs were analysed and the study was then narrowed down to only the three selected Lig-GNPs. The Oxygen Consumption Rate (OCR) was measured (in pmol/min) over time as compounds were injected as part of the mitochondrial respiration analysis. The mitochondrial respiration of HepG2 cells was measured after 3 hours of treatment with the entire range of GNPs. The results are displayed in Figure 5-2.

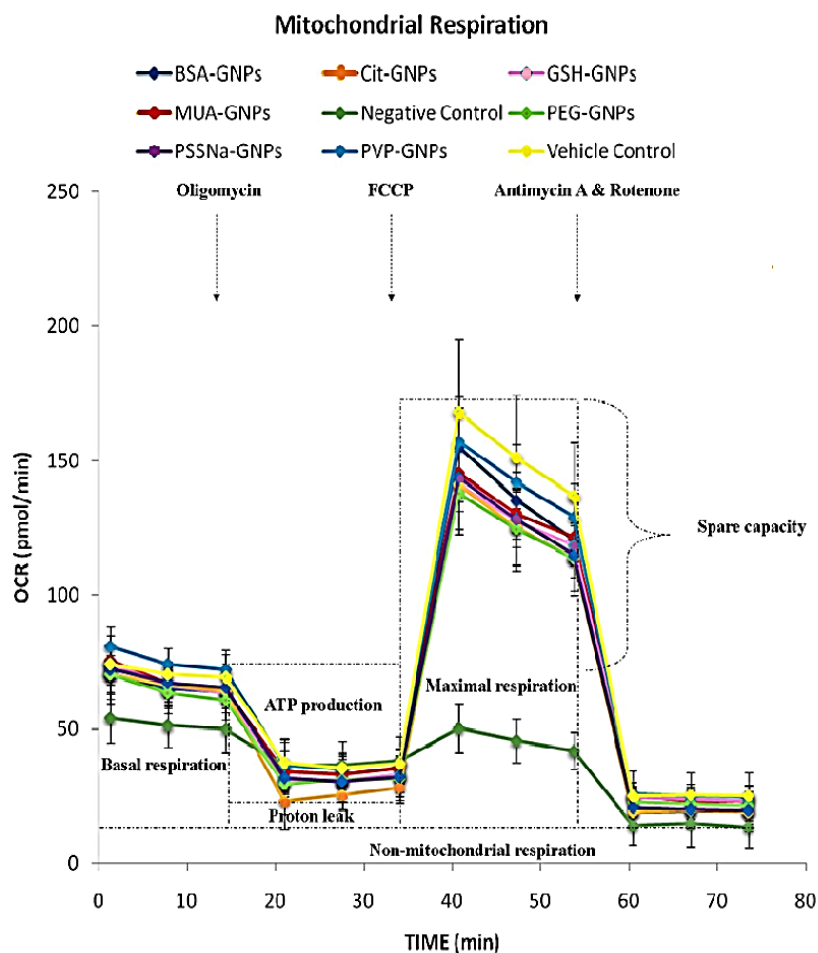


Figure 5-2: Mitochondrial OCR of HepG2 cells after 3 hours of Lig-GNP treatment (Left). Compared to the VC, most treated groups follow the same trend. However, some treated groups have a significantly lower maximal respiration value compared to the VC ($p = 0.03$). The trend indicates alteration (to some extent) in the treated cells' mitochondrial respiration. The only aspects that appeared to be significantly altered between all the Lig-GNP groups were the maximal respiration and spare respiratory capacity.

The three selected Lig-GNPs (PSSNa-GNPs, PVP-GNPs and Cit-GNPs) were separately compared to the VC (Figure 5-3).

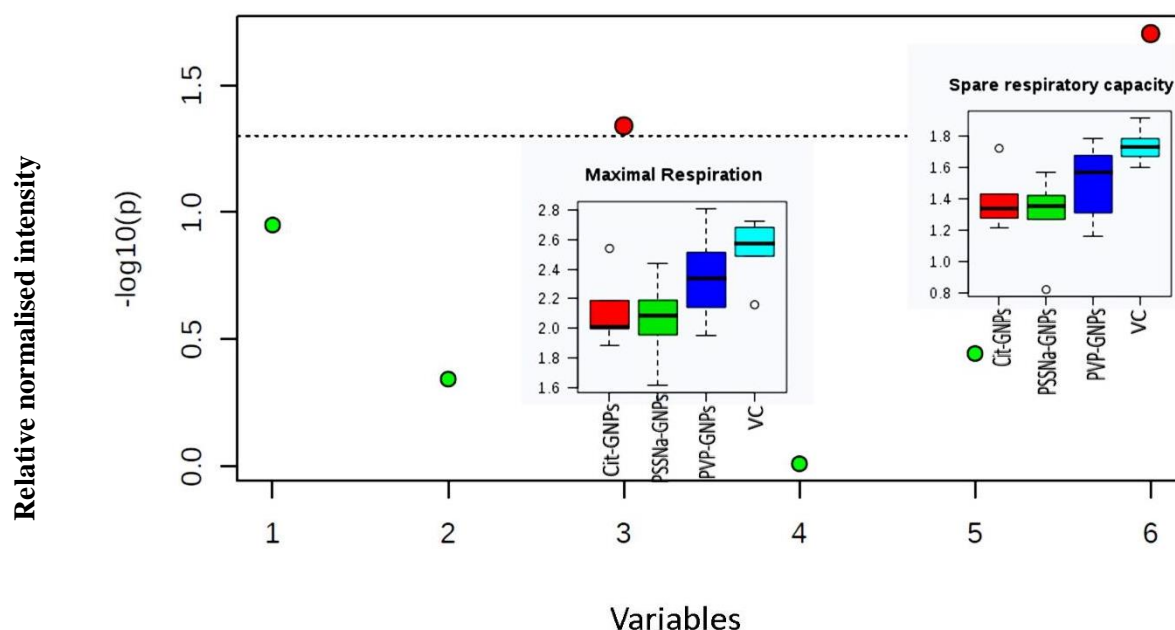


Figure 5-3: One-way ANOVA results showing the maximal respiration and spare respiratory capacity of the 3 selected treatment groups. The dots above the line indicate significance: the higher the dot, the more significant the difference of the respective variable between the groups.

The results show that the maximal respiration ($p = 0.046$) was moderately altered and spare respiratory capacity ($p = 0.02$) of the treated cells was significantly altered when compared to the VC. These results indicate that the electron transport chain and mitochondrial function are affected. ANOVA indicates that the Cit-GNPs, in particular, had overall lower spare respiratory capacity in comparison with the VC group. This means that the number of respiratory units or the function thereof might be affected with the treatment of cells with GNPs. The effect can thus be in the protein chemistry or related to the expression of the units from DNA as these functions are related to one another (Shaughnessy et al., 2014). It also seems that the coatings on the GNPs did improve their biocompatibility in terms of mitochondrial respiration when compared to Cit-GNPs because the results of the Lig-GNP treated cells were similar to the untreated control.

It is hypothesised that the differences observed could be stress related. A study by Shi et al., (2009) suggests that HepG2 cells possibly rely more on glycolysis for energy expenditure (known as the Warburg effect) as a response towards cellular stress. However, non-mitochondrial respiration would more likely affect the basal respiration of the cells, which in this case is not significantly affected. The overall lower maximal respiration could indicate that the cells treated with Cit-GNPs are possibly under stress and therefore other metabolic pathways could be activated to increase energy production (Hayashi et al., 2000; Towler & Hardie, 2007).

5.3.2 Metabolomics analysis

5.3.2.1 NMR (Exometabolome)

NMR analysis was performed on the metabolised culture media of the selected treated groups in order to see if the cells utilise or excrete more metabolites in comparison to the VC. Figure 5-4 illustrates representative box plots showing the differences in the level of selected compounds measured with NMR.

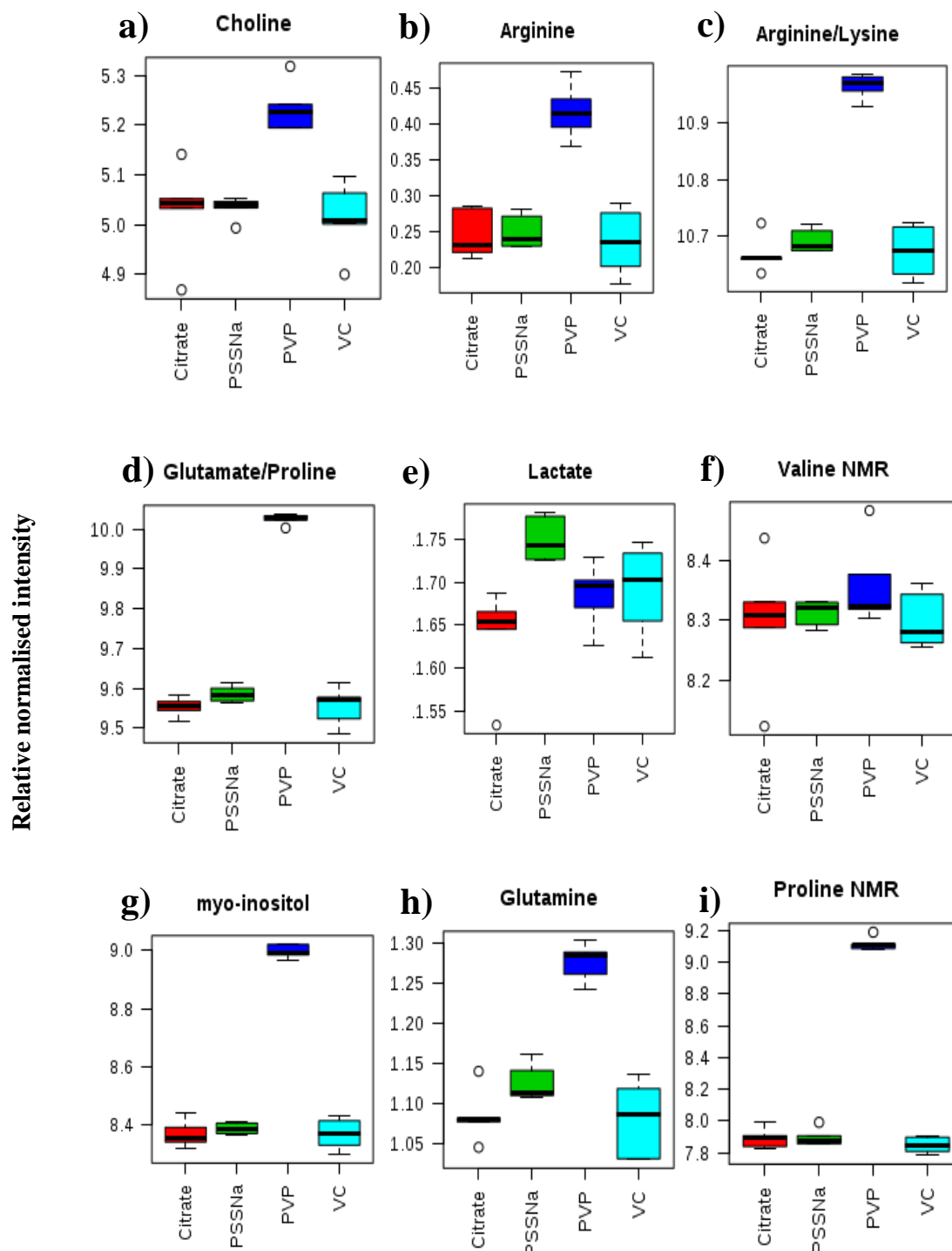


Figure 5.4: Box plots illustrating the differences in compound concentration between the 4 sample groups, from ANOVA statistical analysis. e) Lactate is the only increased metabolite in PSSNa-GNPs. The rest of the metabolites are increased in PVP-treated samples and there is no statistical difference between the VC and Cit-GNPs.

Table 5-3: The p-values of compounds significantly altered in the exometabolome

Metabolite	ID level	p-value	VC -Cit	VC-PSSNa	VC-PVP
Proline	1	<0.001	↔	↔	↑
Glutamate/Proline*	2	<0.001	↔	↔	↑
Myo-inositol	1	<0.001	↔	↔	↑
Arginine/Lysine*	2	<0.001	↔	↔	↑
Glutamine	1	<0.001	↔	↑	↑
Arginine	1	<0.001	↔	↔	↑
Choline	1	<0.001	↔	↔	↑
Lactate	1	0.006	↔	↑	↔

*Overlapping peaks can be either of the compounds.

Table 5-3 shows the metabolites that were significantly altered in the culture media due to GNP treatment as measured via NMR. The concentrations of 8 metabolites were increased, in the media of the cells treated with PVP-GNPs (when compared to the VC). This then indicates that the PVP-GNP treated cells excreted more of these compounds into the media or that they used less of these compounds. Statistical evaluation using principal component analysis (PCA) showed separation of the Lig-GNP treated groups from the VC, indicating that the exometabolome of these groups are markedly different from the VC and each other (despite relatively few metabolites being significantly different).

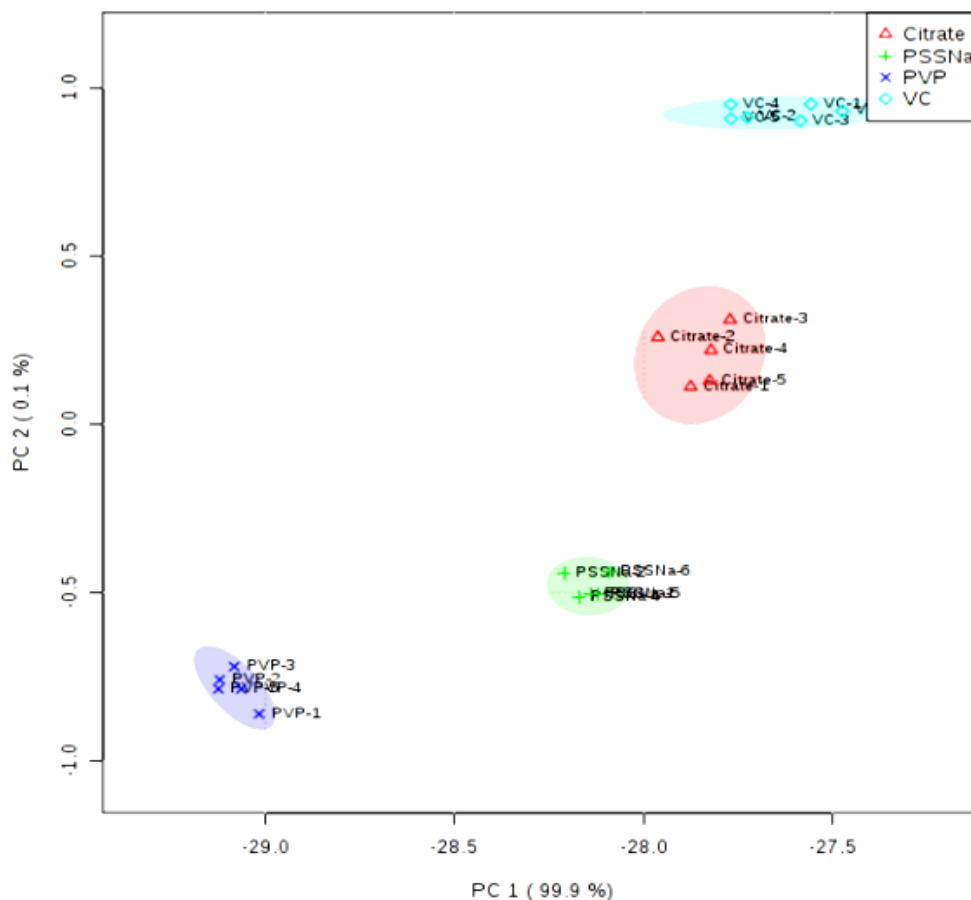


Figure 5-5: PCA scores plot of 8 compounds altered within the exometabolome of HepG2 cells (Table 5.3) as measured with NMR. Ellipses showing 90 % confidence level, and grouping of the Lig-GNP treatment groups, were included. All three Lig-GNP groups separated completely from the VC and each other, showing statistically significant differences between all the treatment groups.

These affected metabolites are associated with cellular energy production and amino acid metabolism. Proline, glutamine, arginine, lysine and glutamate were all significantly higher in the treated groups, indicating that the amino acid metabolism is affected, especially the PVP-GNPs treated cells. The cells either excreted more of these compounds or consumed less thereof, which may have been present in the cRPMI media. According to literature references, cationic molecules attached to the surface of a GNP (such as PVP) can alter the cellular membrane due to attraction forces between the positively charged GNP and negatively charged cellular membrane (Goodman et al., 2004). However, negatively charged PSSNa-GNPs also had a significant effect on the lactate and glutamine levels. The ICP-MS results from chapter 4 showed the internalisation of PVP-GNPs and PSSNa-GNPs as 31.86 %

and 22.91 %, respectively; therefore the percentage of PVP-GNPs taken up by the cells induced metabolic variation within the cells, and the exometabolome effects were likely to be due to particles in the media.

The results indicate that metabolic variation occurred within the exometabolome of HepG2 cells treated with the Lig-GNP treatment groups. The metabolites represent a footprint on the exterior environment of the cell, which could give an indication of the mechanisms triggered when interaction with Lig-GNPs occurs.

5.3.2.2 Endometabolome results (GC-MS & LC-MS/MS)

The untargeted GC-MS and targeted LC-MS/MS data matrixes were combined. Changes within the endometabolome were found in 41 metabolites, of which 8 were significant on both the GC-MS as well as LC-MS/MS. Table 5-4 shows the analytical platform, ID levels (Section 2.9.1.4), p-values and significant difference of each treatment group, compared with the VC, measured with Fisher's post-hoc.

Table 5-4: ID levels, p-values and significant difference of each treatment group, compared with the VC, measured with Fisher's LSD.

	Analytical Platform	Metabolite	ID Level	p-value	VC-Citrate	VC-PSSNa	VC-PVP
1	LC-MS/MS	Acetyl carnitine	1	0.001	↓	↓	↓
2	LC-MS/MS GC-MS	Alanine	1	0.003 0.007	↓	↓	↓
3	LC-MS/MS	Asparagine	1	0.004	↓	↓	↓
4	LC-MS/MS GC-MS	Aspartic acid	1	0.040 <0.001	↓	↓	↓
5	LC-MS/MS	Butyryl carnitine	1	0.012	↓	↓	↓
6	LC-MS/MS	Citrulline	1	0.002	↓	↓	↓
7	LC-MS/MS	Creatine	1	0.016	↓	↓	↓
8	GC-MS	Fructose	3	0.010	↔	↓	↓

9*	GC-MS	Glucose	2	<0.001	↔	↓	↓
	GC-MS	Glucose	2	0.031	↔	↓	↓
10	GC-MS	Glutamic acid	1	0.001	↓	↓	↓
11	LC-MS/MS	Glutamine	1	0.016	↓	↓	↓
12	GC-MS	Glycerol	3	0.006	↔	↓	↔
13	GC-MS	Glycine	1	0.001	↓	↓	↓
14	LC-MS/MS	Glycine	1	0.002	↓	↓	↓
15	LC-MS/MS	Histidine	1	0.022	↓	↓	↓
16	LC-MS/MS	Homocysteine	1	0.049	↑	↑	↔
17	GC-MS	Isoleucine	1	0.004	↔	↓	↓
18	GC-MS	Lactic acid	1	0.038	↔	↓	↓
19	LC-MS/MS	Leucine	1	0.034	↓	↓	↓
	GC-MS			0.003			
20	LC-MS/MS	Lysine	1	0.012	↓	↓	↓
21	GC-MS	Methionine	1	0.029	↓	↓	↓
22	GC-MS	Myo-inositol	3	<0.001	↔	↓	↓
23	LC-MS/MS	Ornithine	1	0.018	↓	↓	↓
24	GC-MS	Oxalic acid	2	0.017	↔	↔	↓
25	LC-MS/MS	Phenylalanine	1	0.010	↓	↓	↓
	GC-MS			0.038			
26	GC-MS	Phosphate	1	0.029	↔	↓	↓
27	LC-MS/MS	Proline	1	0.017	↓	↓	↓
	GC-MS			0.003			
28	LC-MS/MS	Pyroglutamic acid	1	0.006	↔	↓	↓
	GC-MS		2	0.003			
29	GC-MS	Pyruvate	1	0.033	↓	↓	↓
30*	GC-MS	Ribitol	3	0.004	↓	↓	↓
	GC-MS	Ribitol	3	0.025	↓	↓	↓

31	GC-MS	Ribose	3	0.017	↓	↓	↓
32	GC-MS	Serine	1	0.003	↓	↓	↓
33*	GC-MS	Sorbose	3	0.007	↔	↓	↓
	GC-MS	Sorbose	3	0.015	↔	↓	↓
34*	GC-MS	Tagatose	3	0.001	↔	↓	↓
	GC-MS	Tagatose	3	0.013	↔	↓	↓
35	LC-MS/MS	Threonine	1	0.006	↓	↓	↓
	GC-MS			0.003			
36	LC-MS/MS	Tryptophan	1	0.022	↓	↓	↓
37	GC-MS	Turanose	3	<0.001	↓	↓	↓
38	LC-MS/MS	Tyrosine	1	0.002	↓	↓	↓
40	LC-MS/MS	Valeryl carnitine	1	0.005	↓	↓	↓
41	LC-MS/MS	Valine	1	0.005	↓	↓	↓
	GC-MS			0.003			

*Some sugars were detected as two peaks; the second peak could be a different sugar as the GC-MS is not very accurate in identifying sugars.

Figure 5-6 shows box plots of some of the metabolites affected within the endometabolome. The rest of the box plots are shown in Addendum F.

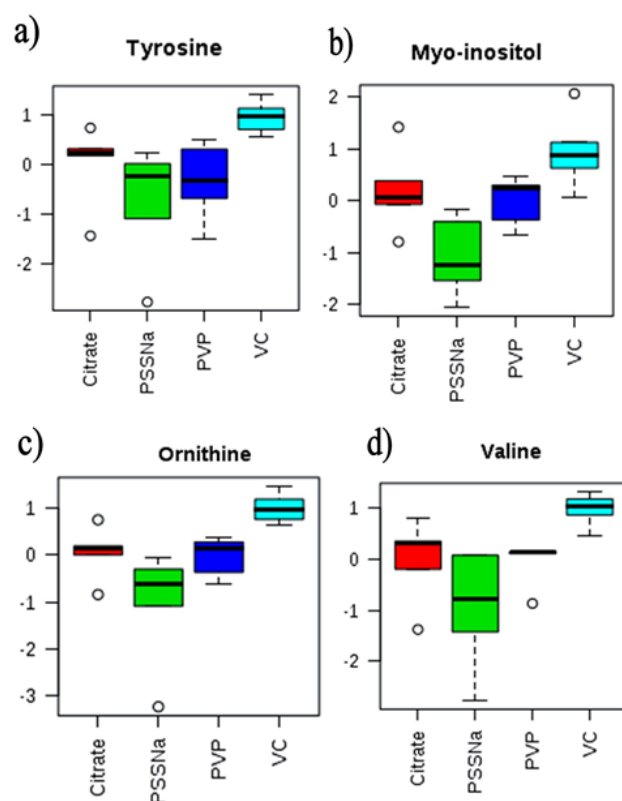


Figure 5-6: Box plots illustrating the differences in compound concentration of 4 metabolites within the endometabolome between the 4 Lig-GNP sample groups, from ANOVA statistical analysis. a) Tyrosine, b) myo-inositol, c) ornithine, and d) valine levels are all decreased when compared to the VC. The box plots were selected based on visual differences noted between the groups and the VC.

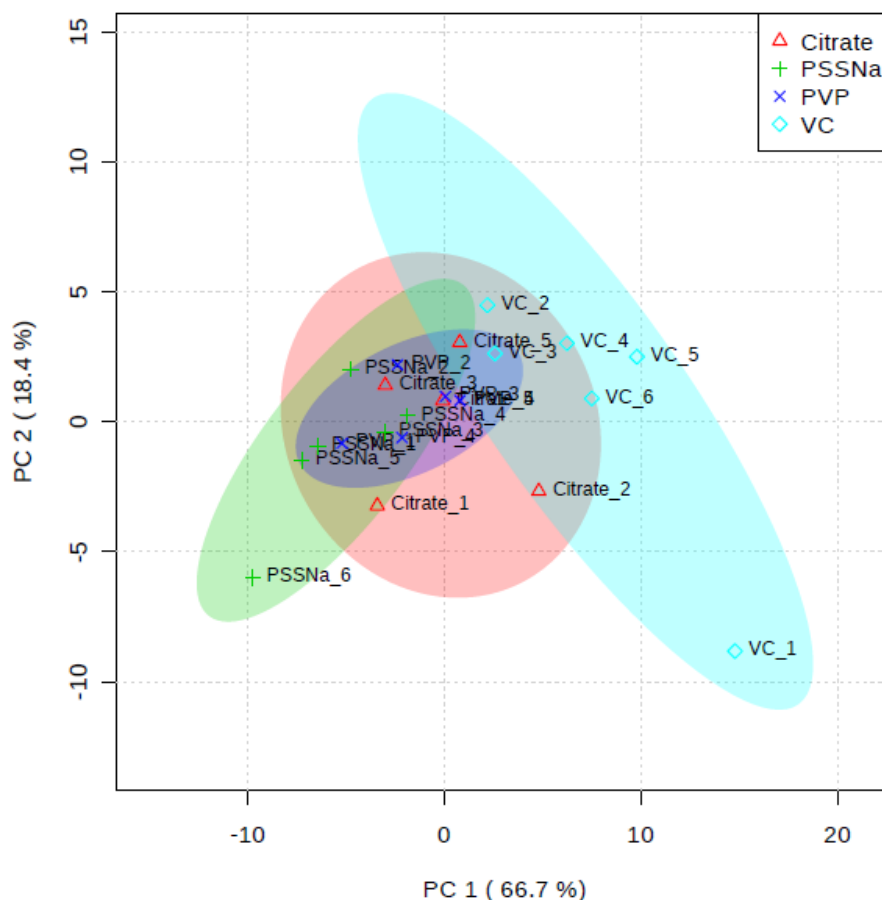


Figure 5-7: PCA scores plot of the metabolites altered within the endometabolome of Lig-GNP treated HepG2 cells as measured by GC-MS and LC-MS/MS, respectively. Grouping is done via 90 % confidence ellipses to show separation of the treatment groups. Partial separation from the VC is observed among all the Lig-GNP treatment groups.

The endometabolome results revealed metabolic variation in ~41 metabolites. Most of the metabolite concentrations were lower in the treated cells compared to the VC. These metabolites are associated with the energy metabolism and play key roles in ATP production, amino acid metabolism, urea biosynthesis and acyl carnitine metabolism. Carbohydrates that were detected include sorbitol, glucose, fructose and ribitol, which serve as biomarkers that indicate affected carbohydrate metabolism. The reason for this decrease is hypothesised later in this chapter.

From this table it is also clear that the analytical platforms not only complemented each other but also confirmed some of the findings. For example, several amino acids detected by LC-

MS/MS and GC-MS gave the exact same group trends (albeit with some slight differences in variance). Some sugars were detected as two peaks; the second peak could be a different sugar as the GC-MS is not very accurate in identifying sugars, and therefore they were identified as level 3. Other compounds that were detected could not be identified, however the main focus in this section is biological interpretation of the data, and unknown compounds would not attribute to the conclusion. The rest of the compounds were identified according to the metabolite identification levels described by (Schymanski et al., 2014) (Section 2.9.1.4) as ID levels 1 & 2.

In contrast with the exometabolome results, covariance of the endometabolites showed less significant separation between the groups, despite having numerous metabolites that differed. The reason for this lack of separation is unclear, but could it be due to the relatively large variation seen in several samples and metabolites (as depicted by the variance within each group).

All endo- and exometabolome compounds were found to differ significantly between the treatment groups, using one-way ANOVA as shown in Figure 5-8. In this figure it is clear that the exometabolites (detected with NMR) differed much more in terms of p-values. This could also explain the clear PCA separation obtained from these results: although only a few compounds differed markedly, the difference of these compounds were so profound that it resulted in better separation.

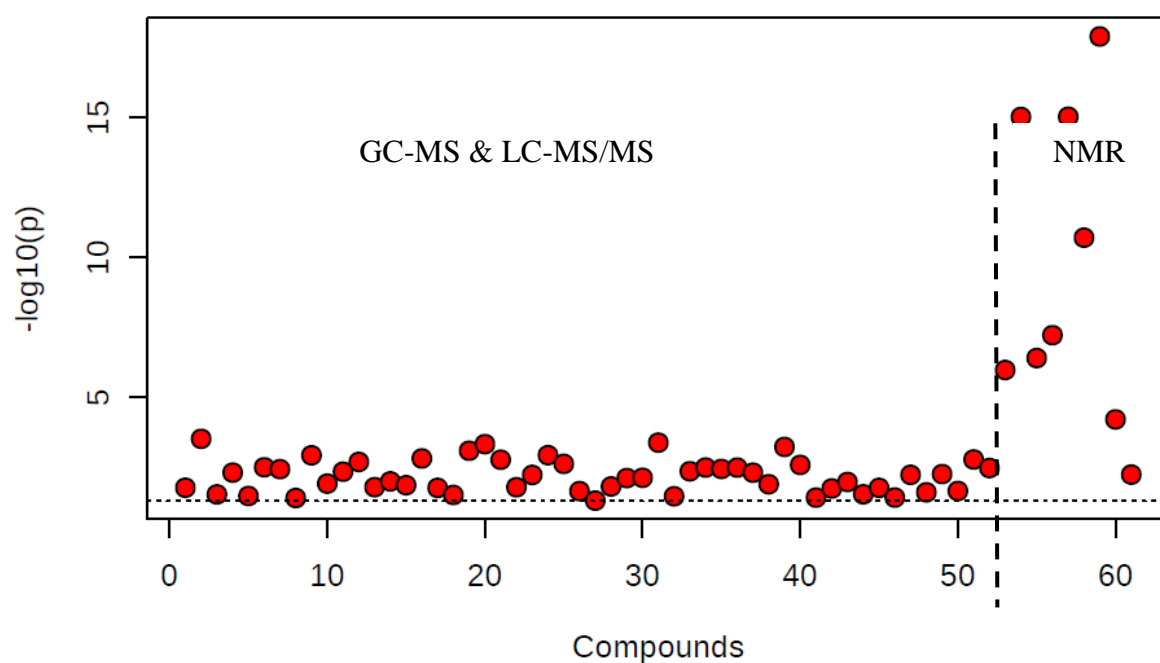


Figure 5-8: One way ANOVA statistical analysis on the treated groups; PVP-GNPs, PSSNa-GNPs, Cit-GNPs and the VC. Sixty compounds in total were significantly altered (indicated with red dots on the graph).

The covariance of all the affected endo- and exometabolites were tested with PCA analysis. The groups separated with the VC, where PVP-GNPs separated the most effectively, followed by PSSNa-GNPs and then Cit-GNPs slightly overlapping with the VC. These results give a holistic view of the degree of metabolic variation induced by the different Lig-GNPs according to their surface and physicochemical properties.

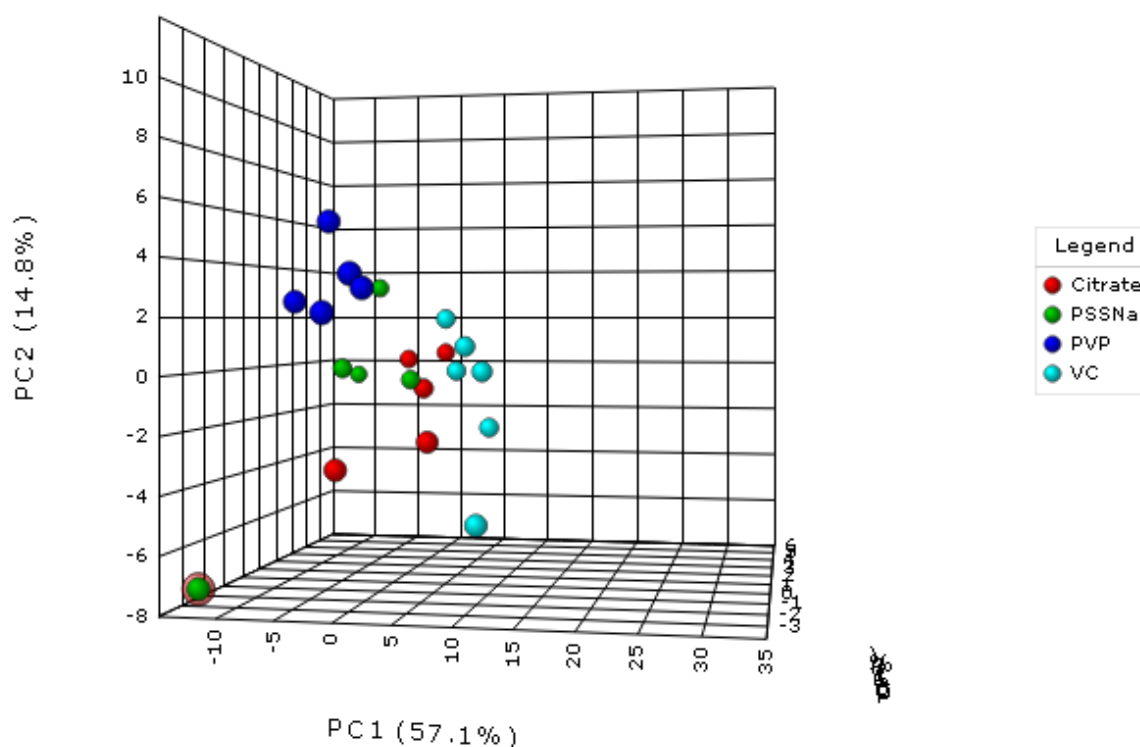


Figure 5-9: PCA score plot of the three Lig-GNP treatment groups using all significantly affected metabolites. Forty nine metabolites were significantly altered in total, of which 8 originated from the exometabolome and 41 from the endometabolome.

PCA analysis revealed the separation of the treatment groups with the VC, emphasising that the Lig-GNP treatment groups did in fact induce metabolic variation in HepG2 cells. Among these altered metabolites are compounds which are associated with energy metabolism, carbohydrate metabolism, amino acid metabolism, acylcarnitine metabolism and lipid metabolism. Table 5-5 is a summary of all the altered metabolites, their ID confidence, and the respective pathways with which it can be associated. All duplicate compounds were removed (such as the amino acids seen with the two analytical platforms) to obtain a list of metabolites for interpretation.

Table 5-5: A summary of the affected metabolism class, metabolites, ID levels and p-values of all the Lig-GNP treatment groups.

	Class	Metabolite	ID level	p-value	Cit-GNPs	PSSNa-GNPs	PVP-GNPs
	Amino acid metabolism	Alanine	1	0.008	↓	↓	↓
		Asparagine	1	0.004	↓	↓	↓
		Aspartic acid	1	0.04	↓	↓	↓
		Citrulline	1	0.002	↓	↓	↓
		Glutamic acid	1	0.002	↓	↓	↓
		Glutamine	1	0.017	↓	↓	↓
		Glycine	1	0.002	↓	↓	↓
		Histidine	1	0.023	↓	↓	↓
		Homocysteine	1	0.049	↑	↑	↔
		Isoleucine	1	0.004	↔	↓	↓
		Leucine	1	0.003	↓	↓	↓
		Lysine	1	0.013	↓	↓	↓
		Methionine	1	0.030	↓	↓	↓
		Ornithine	1	0.018	↓	↓	↓
		Phenylalanine	1	0.010	↓	↓	↓
		Proline	1	0.003	↓	↓	↓
		Pyroglutamic acid	1	0.003	↔	↓	↓
		Serine	1	0.003	↓	↓	↓
		Threonine	1	0.006	↓	↓	↓
		Tryptophan	1	0.022	↓	↓	↓
		Tyrosine	1	0.002	↓	↓	↓
		Valine	1	0.003	↓	↓	↓
Endometabolome	Carbohydrate metabolism	Turanose	3	<0.001	↓	↓	↓
		Fructose	1	0.010	↔	↓	↓
		Glucose	1	0.031	↔	↓	↓
		Myo-inositol	3	<0.001	↔	↓	↓
		Ribitol	3	0.025	↓	↓	↓
		Ribose	2	0.017	↓	↓	↓
		Sorbose	3	0.015	↔	↓	↓
		Tagatose	3	0.013	↔	↓	↓
	Energy metabolism	Creatine	1	0.016	↓	↓	↓
		Phosphate	1	0.029	↔	↓	↓
		Lactic acid	1	0.039	↔	↓	↓
		Pyruvate	1	0.034	↓	↓	↓
		Oxalic acid	2	0.017	↔	↔	↓

	Acylcarnitine metabolism	Acyl carnitine	1	0.001	↓	↓	↓
		Butyryl carnitine	2	0.012	↓	↓	↓
		Valeryl carnitine	2	0.004	↓	↓	↓
	Lipid metabolism	Glycerol	1	0.006	↔	↓	↔
Exometabolome	Amino acid metabolism	Arginine	1	<0.001	↔	↔	↑
		Glutamic acid	1	<0.001	↓	↓	↓
		Glutamine	1	<0.001	↔	↔	↑
		Arginine/Lysine	2	<0.001	↔	↔	↑
		Glutamate/Proline	2	<0.001	↔	↔	↑
		Valine	1	<0.001	↔	↔	↑
	Carbohydrate metabolism	Myo-inositol	1	<0.001	↔	↔	↑
	Energy metabolism	Lactic acid	1	0.006	↔	↑	↔
	Lipid metabolism	Choline	1	<0.001	↔	↔	↑

Figures 5-10 and 5-11 illustrate a metabolic map showing the compounds of interest as well as box plots to give an indication of how each metabolite is altered.

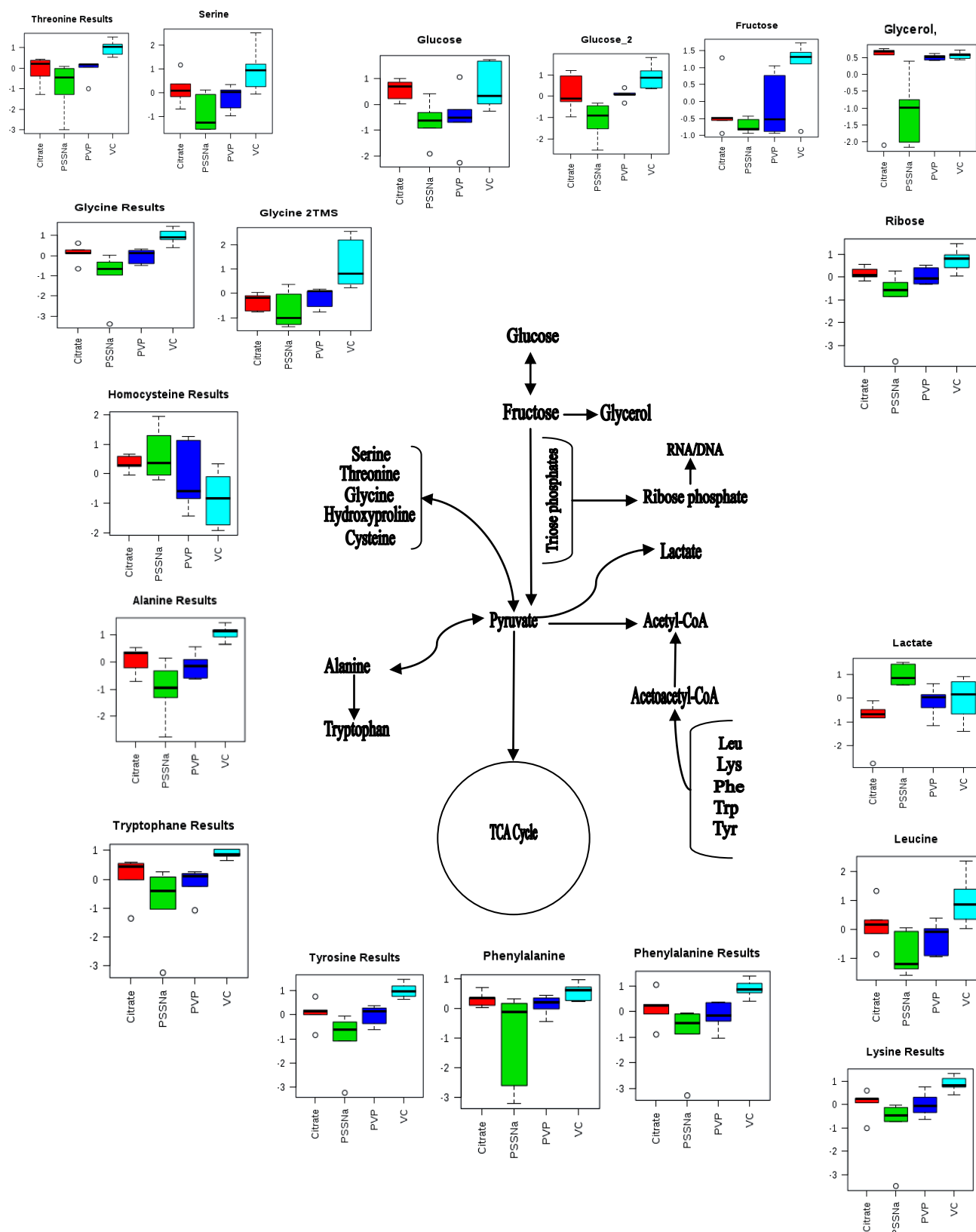


Figure 5-10: Metabolic pathway and box plots of altered compounds playing key roles in glycolysis and the metabolism of amino acids in cellular ATP production. All of these metabolites are statistically significant, showing that the treatment groups had a great impact on the cellular metabolome.

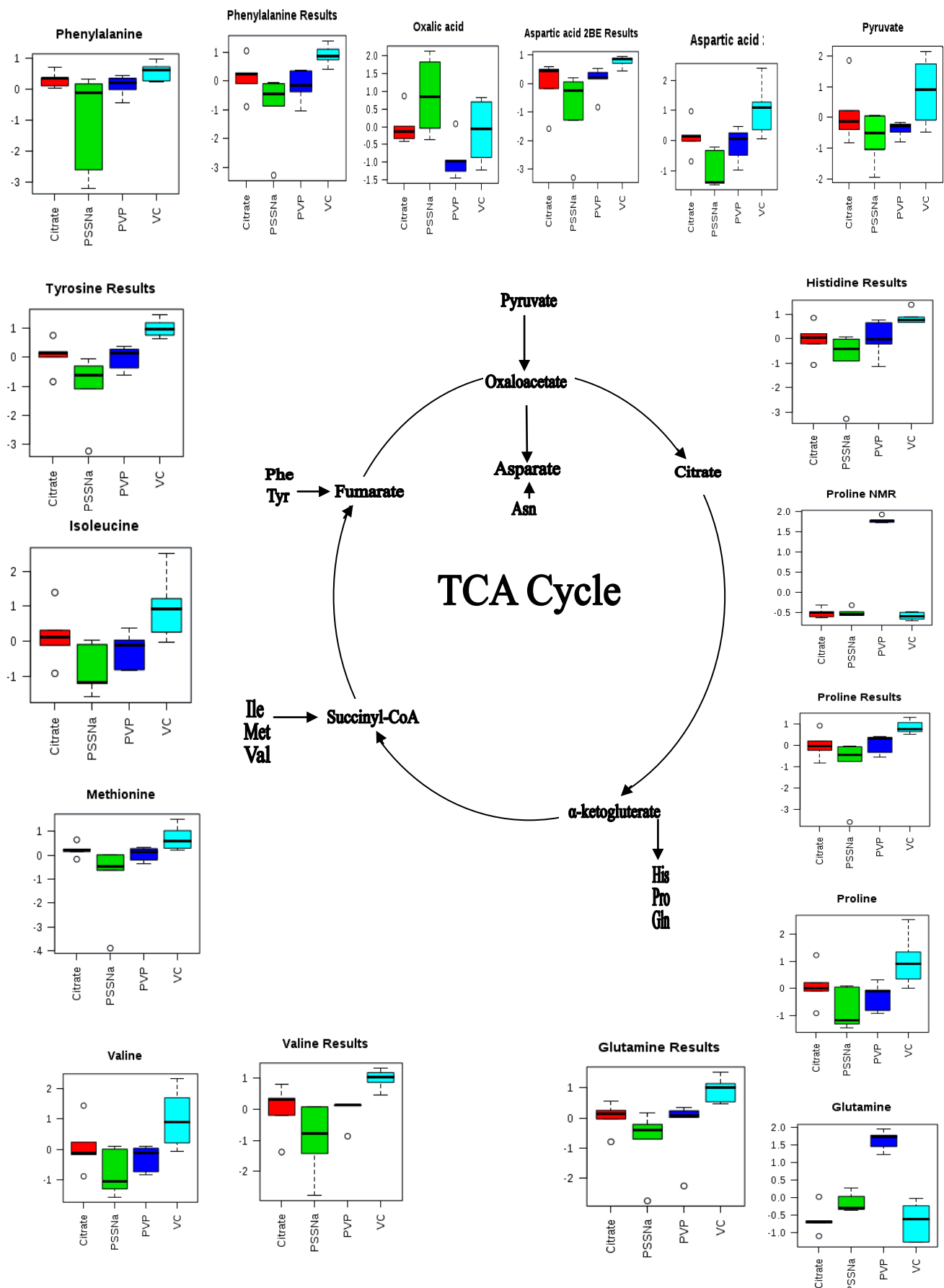


Figure 5-11: Metabolic pathway and box plots of altered compounds associated with the TCA cycle as well as amino acids present in cellular ATP production.

Compared to the VC, most of the Lig-GNP treatment groups had a decreasing effect on the metabolite levels, with the exception of oxalic acid and homocysteine which is increased with PSSNa-GNP treatment, as well as proline and glutamine which is increased with PVP-GNP treatment. Decreased cellular respiration would indicate an increase in metabolites, which is not observed in this case. Instead, the Seahorse XF analysis revealed a decrease in cellular respiration of Cit-GNP treated cells and no significant effects due to any of the other Lig-GNPs. Leakage of metabolites due to loss in membrane integrity could describe the decrease observed in metabolites. However, the NMR data showed the presence of metabolites outside the cell for PVP-GNP treatment but not for the other Lig-GNPs, therefore, the lowered metabolite levels in the endometabolome data are not necessarily ascribed to loss in membrane integrity.

When evaluating the carbohydrate metabolism, the glycolysis pathway intermediates are decreased, including sugars such as glucose and fructose. Lowered glycerol levels indicate that fatty acid metabolism is also altered, and lowered ribose phosphates links to an effect with DNA and RNA. The levels of most amino acids were decreased, indicating that amino acid metabolism is particularly affected as well as the urea cycle (indicated by the decreased citrulline and ornithine levels). Several identified amino acids play key roles as predecessors of TCA cycle intermediates as well as predecessors of acetyl-coA and pyruvate.

It can further be hypothesised that a lower influx of amino acids into the TCA cycle would trigger more carbohydrates to replenish the cycle, which could lead to the drop in several carbohydrate levels. This hypothesis is supported by the lower TCA cycle intermediates. Therefore, considering the application of Lig-GNPs as drug delivery tools, the overall safety and biocompatibility of this delivery method is questioned. However, more research is required to confirm the above statements.

A possible explanation for the decrease in metabolites could be that the initial ligand on the surface of the GNP is displaced by the metabolites, thus lowering the cellular metabolite levels. However, Gioria et al., (2015) evaluated the proteome of GNP treated cells and discovered that Cit-GNPs alter the PSAT1 protein levels which are involved in amino acid biosynthesis. They also found that AHCY was over-expressed, which catalyses the hydrolysis

of S-adenosylhomocysteine to adenosine and homocysteine, possibly explaining the increase in homocysteine levels noted in the endometabolome. Therefore, the effects observed could be that the metabolites bind to the GNP surface, or that the Lig-GNPs affect DNA and protein expression, which finally influences the metabolome. In reality, it is probably a matter of both, however the effects are not yet fully understood.

Regarding that cellular metabolism, protein- and DNA expression are complex networks which affect one another; this study, in correlation with literature references reveals that GNPs affect the metabolome as well as other cellular processes. Biocompatibility of Lig-GNPs is not necessarily charge or size specific, although these aspects do play a role in their behaviour. Positively charged Lig-GNPs (specifically PVP-GNPs) seem to affect the exometabolome, whereas all the treatment groups affect the endometabolome.

5.4 Conclusive summary

The Seahorse XF⁹⁶ analysis revealed a significant decrease in spare respiratory capacity of Cit-GNP treated HepG2 cells. The Lig-GNPs (PVP-GNPs and PSSNa-GNPs) had no significant effect on the cellular respiration when compared to the VC, which possibly indicates improved biocompatibility

However, metabolomics analysis showed alterations for the selected Lig-GNP treatment groups in the exometabolome (NMR analysis) as well as within the endometabolome (GC-MS & LC-MS/MS analysis). The variation observed could potentially be attributed to the binding of specific compounds to the GNPs, or it could be that the Lig-GNPs cause alterations on DNA and protein level (Gioria et al., 2015; Mulder et al., 2016). It is hypothesised that the effects are related to oxidative stress because of the ability of GNPs to change the redox status of cells (Gao et al., 2011) and induce changes in the genome of oxidative stress related pathways as described by (Li et al., 2010).

Whether this effect is non-safe or toxic remains unclear, especially in light of the fact that an accumulation of metabolites (such as during enzyme inhibition) are associated with toxicity and not a decrease of metabolites. One possible outcome pointing to a negative effect of the GNPs on cellular metabolism is the increased levels of specific metabolites in the exometabolome (of PVP-GNP treated cells) which could indicate that the cell's membrane integrity is altered (Pan et al., 2007). The charge-dependent effects observed in this study correlate with the findings of Goodman et al., (2004), and the effect of size also plays a role in how the metabolome and overall biocompatibility is affected; however, these observations could be ligand specific.

Chapter 6: Conclusion

This study was conducted to evaluate the effects that differentially functionalised gold nanoparticles (Lig-GNPs) have on the metabolome of cells. By performing ligand exchange, Lig-GNPs is believed to improve the stability and biocompatibility of GNPs (Fraga et al., 2013). However, research in the field of GNPs in combination with metabolomics is very scant (Gioria et al., 2015). Moreover, the use of unstandardised protocols and unreliable viability assays lead to inaccurate conclusions made in the literature (Alkilany & Murphy, 2010, Kong et al., 2011). The aim of this study was to synthesise GNPs, perform ligand exchange, and evaluate how treatment of Lig-GNPs influences the metabolome of HepG2 cells. The objectives included standardisation, a pilot study to evaluate the dosage used, and finally, the main study, where the effect of GNPs on the metabolome was evaluated. Standardisation included the synthesis of Lig-GNPs and characterisation of the particles. Citrate-capped gold nanoparticles (Cit-GNPs) were synthesised using the Turkevich method and differentially functionalised by performing ligand exchange. Thereafter, characterisation was performed to determine the size, morphology and surface charge of the Lig-GNPs by using methods published in the literature. Also, the stability of the particles was determined in a resembling physiological environment to get an indication of whether differential functionalisation improves the biocompatibility of Lig-GNPs. For the pilot study, cell biology methods were standardised using two independent viability assays (WST-1 and APOPercentage assays) and by determining the cellular uptake of Lig-GNPs into the cells via ICP-MS. The WST-1 assay was performed to get an indication of the dosage to be used for the main study, and the APOPercentage apoptosis assay was performed to establish whether the treatment groups induce necrosis or apoptosis, and to evaluate the link between the metabolome and apoptosis in cells (Gioria et al., 2015). Finally, the main study included mitochondrial respiration analysis (Seahorse XF⁹⁶ analyser) and evaluation of two selected Lig-GNP treatment groups to determine the effect on the exo- and endometabolome of HepG2 cells. NMR was used for the exometabolome, and GC-MS and LC-MS/MS was used for the endometabolome.

The results have shown that differentially functionalising GNPs does improve their overall stability and biocompatibility to some extent. The stability evaluation showed an overall increase in the stability of Lig-GNPs in similar physiological conditions, in contrast to Cit-GNPs, which were used as reference particles. Different patterns in viability and cellular uptake were noted with each Lig-GNP, which correlates with the physico-chemical properties of the particles (size, morphology and surface net charge). Goodman et al. (2004) observed that cationic particles seem to be moderately toxic, whereas anionic particles are nontoxic; however, our data suggest that although surface charge plays a role, the size and structure should also be brought into consideration when evaluating the effects of GNPs on cells.

The APOPercentage apoptosis assay confirmed that the treatment groups do initiate apoptosis instead of necrosis; however, some Lig-GNPs induce a higher level of apoptosis than others (PVP-GNPs vs PSSNa-GNPs), even when the IC₃₀ values of the compared Lig-GNPs are similar, according to the WST-1 assay. No specific link was observed between apoptosis and the metabolomics results; however, there was a link in apoptotic induction time and DNA damage, which, in turn, correlated with the cellular respiration results of this study. Mulder et al. (2016) found a link between the apoptotic induction time points and DNA damage; therefore this time point (3 hours after treatment) was selected to correlate the DNA damage and repair with the metabolome. They found that the Lig-GNPs of interest caused DNA damage, but only some (PVP-GNPs and PSSNa-GNPs included) showed DNA repair after 24 hours. Cit-GNPs showed no repair, which is hypothesised to be due to the instability of the particles in physiological environments. This observation also relates to the mitochondrial respiration data, where the effects of PVP-GNPs and PSSNa-GNPs were not significant, but a decrease was noted in the spare capacity of Cit-GNP treated cells. It is hypothesised that the mitochondria is affected due to mitochondrial-nuclear interactions as described by Shaughnessy et al. (2014), or by the particles themselves; however, the exact mechanisms are not yet understood.

Metabolomics analysis showed distinctive alterations after treatment with all the treatment groups. Both Lig-GNPs as well as the Cit-GNP reference caused variations when compared to the untreated control (VC). The levels of 49 metabolites in total (41 endometabolome and 8 exometabolome) were altered, showing that a number of metabolic pathways were affected.

The main pathways that were affected due to Lig-GNP treatment included energy metabolism, amino acid metabolism, lipid metabolism, acylcarnitine metabolism and carbohydrate metabolism. Analysis of the exometabolome using NMR showed increased metabolite concentrations when treated with PVP-GNPs. It seems as if the HepG2 cells are either excreting or consuming less of these compounds in the media. Studies in the literature associate cationic structures such as PVP-GNPs with cytotoxicity, because these species are likely to interact with the negatively charged cellular membrane; thus possibly reducing the cellular membrane integrity, and finally leading to leakage of internal cellular metabolite content. One hypothetical reason for the increased exo-metabolites is that the PVP ligand on the GNP surface is displaced by molecules with a stronger affinity towards GNPs, resulting in free PVP molecules within the cells. PVP could be degraded or digested by enzymes to form smaller structures of proline, which could have a feedback or feedforward effect on the cellular metabolism.

The endometabolome results showed a decrease in the majority of metabolites, with the exception of homocysteine in Cit-GNPs and PSSNa-GNPs, which was found to be increased. It is hypothesised that DNA damage (as observed by Mulder et. al, 2016) or changes in protein expression could influence the final downstream end products, which is the metabolome. Gioria et al. (2015) found the protein responsible for the hydrolysis of S-adenosylhomocysteine to adenosine and homocysteine to be upregulated in Cit-GNP treated cells, explaining the increase in homocysteine observed in the metabolome during this study. The other metabolites were either unchanged or downregulated. The lower levels of carbohydrates observed could be due to lowered amino acid influx in the TCA cycle, forcing increased usage of carbohydrates to replenish the cycle. These effects could be related to cellular stress response. Moreover, as mentioned previously, the hypothesis of ligand displacement can result in PVP ligand molecules, which possibly bio-mimics the amino acid proline due to similarity in structure. Therefore, the cell could be under the impression that abundant levels of proline are present and thus lower the influx of certain amino acids, especially proline and proline derivatives.

The question remains whether differentially functionalising GNPs improve their biocompatibility as a whole. Several components play a role in biocompatibility and the

genome, cellular respiration, and the metabolome is taken into consideration. Some aspects of the study showed promising results; however, a single field of study cannot give a holistic indication of the effects of Lig-GNPs on cells. Cellular stress mechanisms are complex and further study is required.

In summary, it is hypothesised that the lowered metabolite levels could be due to two possible reasons. Firstly, the treatment groups could induce cellular stress on the DNA and protein levels, disrupting the intracellular homeostatic control system causing deregulation of biological processes (Shi et al., 2009). The second possibility is that the ligands on the Lig-GNP surface is displaced by metabolites in the cell or even adhering to the Lig-GNP to form a complex; thus depleting the normal metabolite levels. Moreover, the free ligands can serve as bio-mimics (or be enzymatically digested into smaller structures, similar to the molecules already present in the cells) which possibly leads to cells falsely regulating their internal milieu. Although this type of variation within the metabolome does not necessarily have a link with cytotoxicity, the normal cellular functions are compromised. However, the exact mechanisms are not yet known, and the abovementioned hypotheses are still to be investigated. These findings are worth elucidating in order to establish how Lig-GNP interaction affects the cellular metabolism and, more importantly, how these findings correlate with the biocompatibility of Lig-GNPs within biological systems. The research in this field remains very limited, and a great deal of research is required to confirm these hypotheses.

Addendum A: Bibliography

AGILENT TECHNOLOGIES INC. 2008. *Metabolomics: Approaches using mass spectrometry*.

Viewed 3 November 2016 <http://www.agilent.com/cs/library/primers/Public/5990-4314EN.pdf>

ALKILANY, A. & MURPHY, C. 2010. Toxicity and cellular uptake of gold nanoparticles: What we have learned so far? *Journal of nanoparticle research*, 12, 2313-2333.

ALLOYEAU, D., MOTTET, C. & RICOLLEAU, C. 2012. *Nanoalloys: Synthesis, structure and properties*, London, New York: Springer.

BAJAK, E., FABBRI, M., PONTI, J., GIORIA, S., OJEA-JIMÉNEZ, I., COLLOTTA, A., MARIANI, V., GILLILAND, D., ROSSI, F. & GRIBALDO, L. 2015. Changes in Caco-2 cells transcriptome profiles upon exposure to gold nanoparticles. *Toxicology letters*, 233, 187-199.

BASIRUDDIN, S., SAHA, A., PRADHAN, N. & JANA, N. R. 2010. Advances in coating chemistry in deriving soluble functional nanoparticle. *The journal of physical chemistry C*, 114, 11009-11017.

BHATTACHARYA, R., PATRA, C. R., EARL, A., WANG, S., KATARYA, A., LU, L., KIZHAKKEDATHU, J. N., YASZEMSKI, M. J., GREIPP, P. R. & MUKHOPADHYAY, D. 2007. Attaching folic acid on gold nanoparticles using noncovalent interaction via different polyethylene glycol backbones and targeting of cancer cells. *Nanomedicine: Nanotechnology, biology and medicine*, 3, 224-238.

BRUST, M. & KIELY, C. J. 2002. Some recent advances in nanostructure preparation from gold and silver particles: A short topical review. *Colloids and surfaces A: Physicochemical and engineering aspects*, 202, 175-186.

BUESEN, R., LANDSIEDEL, R., SAUER, U. G., WOHLLEBEN, W., GROETERS, S., STRAUSS, V., KAMP, H. & VAN RAVENZWAAY, B. 2014. Effects of SiO₂, ZrO₂, and BaSO₄ nanomaterials with or without surface functionalisation upon 28-day oral exposure to rats. *Archives of toxicology*, 88, 1881-1906.

- CAMMACK, R., ATWOOD, T., CAMPBELL, P., PARISH, H., SMITH, A., VELLA, F. & STIRLING, J. 2006. Oxford Dictionary of Biochemistry and Molecular Biology (2nd ed.). Oxford: Oxford University Press.
- CHANANA, M. & LIZ-MARZÁN, L. M. 2012. Coating matters: The influence of coating materials on the optical properties of gold nanoparticles. *Nanophotonics*, 1, 199-220.
- CHEN, G., WANG, Y., TAN, L. H., YANG, M., TAN, L. S., CHEN, Y. & CHEN, H. 2009. High-purity separation of gold nanoparticle dimers and trimers. *Journal of the American Chemical Society*, 131, 4218-4219.
- CHENG, Y., C. SAMIA, A., MEYERS, J. D., PANAGOPOULOS, I., FEI, B. & BURDA, C. 2008. Highly efficient drug delivery with gold nanoparticle vectors for in vivo photodynamic therapy of cancer. *Journal of the American Chemical Society*, 130, 10643-10647.
- CHO, W.-S., CHO, M., JEONG, J., CHOI, M., HAN, B. S., SHIN, H.-S., HONG, J., CHUNG, B. H., JEONG, J. & CHO, M.-H. 2010. Size-dependent tissue kinetics of PEG-coated gold nanoparticles. *Toxicology and applied pharmacology*, 245, 116-123.
- COBLEY, C. M., CHEN, J., CHO, E. C., WANG, L. V. & XIA, Y. 2011. Gold nanostructures: A class of multifunctional materials for biomedical applications. *Chemical society reviews*, 40, 44-56.
- CONNOR, E. E., MWAMUKA, J., GOLE, A., MURPHY, C. J. & WYATT, M. D. 2005. Gold nanoparticles are taken up by human cells but do not cause acute cytotoxicity. *Small*, 1, 325-327.
- CORNING. 2007. *Surface areas and recommended medium volumes for Corning cell culture vessels*. Viewed 3 November 2016
http://csmedia2.corning.com/LifeSciences/Media/pdf/cc_surface_areas.pdf

- DANIEL, M.-C. & ASTRUC, D. 2004. Gold nanoparticles: Assembly, supramolecular chemistry, quantum-size-related properties, and applications toward biology, catalysis, and nanotechnology. *Chemical reviews*, 104, 293-346.
- DI PASQUA, A. J., MISHLER II, R. E., SHIP, Y.-L., DABROWIAK, J. C. & ASEFA, T. 2009. Preparation of antibody-conjugated gold nanoparticles. *Materials letters*, 63, 1876-1879.
- DONG, W., DONG, C., SHUANG, S. & CHOI, M. M. 2010. Near-infrared luminescence quenching method for the detection of phenolic compounds using N-acetyl-L-cysteine-protected gold nanoparticles-tyrosinase hybrid material. *Biosensors and bioelectronics*, 25, 1043-1048.
- FRAGA, S., FARIA, H., SOARES, M. E., DUARTE, J. A., SOARES, L., PEREIRA, E., COSTA-PEREIRA, C., TEIXEIRA, J. P., DE LOURDES BASTOS, M. & CARMO, H. 2013. Influence of the surface coating on the cytotoxicity, genotoxicity and uptake of gold nanoparticles in human HepG2 cells. *Journal of applied toxicology*, 33, 1111-1119.
- GAO, W., XU, K., JI, L. & TANG, B. 2011. Effect of gold nanoparticles on glutathione depletion-induced hydrogen peroxide generation and apoptosis in HL7702 cells. *Toxicology letters*, 205, 86-95.
- GHOSH, D., SARKAR, D., GIRIGOSWAMI, A. & CHATTOPADHYAY, N. 2011. A Fully Standardised Method of Synthesis of Gold Nanoparticles of Desired Dimension in the Range 15 nm–60 nm. *Journal of nanoscience and nanotechnology*, 11, 1141-1146.
- GHOSH, H. & BÜRGI, T. 2013. Adsorption of gold and silver nanoparticles on polyelectrolyte layers and growth of polyelectrolyte multilayers: an in situ ATR-IR study. *The journal of physical chemistry C*, 117, 26652-26658.
- GHOSH, P., HAN, G., DE, M., KIM, C. K. & ROTELLO, V. M. 2008. Gold nanoparticles in delivery applications. *Advanced drug delivery reviews*, 60, 1307-1315.
- GIORIA, S., LOBO VICENTE, J., BARBORO, P., LA SPINA, R., TOMASI, G., URBÁN, P., KINSNER-OVASKAINEN, A., ROSSI, F. & CHASSAIGNE, H. 2015. A combined proteomics and metabolomics approach to assess the effects of gold nanoparticles *in vitro*. *Nanotoxicology*, 1-59.
- GOLDBURG, W. 1999. Dynamic light scattering. *American journal of physics*, 67, 1152-1160.

- GOODACRE, R., VAIDYANATHAN, S., DUNN, W. B., HARRIGAN, G. G. & KELL, D. B. 2004. Metabolomics by numbers: Acquiring and understanding global metabolite data. *Trends in biotechnology*, 22, 245-252.
- GOODMAN, C. M., MCCUSKER, C. D., YILMAZ, T. & ROTELLO, V. M. 2004. Toxicity of gold nanoparticles functionalised with cationic and anionic side chains. *Bioconjugate chemistry*, 15, 897-900.
- GU, Y.-J., CHENG, J., LIN, C.-C., LAM, Y. W., CHENG, S. H. & WONG, W.-T. 2009. Nuclear penetration of surface functionalised gold nanoparticles. *Toxicology and applied pharmacology*, 237, 196-204.
- HALL, R. D. 2006. Plant metabolomics: From holistic hope, to hype, to hot topic. *New phytologist*, 169, 453-468.
- HANAUER, M., PIERRAT, S., ZINS, I., LOTZ, A. & SÖNNICHSEN, C. 2007. Separation of nanoparticles by gel electrophoresis according to size and shape. *Nano letters*, 7, 2881-2885.
- HO, C. S., LAM, C. W. K., CHAN, M. H. M., CHEUNG, R. C. K., LAW, L. K., LIT, L. C. W., NG, K. F., SUEN, M. W. M. & TAI, H. L. 2003. Electrospray ionisation mass spectrometry: Principles and clinical applications. *The clinical biochemist reviews*, 24, 3-12.
- HONG, R., HAN, G., FERNÁNDEZ, J. M., KIM, B.-J., FORBES, N. S. & ROTELLO, V. M. 2006. Glutathione-mediated delivery and release using monolayer protected nanoparticle carriers. *Journal of the American Chemical Society*, 128, 1078-1079.
- HOROVITZ, O., TOMOAIA, G., MOCANU, A., YUPSANIS, T. & TOMOAIA-COTISEL, M. 2007. Protein binding to gold colloids. *Gold bulletin*, 40, 213-218.
- HUANG, Y., LÜ, X., QU, Y., YANG, Y. & WU, S. 2015. MicroRNA sequencing and molecular mechanisms analysis of the effects of gold nanoparticles on human dermal fibroblasts. *Biomaterials*, 37, 13-24.
- JONES, C. F. & GRAINGER, D. W. 2009. *In vitro* assessments of nanomaterial toxicity. *Advanced Drug Delivery reviews*, 61, 438-456.

- KHULLAR, P., SINGH, V., MAHAL, A., DAVE, P. N., THAKUR, S., KAUR, G., SINGH, J., SINGH KAMBOJ, S. & SINGH BAKSHI, M. 2012. Bovine serum albumin bioconjugated gold nanoparticles: Synthesis, hemolysis, and cytotoxicity toward cancer cell lines. *The Journal of physical chemistry C*, 116, 8834-8843.
- KONG, B., SEOG, J. H., GRAHAM, L. M. & LEE, S. B. 2011. Experimental considerations on the cytotoxicity of nanoparticles. *Nanomedicine*, 6, 929-941.
- LABALA, S., MANDAPALLI, P. K., KURUMADDALI, A. & VENUGANTI, V. V. K. 2015. Layer-by-layer polymer coated gold nanoparticles for topical delivery of imatinib mesylate to treat melanoma. *Molecular pharmaceutics*, 12, 878-888.
- LASAGNA-REEVES, C., GONZALEZ-ROMERO, D., BARRIA, M. A., OLMEDO, I., CLOS, A., SADAGOPA RAMANUJAM, V. M., URAYAMA, A., VERGARA, L., KOGAN, M. J. & SOTO, C. 2010. Bioaccumulation and toxicity of gold nanoparticles after repeated administration in mice. *Biochemical and biophysical research communications*, 393, 649-655.
- LEE, H., LEE, M.-Y., BHANG, S. H., KIM, B.-S., KIM, Y. S., JU, J. H., KIM, K. S. & HAHN, S. K. 2014. Hyaluronate–gold nanoparticle/cocilizumab complex for the treatment of rheumatoid arthritis. *ACS nano*, 8, 4790-4798.
- LEITE, P. E. C., PEREIRA, M. R., DO NASCIMENTO SANTOS, C. A., CAMPOS, A. P. C., ESTEVES, T. M. & GRANJEIRO, J. M. 2015. Gold nanoparticles do not induce myotube cytotoxicity but increase the susceptibility to cell death. *Toxicology in vitro*, 29, 819-827.
- LI, H., HUANG, J., LV, J., AN, H., ZHANG, X., ZHANG, Z., FAN, C. & HU, J. 2005. Nanoparticle PCR: Nanogold-assisted PCR with enhanced specificity. *Angewandte chemie international edition*, 44, 5100-5103.
- LI, J. J., HARTONO, D., ONG, C.-N., BAY, B.-H. & YUNG, L.-Y. L. 2010. Autophagy and oxidative stress associated with gold nanoparticles. *Biomaterials*, 31, 5996-6003.
- LIU, D. C., RAPHAEL, A. P., SUNDH, D., GRICE, J. E., SOYER, H. P., ROBERTS, M. S. & PROW, T. W. 2012. The human stratum corneum prevents small gold nanoparticle penetration and their potential toxic metabolic consequences. *J. nanomaterials*, 2012, 7-7.

- LU, X., TIAN, Y., ZHAO, Q., JIN, T., XIAO, S. & FAN, X. 2011. Integrated metabonomics analysis of the size-response relationship of silica nanoparticles-induced toxicity in mice. *Nanotechnology*, 22, 055101.
- MALVERN. 2015. Dynamic light scattering training achieving reliable nano particle sizing. Viewed 3 November 2016. <http://149.171.168.221/partcat/wp-content/uploads/Malvern-Zetasizer LS.pdf>.
- METABOANALYST. 2016. Metaboanalyst. [ONLINE] Available at: <http://www.metaboanalyst.ca/>. [Accessed 3 November 2016].
- MCINTOSH, C. M., ESPOSITO, E. A., BOAL, A. K., SIMARD, J. M., MARTIN, C. T. & ROTELLO, V. M. 2001. Inhibition of DNA transcription using cationic mixed monolayer protected gold clusters. *Journal of the American Chemical Society*, 123, 7626-7629.
- MUKHERJEE, P., BHATTACHARYA, R., WANG, P., WANG, L., BASU, S., NAGY, J. A., ATALA, A., MUKHOPADHYAY, D. & SOKER, S. 2005. Antiangiogenic properties of gold nanoparticles. *Clinical cancer research*, 11, 3530-3534.
- MULDER, D. P., P.J. TAUTE, C.J.F. 2016. Genotoxicity of goldnanoparticles.
- PAINO, I. M. M., MARANGONI, V. S., DE OLIVEIRA, R. D. C. S., ANTUNES, L. M. G. & ZUCOLOTTI, V. 2012. Cyto and genotoxicity of gold nanoparticles in human hepatocellular carcinoma and peripheral blood mononuclear cells. *Toxicology letters*, 215, 119-125.
- PAN, Y., NEUSS, S., LEIFERT, A., FISCHLER, M., WEN, F., SIMON, U., SCHMID, G., BRANDAU, W. & JAHNEN-DECHENT, W. 2007. Size-dependent cytotoxicity of gold nanoparticles. *Small*, 3, 1941-1949.
- PARTS PER MILLION CONVERSION CHART (Fractions and Percent Converter, Percentages And Parts). 2016. Parts Per Million Conversion Chart (Fractions and Percent Converter, Percentages And Parts). [ONLINE] Available at: <http://www.convert-me.com/en/convert/percent/uppm.html>. [Accessed 29 July 2016].

- PATRA, H. K., BANERJEE, S., CHAUDHURI, U., LAHIRI, P. & DASGUPTA, A. K. 2007. Cell selective response to gold nanoparticles. *Nanomedicine: Nanotechnology, biology and medicine*, 3, 111-119.
- PILLAI, G. 2014. Nanomedicines for cancer therapy: An update of FDA approved and those under various stages development. *SOJ pharm. pharm. sci*, 1, 1-13.
- PRIMO, A., CORMA, A. & GARCÍA, H. 2011. Titania supported gold nanoparticles as photocatalyst. *Physical chemistry chemical physics*, 13, 886-910.
- ROBERTSON, D. G. 2005. Metabonomics in toxicology: A review. *Toxicological sciences*, 85, 809-822.
- SABER, R., SHAKOORI, Z., SARKAR, S., TAVOOSIDANA, G., KHARRAZI, S. & GILL, P. 2013. Spectroscopic and microscopic analyses of rod-shaped gold nanoparticles interacting with single-stranded DNA oligonucleotides. *IET nanobiotechnology*, 7, 42-49.
- SADIK, O. A., DU, N., KARIUKI, V., OKELLO, V. & BUSHLYAR, V. 2014. Current and emerging technologies for the characterisation of nanomaterials. *ACS sustainable chemistry & engineering*, 2, 1707-1716.
- SCHNACKENBERG, L. K., SUN, J. & BEGER, R. D. 2012. Metabolomics techniques in nanotoxicology studies. *Nanotoxicity*. Springer.
- SEITZ, O., CHEHIMI, M. M., CABET-DELIRY, E., TRUONG, S., FELIDJ, N., PERRUCHOT, C., GREAVES, S. J. & WATTS, J. F. 2003. Preparation and characterisation of gold nanoparticle assemblies on silanised glass plates. *Colloids and surfaces A: Physicochemical and engineering aspects*, 218, 225-239.
- SU, H., ZHENG, Q. & LI, H. 2012. Colorimetric detection and separation of chiral tyrosine based on N-acetyl-L-cysteine modified gold nanoparticles. *Journal of materials chemistry*, 22, 6546-6548.
- TSAI, C.-S., YU, T.-B. & CHEN, C.-T. 2005. Gold nanoparticle-based competitive colorimetric assay for detection of protein-protein interactions. *Chemical communications*, 4273-4275.

- UBOLDI, C., BONACCHI, D., LORENZI, G., HERMANN, M. I., POHL, C., BALDI, G., UNGER, R. E. & KIRKPATRICK, C. J. 2009. Gold nanoparticles induce cytotoxicity in the alveolar type-II cell lines A549 and NCIH441. *Part fibre toxicol*, 6, 18.
- VAN DYK, H. C. 2016. Evaluating the involvement of mtDNA variants in patients diagnosed with myalgic encephalomyelitis. North-West University.
- WANG, B., CHEN, N., WEI, Y., LI, J., SUN, L., WU, J., HUANG, Q., LIU, C., FAN, C. & SONG, H. 2012. Akt signaling-associated metabolic effects of dietary gold nanoparticles in *Drosophila*. *Sci. rep.*, 2.
- WANG, C.-H., LIU, C.-J., CHIEN, C.-C., CHEN, H.-T., HUA, T.-E., LENG, W.-H., CHEN, H.-H., KEMPSON, I. M., HWU, Y. & HSIAO, M. 2011. X-ray synthesised PEGylated (polyethylene glycol coated) gold nanoparticles in mice strongly accumulate in tumors. *Materials chemistry and physics*, 126, 352-356.
- WANG, D., ROGACH, A. L. & CARUSO, F. 2002. Semiconductor quantum dot-labeled microsphere bioconjugates prepared by Stepwise Self-Assembly. *Nano letters*, 2, 857-861.
- WANG, Z. & MA, L. 2009. Gold nanoparticle probes. *Coordination chemistry reviews*, 253, 1607-1618.
- WILLIAMS, A., KOEKEMOER, G., LINDEQUE, Z., REINECKE, C. & MEYER, D. 2012. Qualitative serum organic acid profiles of HIV-infected individuals not on antiretroviral treatment. *Metabolomics*, 8, 804-818.
- XU, C., YANG, D., MEI, L., LU, B., CHEN, L., LI, Q., ZHU, H. & WANG, T. 2013. Encapsulating gold nanoparticles or nanorods in graphene Oxide shells as a novel gene vector. *ACS applied materials & interfaces*, 5, 2715-2724.
- YANG, C., SUI, H., LI, X., HAN, J., LUO, X., ZHANG, H., SUN, H., SUN, H., ZHOU, Y. & YANG, B. 2013. Gold nanoparticle superstructures with enhanced photothermal effect. *CrystEngComm*, 15, 3490-3497.
- YE, K., QIN, J., PENG, Z., YANG, X., HUANG, L., YUAN, F., PENG, C., JIANG, M. & LU, X. 2014. Polyethylene glycol-modified dendrimer-entrapped gold nanoparticles enhance CT imaging of blood pool in atherosclerotic mice. *Nanoscale research letters*, 9, 1-12.

- ZHENG, M., LI, Z. & HUANG, X. 2004. Ethylene glycol monolayer protected nanoparticles: Synthesis, characterisation, and interactions with biological molecules. *Langmuir*, 20, 4226-4235.
- ZHOU, X., XU, W., LIU, G., PANDA, D. & CHEN, P. 2009. Size-dependent catalytic activity and dynamics of gold nanoparticles at the single-molecule level. *Journal of the American Chemical Society*, 132, 138-146.
- ČUPERLOVIĆ-CULF, M., BARNETT, D. A., CULF, A. S. & CHUTE, I. 2010. Cell culture metabolomics: applications and future directions. *Drug discovery today*, 15, 610-621.

Addendum B: Concentration evaluation of GNPs

This aspect of the study was performed with Cit-GNPs as reference to achieve an indication of the concentrations of the other Lig-GNPs, because ligand exchange induces a shift in the absorbance plasmon peak of GNPs. A serial dilution was prepared and analysed with UV-Vis spectrometry, the concentrations were mathematically calculated and correlated with the sample values and a graph was plotted which was used as a reference for the other Lig-GNP concentrations.

Table B-1: The size and concentration of Cit-GNPs based on the OD of the particles and calculations from Haiss et al.

GNPs (μl)	H ₂ O (μl)	Sample concentration (nM)	Concentration (nM)	OD 450 ($\times 10^{-2}$)
100	0	2.18	2.2	5.45
50	50	1.09	1.1	2.73
25	75	0.54	0.55	1.36
12.5	87.5	0.27	0.27	0.68
6	94	0.14	0.14	0.34

Figure B-1 shows the GNP concentration gradient used as standard model to convert the OD obtained in UV-Vis spectroscopy to convert the value to GNP concentration (in nM).

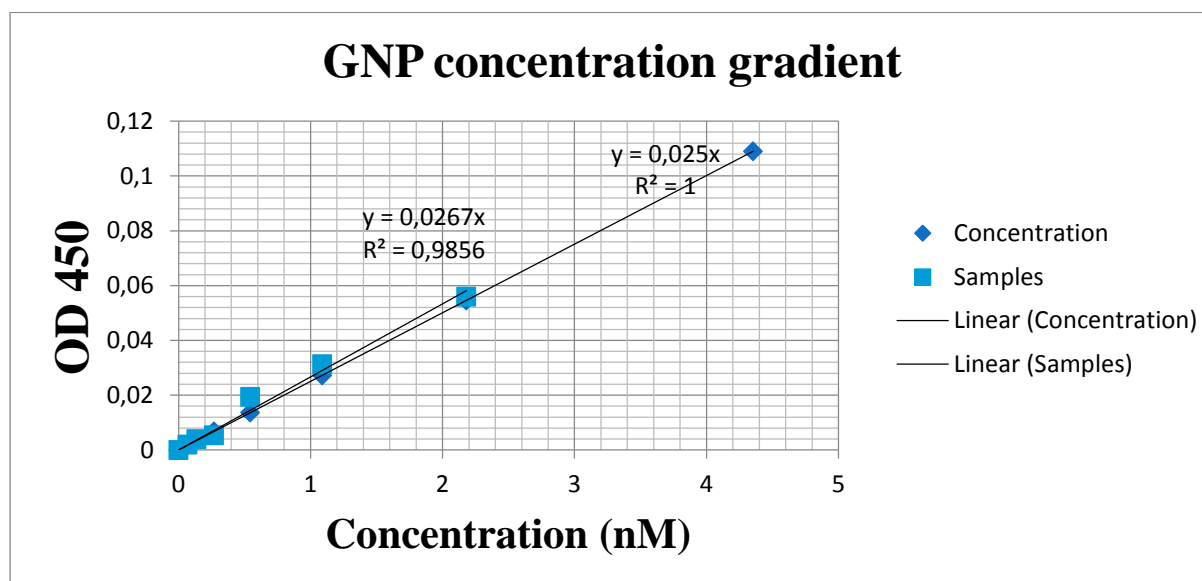


Figure B-1: Concentration gradient of the samples (■) compared with the mathematically calculated (theoretical) concentration gradient (◆). $R^2 = 1$ (or close to 1) shows a linear trend line.

Addendum C: Ligand exchanged GNPs

Ligand exchange is performed (Section 3.2.4). Figure C-1 illustrates the size and surface orientation of each individual Lig-GNP and more specifically the behaviour of the Ligand on the GNP surface. These illustrations give a better understanding as to how each respective Lig-GNP functions based on its physico-chemical properties. For instance, MUA is a small, negatively charged, thiol containing molecule and therefore a large number of MUA molecules are strongly attracted to the surface of the GNP, leading to densely packed MUA molecules. In contrast, BSA is a large protein molecule, which has a less strong affinity towards the GNP core and more spherical hindrance due to the surface orientation and single binding site on the GNP. Finally, polymers such as PEG, PSSNa and PVP are long molecules with multiple attachment points, which allows a single molecule to wrap around the GNP and occupy more than one attachment points. These Lig-GNPs will appear small, even though the ligands on the surface are large.

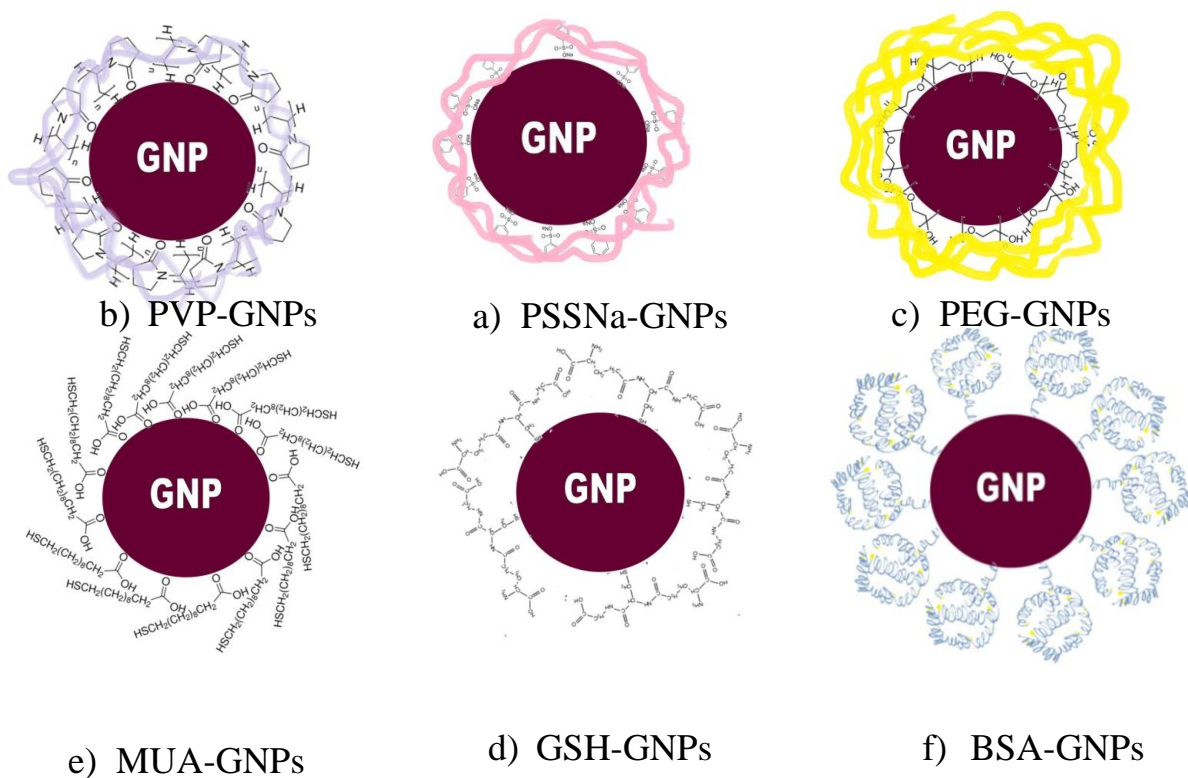


Figure C-1: The spherical orientation of each Lig-GNP (not to scale).

The polymer ligands [which included a) PVP-GNPs, b) PSSNa-GNPs and c) PEG-GNPs] are wrapped around the GNP core due to multiple attachment points on a single molecule. Therefore, even though the ligand is a large molecule, the Lig-GNP will not be significantly large. The Ligands have an electrostatic affinity towards the GNP core and is therefore not as strongly bound as thiol containing molecules. Small ligands such as d) MUA-GNPs are strongly bound due to the GNPs affinity towards the thiol group. The MUA molecules are also densely packed due to their small size. Larger molecules such as e) GSH and f) BSA contribute to increasing the diameter of the Lig-GNP. Each large molecule only has one attachment point, leading to a few molecules on the surface of the particle which are less densely packed due to their large size and spherical orientation.

Addendum D: Stability analysis

Each Lig-GNP treatment group was evaluated to determine the stability of the functionalised GNPs when introduced to chemical environmental changes which represent the circumstances within the cells; such as difference in pH, the presence of salts, organic compounds, media and buffers. In this addendum the method and results will be discussed in more detail.

An initial salt stress test was performed, where concentrated NaCl was added to the Lig-GNPs. Thereafter, a titration range was done with salt and pH. The effect of clean RPMI and complete RPMI media that was used for cell culturing was also evaluated. The experiment was also performed with different buffers, organic molecules and thiols. Table D-1 is a summary of the compounds, concentrations and other specifications used to evaluate the stability of Lig-GNPs. The Lig-GNPs were quantitatively considered stable if no colour change was observed upon addition of the stressor compound. A colour shift from burgundy red to darker purple, blue, grey or black is indicative of instability. The samples were also analysed with UV-Vis spectrometry to confirm the results. Deviation from the reference peak indicates that the particles are unstable. For instance, Figure D-1 shows the difference in absorbance between stable GNPs (PSSNa-GNPs) and particles that are not stable (Cit-GNPs) when exposed to the same stressor compound (50 mM NaCl).

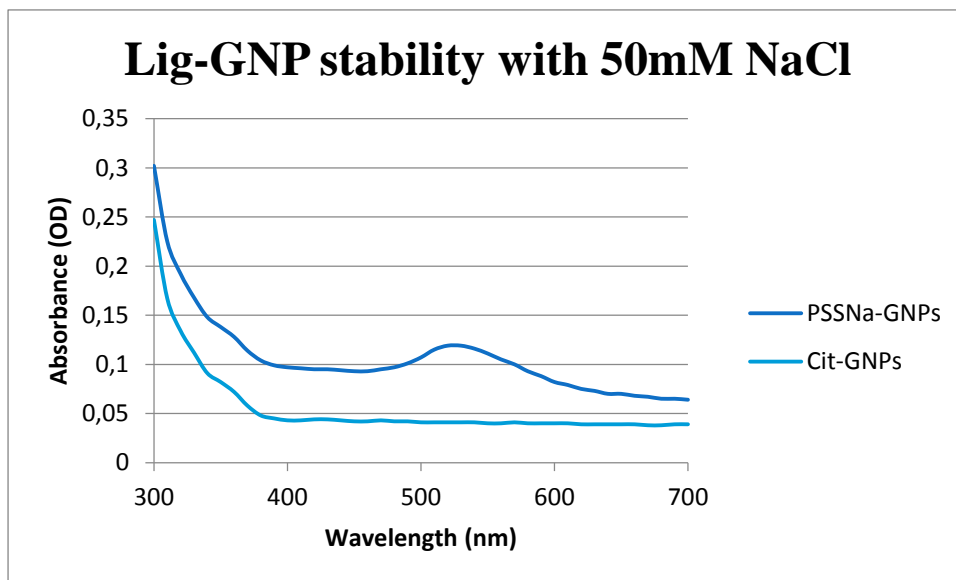


Figure D-1: The absorbance spectrum of Cit-GNPs and PSSNa-GNPs after immediate addition of 50 mM of NaCl.

The Cit-GNPs lack the normal absorbance peak, indicating that the particles are unstable in this particular condition.

Initial salt stress test

After standardisation of ligand exchange, each sample was evaluated in terms of stability with a range of reagents. However, before the evaluation an initial salt stress test was performed with every sample by adding 10 μ l of 1.5 M NaCl to 200 μ l GNPs and visualising whether the particles were stable or not. The aim was to get an approximate indication of stability, where after a more accurate titration series would follow to determine the threshold point.

Stability evaluation

The following reagents represent conditions of the cell that is relevant to the study. Therefore, GNP interaction in each condition was evaluated *in vitro* to predict how stable the samples are to compare stability between the different ligand exchanged particles.

Method:

In 96 well plates; the effect of salt, buffers, culture media, organic compounds, thiols and pH was monitored using UV-Vis spectroscopy. An immediate read was done, then after 1 hour, 2 hours, 6 hours, 24 hours and 48 hours.

A salt titration was performed with 1 mM, 10 mM, 50 mM and 100 mM.

Buffers used included EDTA (0.5 ×, 1 ×, 2.5 ×, 5 ×), 10 mM MOPS (pH 9 and pH 10), 100mM HEPES (pH 7 and pH 8) and PBS (0.5 ×, 1 ×, 2.5 ×, 5 ×).

Complete cell culture media (cRPMI) compared with clean media (RPMI).

Organic molecules used include citrate pH 4, 5 & 6 and glycine pH 2, 3, 9 & 10.

To represent the presence of thiol containing compounds, 20 µl β-Mercaptoethanol was used on 30 µl of GNPs.

Water with a pH range of pH 3-10 was used to determine the effect of pH change after ligand exchange has taken place. (pH adjusted with NaOH and HCl)

Table D-1 presents a summary of the compounds used to perform the evaluation.

Table D-1: A list of compounds and concentrations/ pH values used to determine the stability of GNPs in a physiological environment.

Compound	Specification	
Salt titration	NaCl	1 mM, 10 mM, 50 mM and 100 mM
Buffers	EDTA	(0.5×, 1×, 2.5×, 5×),
	10mM MOPS	(pH 9 and pH 10),
	100mM HEPES	(pH 7 and pH 8)
	PBS	(0.5×, 1×, 2.5×, 5×),
Culture media	Complete media	1×
	Clean media	1×
Organic molecules	Citrate	pH 4,5 & 6
	Glycine	pH 2,3,9 & 10
Thiols	β-Mercaptoethanol	20 μl
pH	HCl, NaOH	pH 3, 4, 5, 6, 7, 8, 9 & 10

After UV-Vis Spectrometry analysis, the spectra of the Lig-GNPs which remained similar to the untreated control were considered to be stable. The spectra which shifted or decreased were not stable. Table D-2 is a summary showing which Lig-GNPs were stable after treatment.

Table D-2: The stability of Lig-GNPs under different conditions resembling the cellular environment.

		Citrate-GNPs	PSSNa-GNPs	PVP-GNPs	BSA-GNPs	MUA-GNPs	PEG-GNPs	GSH-GNPs
pH	pH	6<pH<10	4<pH<10	4<pH<10	5<pH<10	4<pH<10	5<pH<10	5<pH<10
Salt	[NaCl] (mM)	1-10	1-50*	1-50*	1-100	1-100	1-50*	1-50*
Buffers	10mM MOPS	9<pH<10*	9<pH<10*	9<pH<10*	9<pH<10	9<pH<10	9<pH<10	9<pH<10
	100mM HEPES	7<pH<8*	7<pH<8*	7<pH<8*	7<pH<8	7<pH<8	7<pH<8*	7<pH<8
	PBS	Not stable	Not stable	Not stable	Stable	Not stable	Not stable	Not stable
	EDTA	>0.01M	>0.01M	>0.05M*	>0.05M	>0.01M	>0.01M*	>0.01M
Organic	Glycine	3<pH<10	2<pH<10	2<pH<10	9<pH<10	3<pH<10	2<pH<10	9<pH<10
	Citrate	4<pH<6*	4<pH<6*	4<pH<6*	4<pH<6*	4<pH<6*	4<pH<6*	pH 6
Thiols	B-Mercapto-ethanol	Not stable	>1h*	>1h*	>1h*	>1h*	>1h*	>1h*
Media	cRPMI	Stable	Stable	Stable	Stable	Stable	Stable	NOT Stable
	RPMI	Not Stable	Not Stable	Not Stable	Not Stable	Not Stable	Not Stable	Not Stable

* Initially stable but decreased in stability over time

Table D-2 shows the ranges where the Lig-GNPs were stable. The values indicated with asterisks (*) is where the stability decreases over time. The GNPs that were selected for the

metabolomics study (Citrate-GNPs, PSSNa-GNPs and PVP-GNPs) were stable in the physiological NaCl range. All the Lig-GNPs were stable in cRPMI and most of the particles were unstable in PBS, therefore ddH₂O was used as vehicle control. The particles were initially stable in the buffers and organic molecules. However, at the 6h time point the stability with these compounds are being compromised as the particles start to react with these molecules over time. All of the Lig-GNPs interacted with the B-Mercaptoethanol, indicating that the Lig-GNPs are vulnerable towards displacement by thiols within the cells.

Addendum E: Cell viability assays

WST-1 data

The following graph, Figure E-1, shows the WST-1 cytotoxicity assay results for all the Lig-GNPs.

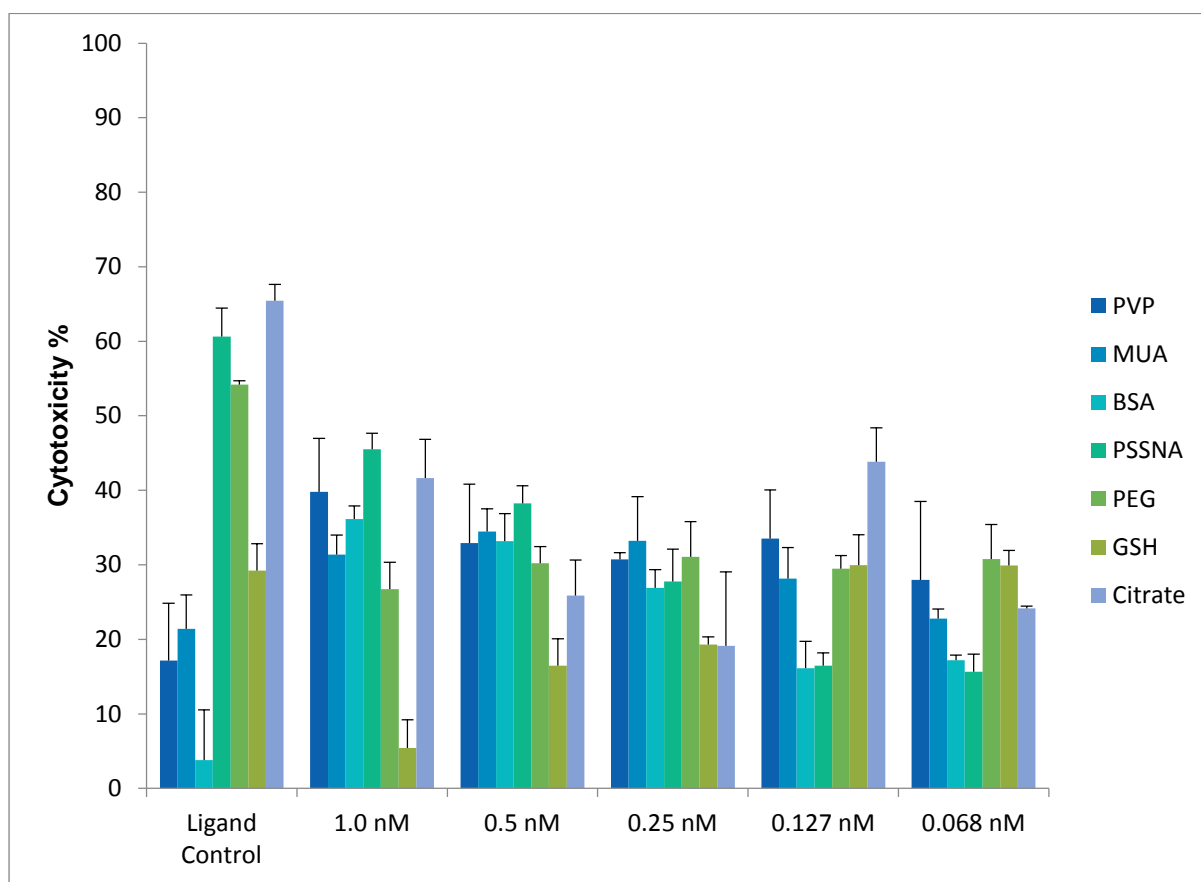


Figure E-1: The WST-1 cytotoxicity results of HepG2 cells treated with a range of Lig-GNP concentrations to determine the IC_{30} values for each treatment.

In most cases, cytotoxicity increased with increase in Lig-GNP concentration, with the exception of GSH-GNPs.

Figure E-2 shows the FI values for all the Lig-GNP treated HepG2 cells

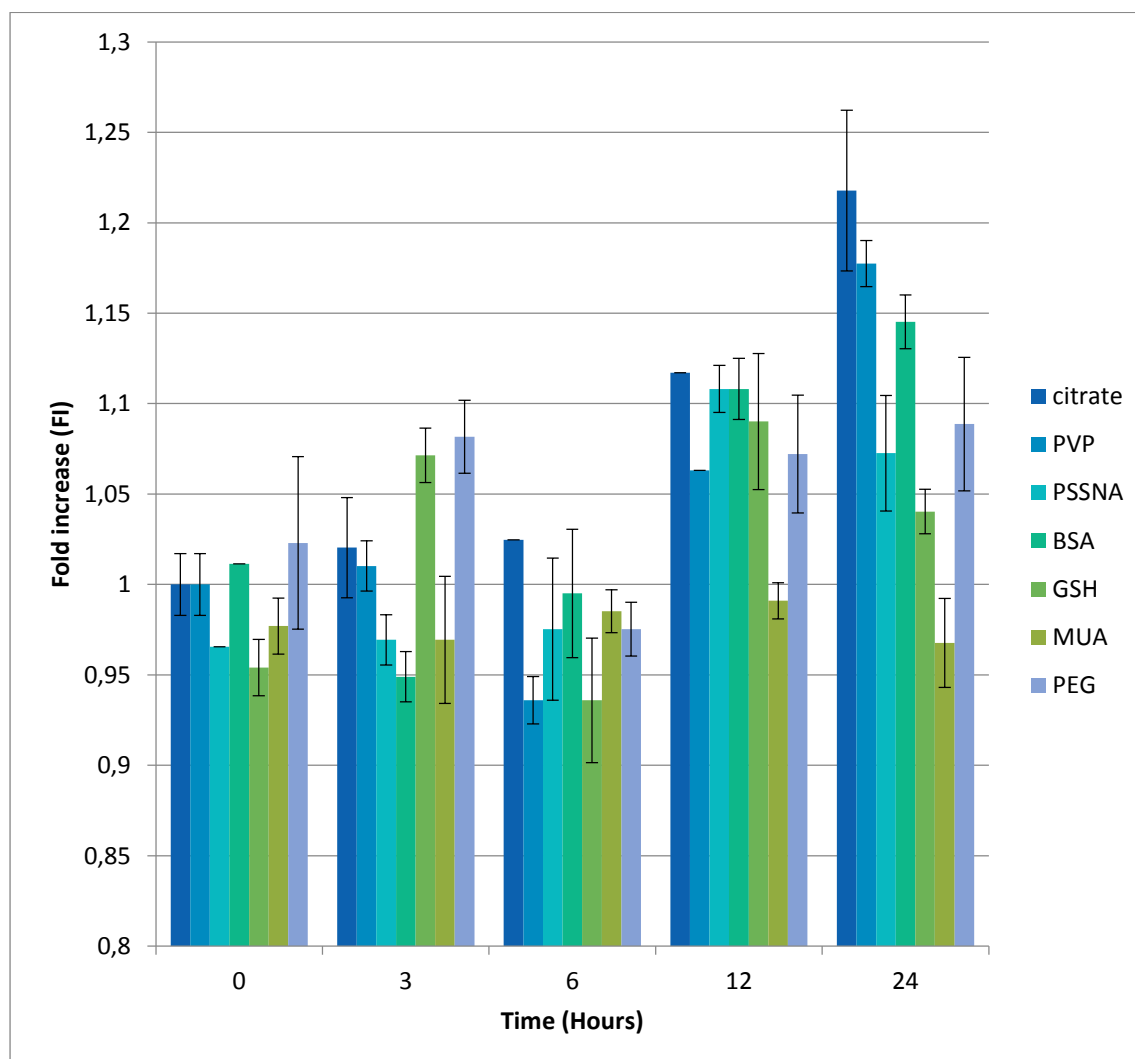
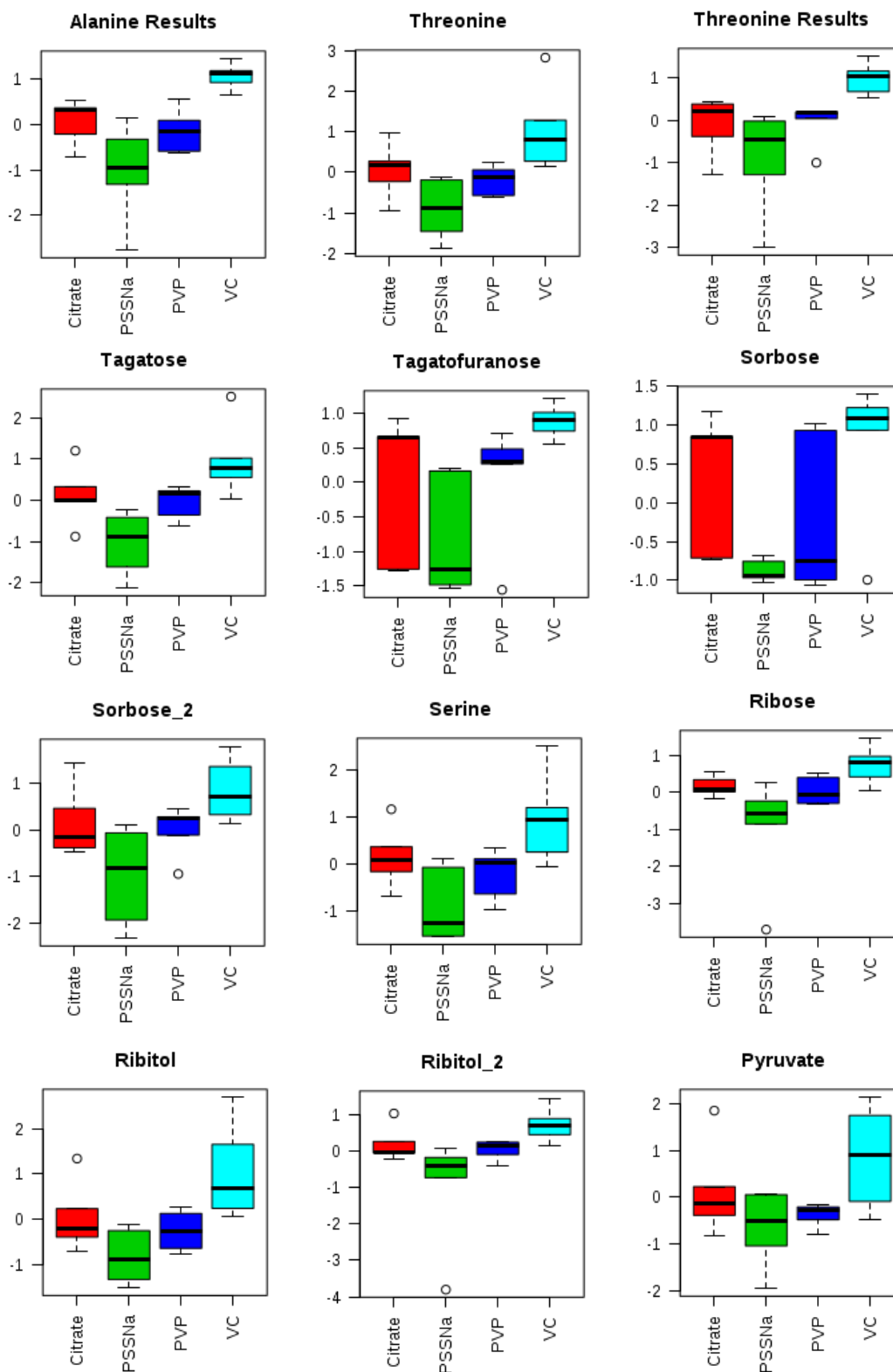
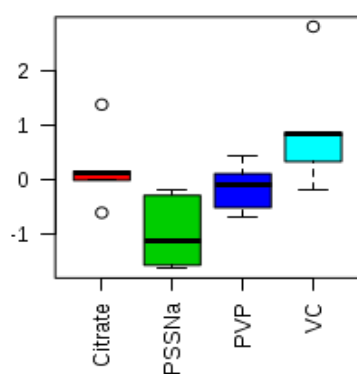
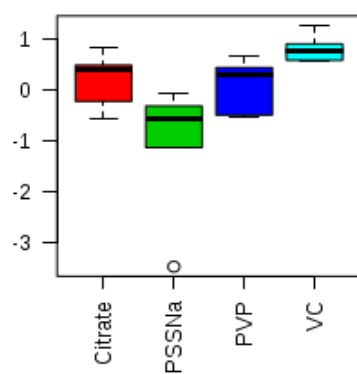
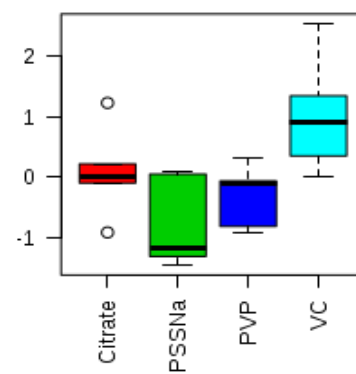
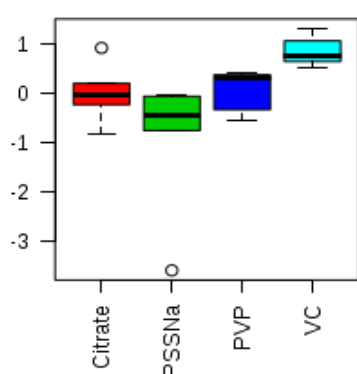
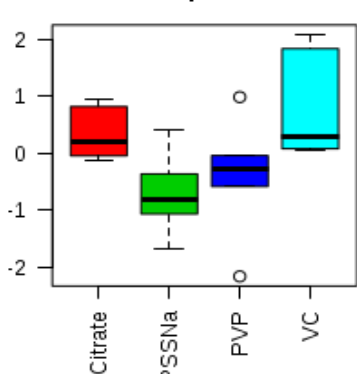
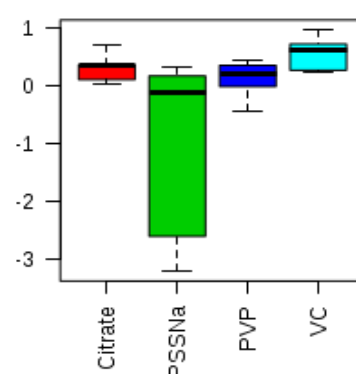
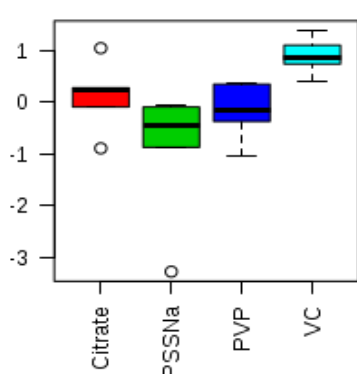
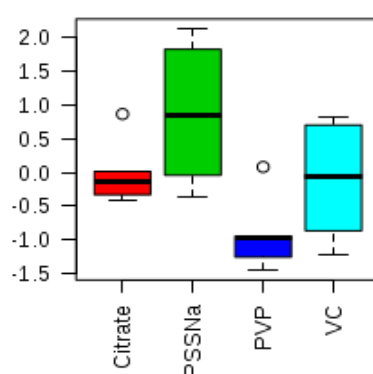
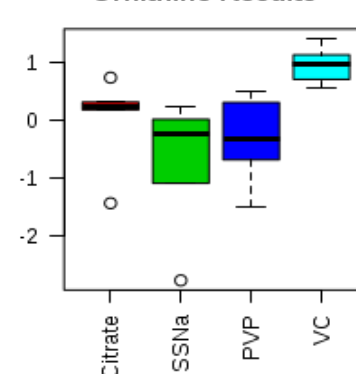
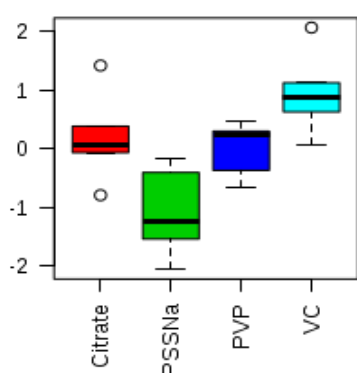
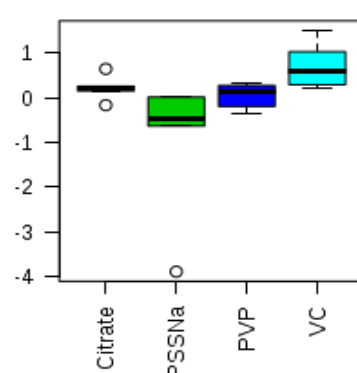
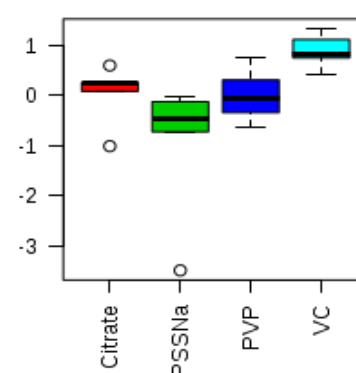


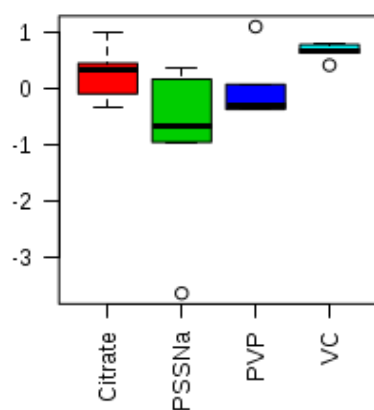
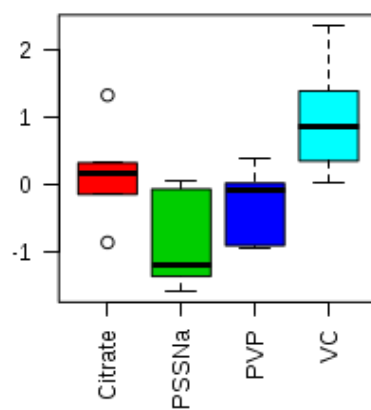
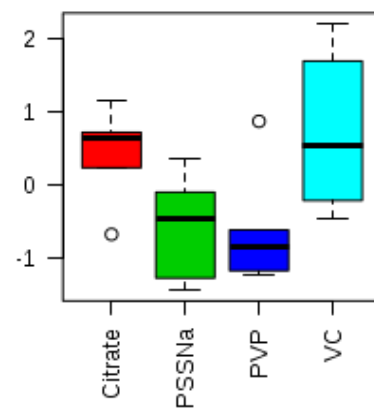
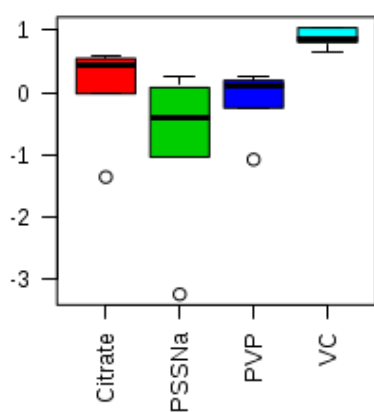
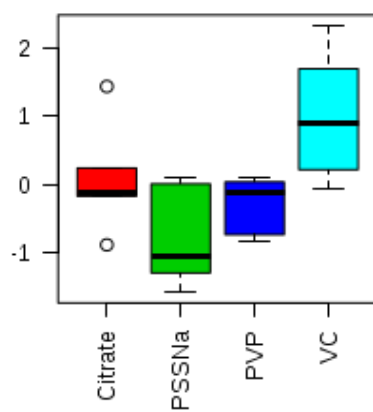
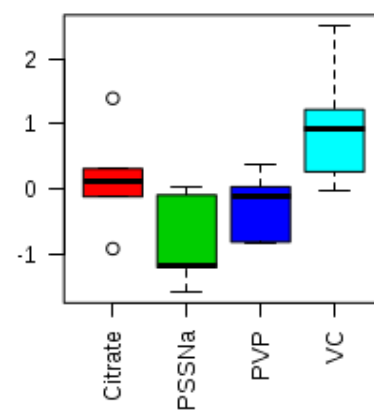
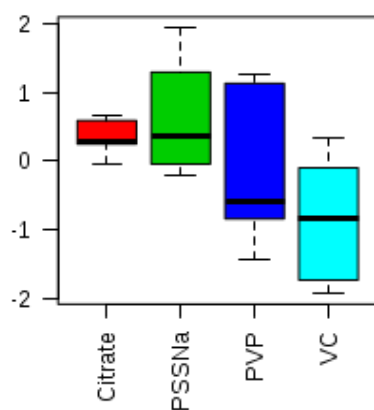
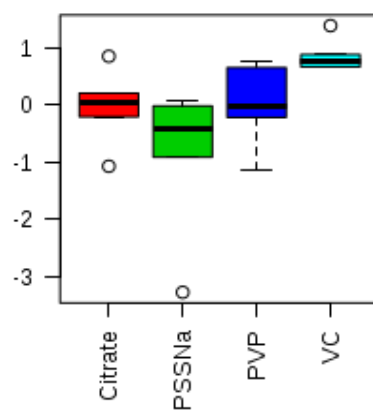
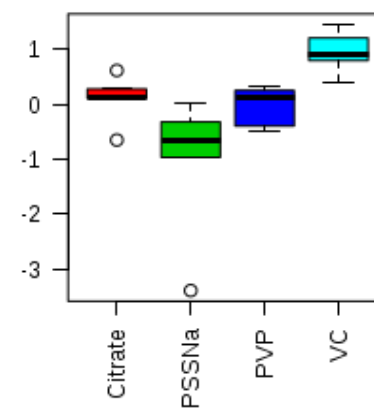
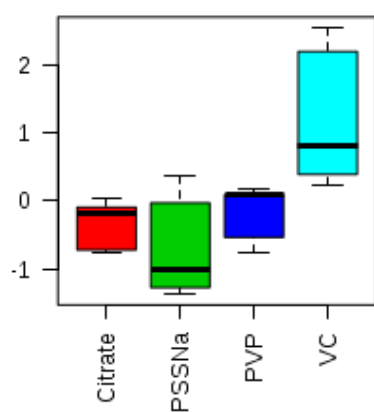
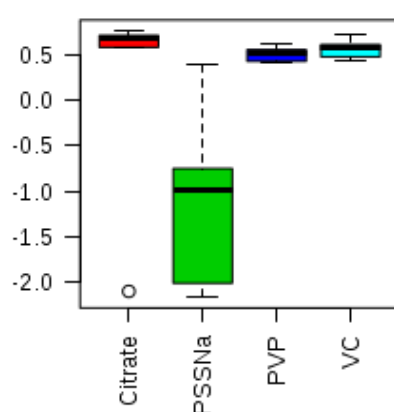
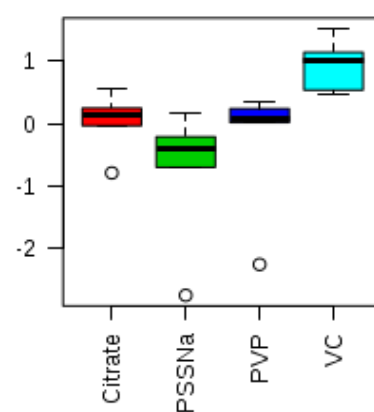
Figure E-2: The Apo % results of HepG2 cells treated with a range of Lig-GNP concentrations.

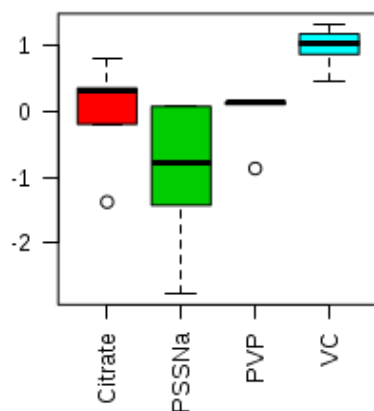
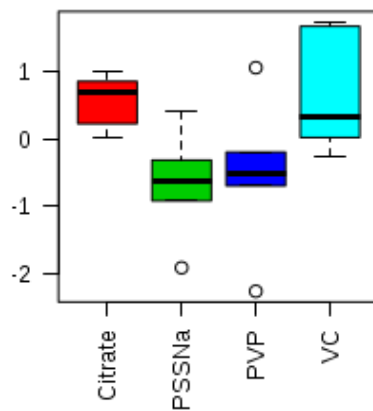
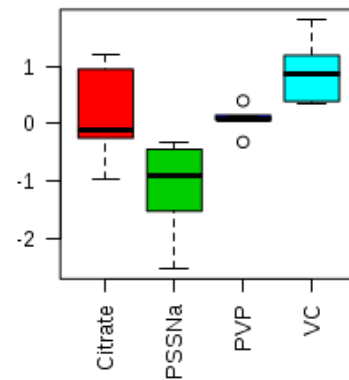
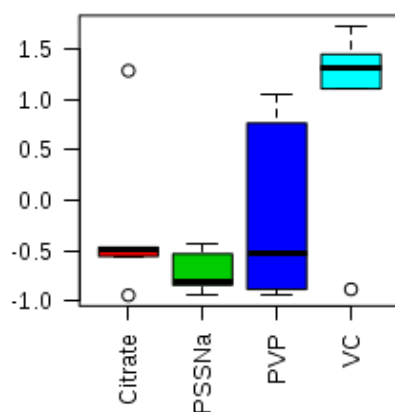
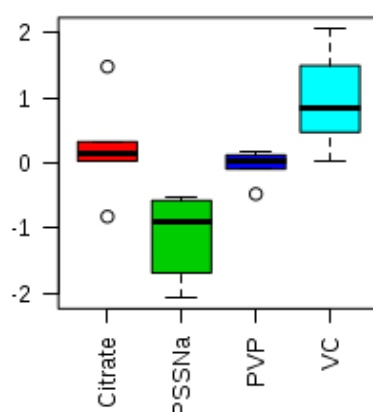
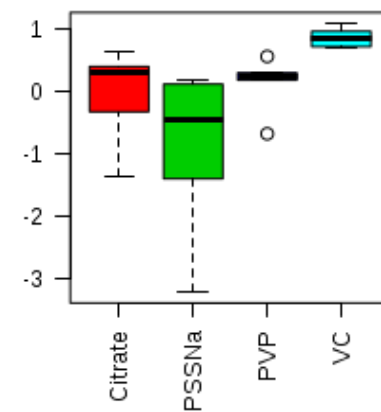
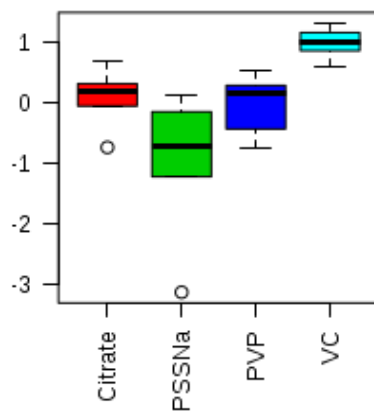
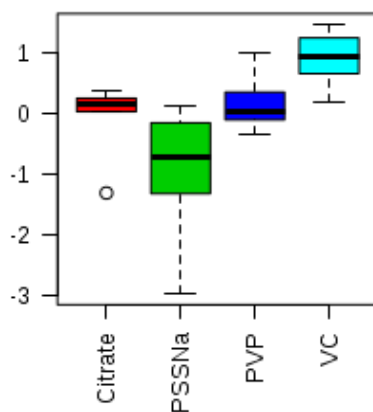
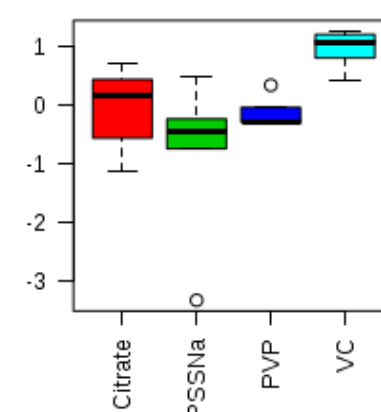
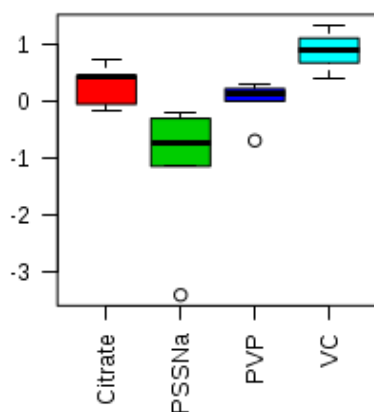
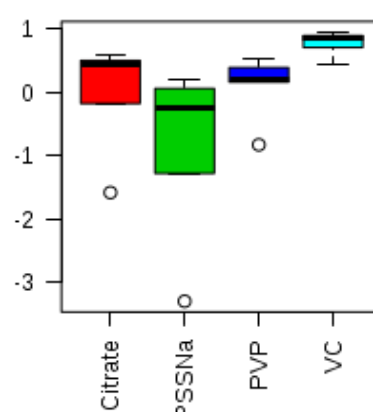
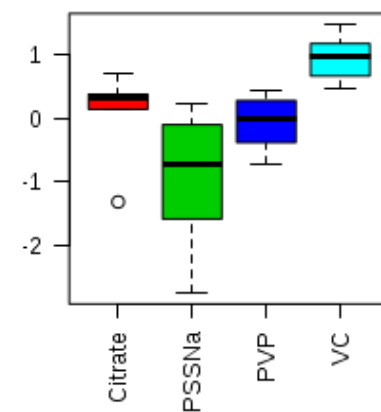
Addendum F: Metabolomics data

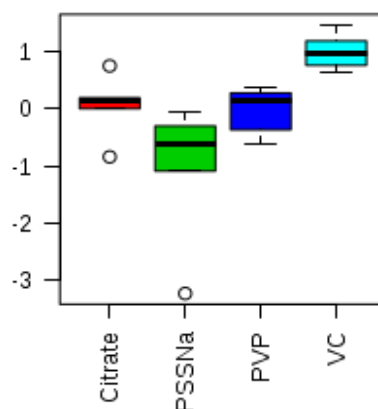
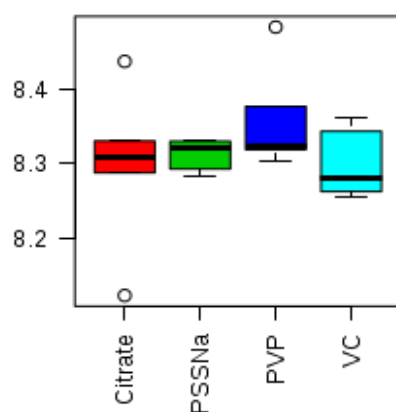
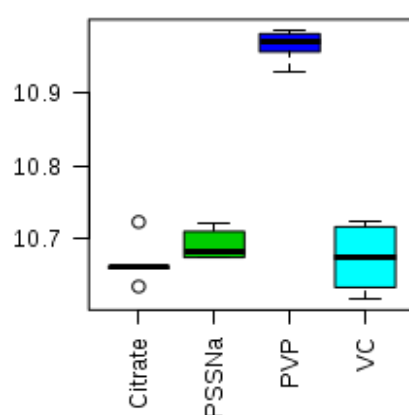
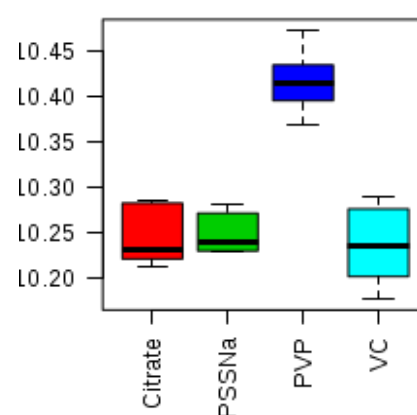
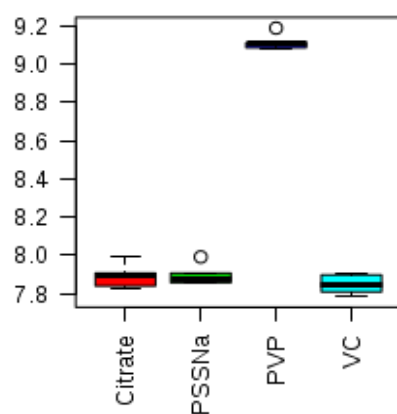
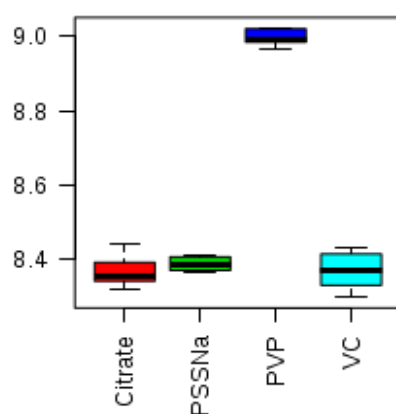
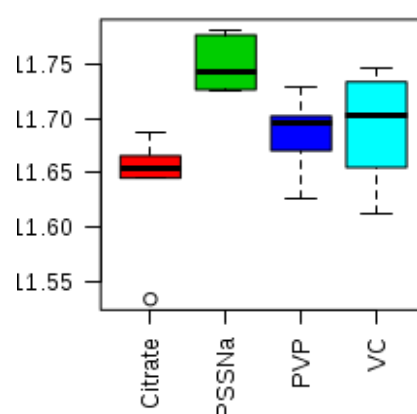
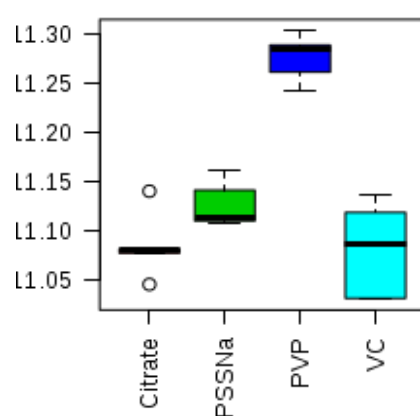
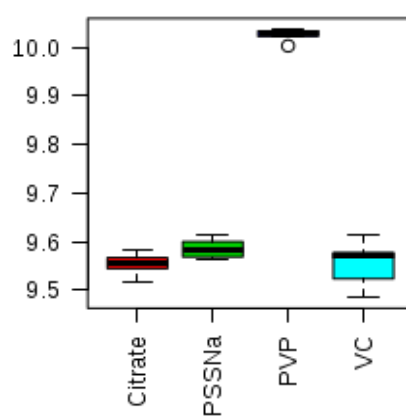
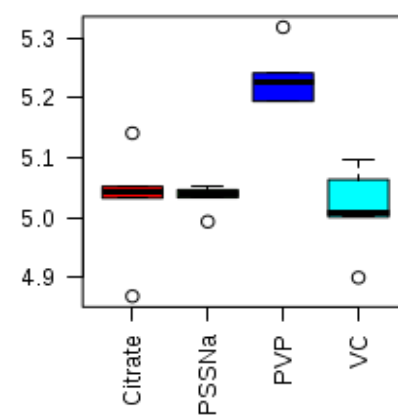
The following box plots show the metabolic variation for each treatment group.



Pyroglutamic acid**Pyroglutamic acid Results****Proline****Proline Results****Phosphate****Phenylalanine****Phenylalanine Results****Oxalic acid****Ornithine Results****Myo-inositol****Methionine****Lysine Results**

Leucine_Isoleucine Results**Leucine****Lactic acid****Tryptophane Results****Valine****Isoleucine****Homocysteine Results****Histidine Results****Glycine Results****Glycine 2TMS****Glycerol, tris(trimethylsilyl) ether.1****Glutamine Results**

Valine Results**Glucose****Glucose_2****Fructose****D-Turanose, heptakis(trimethylsilyl)****Creatine Results****Citrulline Results****C5 Results****C4 Results****C2 Results****Aspartic acid 2BE Results****Asparagine Results**

Tyrosine Results**Valine NMR****Arginine/Lysine****Arginine****Proline NMR****myo-inositol****Lactate****Glutamine****Glutamate/Proline****Choline**

Addendum G: Materials, suppliers and preparation of stock solutions.

Materials and suppliers

0.2µm filter	GVS	L1133912
2-ethanesulfonic acid (MES)	Sigma Aldrich	M2933-100G
3-(N-Morpholino)-propanesulfonic acid, (MOPS)	Sigma Aldrich	M1254-250G
96 well plates (Lasec, Cellstar)	(Lasec, Cellstar)	655180
β-mercaptoethanol	Sigma Aldrich	444203-250ml
Acetone	Honeywell	67-64-1
Agarose	Merck	1.01236.0100
Ammoniumbicarbonate (AMBIC)	Sigma Aldrich	1043492
APOPercentage™ assay kit (Apo %)	Biocolor	A1000
Aurotetrachlorotrihydrate (HAuCl ₄ .3H ₂ O)	Sigma / Merck	254169-500MG
Boric acid (Ortho boric acid)	Merck	B6768-1kg
Bovine Serum Albumin (BSA)	HyClone®	SH30574.02
Disodium Phosphate	Sigma Aldrich	S9763
Ethylenediaminetetraacetic acid (EDTA)	Merck	324503
Falcon tube (15 ml, Lasec (Cellstar))	Lasec (Cellstar)	188261
Falcon tube (50 ml, Lasec (Cellstar))	Lasec (Cellstar)	227261
Glutathione, reduced (GSH)	Merck	1.04090.0005
Glycerol	Merck	1.04092.1000
Glycine	Sigma Aldrich	G71260-100G

Hydrochloric acid (HCl)	Merck	1.00313.2500
L-Cysteine (L-Cys)	Sigma Aldrich	W326305-100G
Methoxyamine Hydrochloride	Sigma Aldrich	593-56-6
Mercaptopropionic acid (MPA)	Merck	8.22087.0100
Mercaptosuccinic acid (MSA)	Merck	8.20763.0100
Mercaptoundecanoic acid (MUA)	Sigma Aldrich	450561-5G
Microcentrifuge tube (1.5 ml, Eppendorf)	Merck	54100N
N-(2-Hydroxyethyl)-piperazine- -ethanesulfonic acid, (HEPES)	Sigma	H3375-100G
N-acetyl-L-Cysteine (NAC)	Merck	616-91-1
N-mercaptopropionyl glycine (MPG)	Sigma Aldrich	M6635-10G
Poly-ethylene Glycol (PEG) 6000	Sigma Aldrich	81323-250G
Polyethylene imine (PEI)	Sigma Aldrich	408700-250ml
Polyethylene oxide 100k (PEO)	Sigma Aldrich	818986-250G
Polystyrenesulfonate (PSS)	Sigma Aldrich	561967
Polystyrene cuvettes (Malvern)	Malvern	DT50012
Polyvinylpyrrolidone (PVP)	Sigma Aldrich	PVP-40-100G
Potassium Phosphate	Sigma Aldrich	P3786
Sodium Carbonate (Na ₂ CO ₃)	Sigma Aldrich	S6014-500G
Sodium chloride, (NaCl)	Merck	230952-100G
Sodium hydroxide (NaOH)	Merck	1.06462.1000
Thioglyconic acid (TGA)	Merck	1.00700.0100

Trisodium Citrate	Sigma Aldrich	S4641-500G
Trypsin	Lonza	BE02-007E
Tween-20	Merck	8.22184.0500
Tween-80	Merck	8.22187.0500
WST-1 Cell viability / Cytotoxicity Reagent	Roche	11644807001

Stock solutions and buffers

Aqua regia: One Part nitric acid (HNO_3) slowly added to three parts hydrochloric acid (HCl). Caution, corrosive, exothermic reaction

Assay medium (not buffered), Seahorse XF analysis: 8.3 g Sigma D5030 powder was dissolved in autoclaved 990 ml tissue culture-grade H_2O . The solution was supplemented with NaCl (final concentration 143 mM); 0.5 % Phenol Red solution (Sigma P0290, final concentration of 3mg/L); GlutaMAX solution for a final concentration of 2 mM. The pH was adjusted with 0.5 M NaOH . Stored at 4 °C

Aurotetrachlorotrihydrate solution, methanolic: 50mM tetrachloroauratetrihydrate ($\text{HAuCl}_4 \cdot 3\text{H}_2\text{O}$) was prepared in 50 ml methanol, covered with aluminium foil and stored at 4°C.

HEPES Buffer: HEPES solution was prepared from a 0.5 M stock solution to a final concentration of 20 mM in dH_2O . The pH was adjusted to pH 8 and stored at room temperature.

MES Buffer: MES solution was prepared from a 0.5 M stock solution to a final concentration of 20 mM in dH_2O . The pH was adjusted to pH 6 and stored at room temperature.

Methoxyamine in pyridine: MOX solution was prepared by adding 0.02g MOX reagent to 10 ml pyridine to a final concentration of 2000 ppm. Caution; hazardous, toxic, flammable.

TBE Buffer (Tris/Borate/EDTA) (10x): 0.9 M Tris (pH 8.3), 0.89 M boric acid and 25 mM EDTA dissolved in dH₂O. The solution pH was adjusted to pH 8.3 with NaOH and then autoclaved. The stock solution was stored at room temperature and diluted ten-fold when needed.

TAE Buffer (Tris/Acetic acid/EDTA): 40 mM Tris, 20 mM acetic acid, and 1mM EDTA dissolved in dH₂O. The solution pH was adjusted to pH 8 with NaOH and stored at room temperature.

PBS Buffer (Phosphate buffered saline) (10x) : 1.37 M NaCl, 27 mM KCl, 100 mM Na₂HPO₄ and 18 mM KH₂PO₄ was dissolved in 500 ml dH₂O and stores at room temperature. The stock solution was stored at room temperature and diluted ten-fold when needed.

Addendum H: Comet assay results reported by Mulder et al., (2016)

Mulder et. al (2016) reported DNA damage in HepG2 cells treated with various Lig-GNPs. The comet assay (alkaline single cell gel electrophoresis) was used to determine DNA damage in single cells by gel electrophoresis. The head of the comet is densely packed DNA and the tail shows fragmented and relaxed DNA. The ratio of the head versus the tail fluorescence is used to determine the amount of DNA damage. The following images show DNA damage of cellular nuclei determined with the comet assay. Figure H-1: 0 hours after treatment; Figure H-2: 3 hours after treatment; Figure H-3: 24 hours after treatment. (With permission from Mulder et. al 2016)

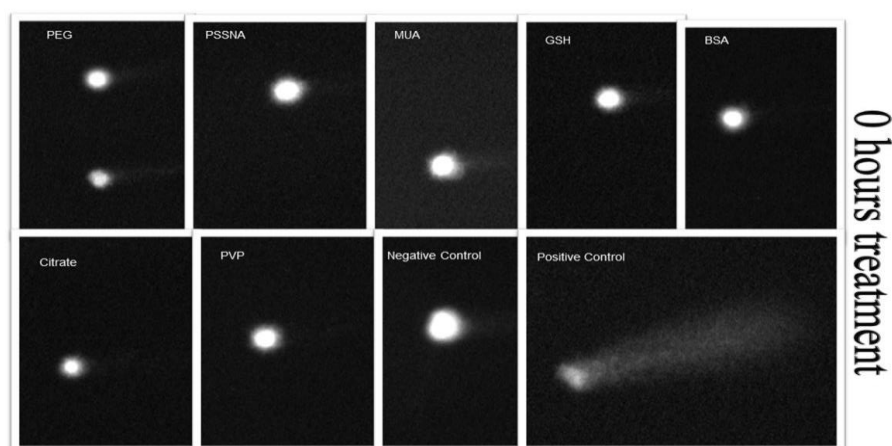


Figure H-1: Comet assay results of Lig-GNP treated HepG2 cells 0 hours after treatment. DNA damage is limited, indicated by absence of comet tails (as noted in the positive control)

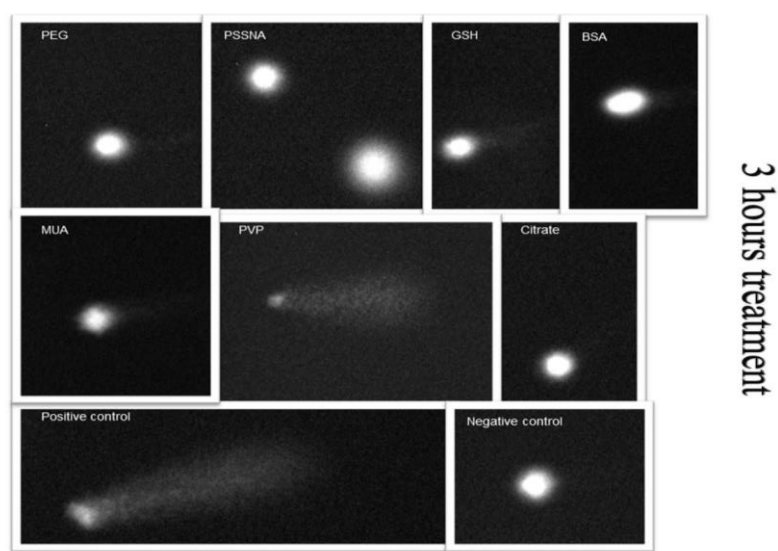


Figure H-2: Comet assay results of Lig-GNP treated HepG2 cells 3 hours after treatment. PVP-GNPs show DNA degradation characterised by the comet shape noted.

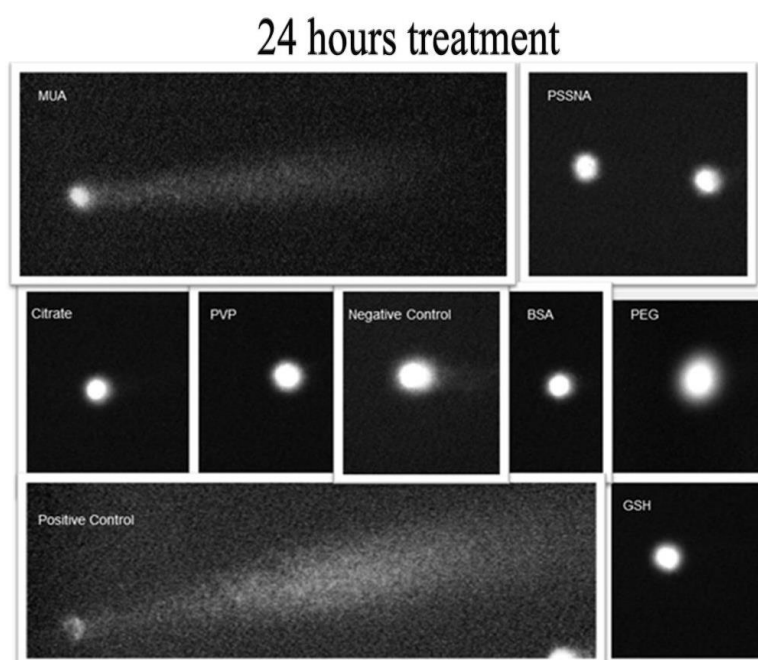


Figure H-3: Comet assay results 3 results of Lig-GNP treated HepG2 cells 24 hours after treatment. MUA shows visible DNA damage, where PVP shows no comet tail. The absence in comet tail for PVP indicates that the cells were able to repair the DNA damage.

Addendum I: Ligand exchange ppm-mol calculations

GNPs in 2 ml (For ligand exchange)		2,18nM	2000 µl		4,36E-12 ppm
Volume		V1 (µl)	V2 (µl)	V1 (l)	V2 (l)
		2100	100	0,0021	1E-04
		2120	120	0,00212	1E-04
		2140	140	0,00214	1E-04
		2160	160	0,00216	2E-04
		2180	180	0,00218	2E-04
		2200	200	0,0022	2E-04
GSH	Concentration	Mol ligand		~ Ligand: GNP	ppm ratio
0,0001	0,025	M		573394	0,6
0,00012			mol	688073	0,7
0,00014			mol	802752	0,8
0,00016			mol	917431	0,9
0,00018			mol	1032110	1
0,0002			mol	1146789	1,1
PEG	Concentration	Mol ligand		~ Ligand: GNP	ppm ratio
0,0001	0,025	M		573394	0,6
0,00012			mol	688073	0,7
0,00014			mol	802752	0,8
0,00016			mol	917431	0,9
0,00018			mol	1032110	1
0,0002			mol	1146789	1,1
PVP	Concentration	Mol ligand		~ Ligand: GNP	ppm ratio
0,0001	0,003	M		57339	0,6
0,00012			mol	68807	0,7
0,00014			mol	80275	0,8
0,00016			mol	91743	0,9
0,00018			mol	103211	1
0,0002			mol	114679	1,1

MUA	Concentration	Mol ligand	Ligand (ppm)	~ Ligand: GNP	ppm ratio
0,0001	1E-04	M	1E-08	2294	2300
0,00012			1,2E-08	2752	2700
0,00014			1,4E-08	3211	3200
0,00016			1,6E-08	3670	3600
0,00018			1,8E-08	4128	4100
0,0002			2E-08	4587	4500
Citrate	Concentration	Mol ligand	Ligand (ppm)	~ Ligand: GNP	ppm ratio
0,0001	9E-04	M	8,7E-08	19954	20000
0,00012			1,044E-07	23945	24000
0,00014			1,218E-07	27936	28000
0,00016			1,392E-07	31927	32000
0,00018			1,566E-07	35917	36000
0,0002			1,74E-07	39908	40000
BSA (1 mg/ ml)	Concentration	Mol ligand	Ligand (ppm)	Ligand: GNP	ppm ratio
0,0001	1	mg/ml	-	100	3,81E-17
0,00012			-	120	4,57E-17
0,00014			-	140	5,33E-17
0,00016			-	160	6,09E-17
0,00018			-	180	6,85E-17
0,0002			-	200	7,62E-17
BSA (1 mg/ ml)	Concentration	Mol ligand	Ligand (ppm)	Ligand: GNP	ppm ratio
0,0001	1	mg/ml	0,0001	100	2,29E+01
0,00012			0,00012	120	2,75E+01
0,00014			0,00014	140	3,21E+01
0,00016			0,00016	160	3,67E+01
0,00018			0,00018	180	4,13E+01
0,0002			0,0002	200	4,59E+01

1 ppm is equal to the ratio of 1 mol GNPs to 1×10^6 mol capping material.

Calculate the amount of moles in 2 ml of 2.18 nM GNPs as follows:

$$n = C \times V$$

$$n = (2.18 \times 10^{-9} \text{ M}) \times (2000 \times 10^{-6} \text{ L})$$

$$n = 4.36 \times 10^{-12} \text{ mol GNPs}$$

Ligand exchange calculations: (GSH as example)

25 mM GSH in different volumes GNPs (100-200 μ l)

$$n = C \times V$$

$$n = (0.025 \text{ mol/L}) \times (0.0001 \text{ L})$$

$$n = 0.0000025 \text{ mol}$$

$$n = 2.5 \text{ } \mu\text{mol}$$

Therefore, ppm ratio is equal to the amount of mol GSH ligand divided by the amount of mol GNPs.

$$ppm = \frac{2.5 \text{ } \mu\text{mol GSH ligand}}{4.36 \text{ pmol GNPs}}$$

$$ppm = 573394.495$$

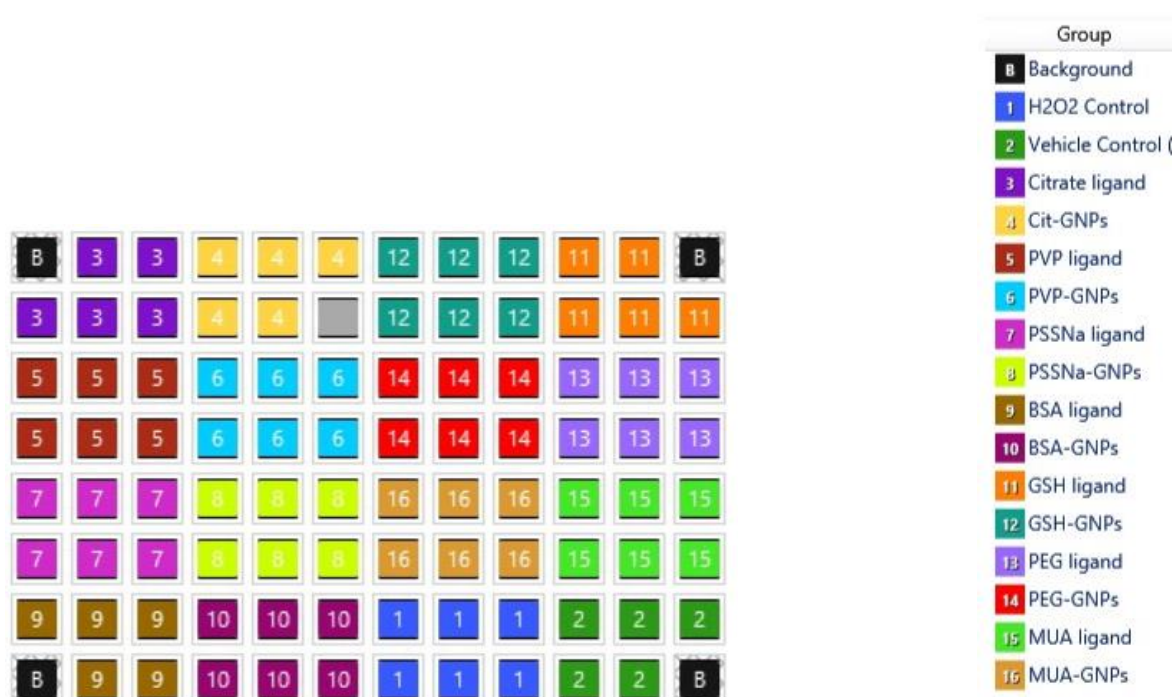
$$= \sim 600\,000 \text{ to } 1$$

Therefore, the ratio of capping material to GNPs was 0.6 ppm.

Addendum J: Seahorse XF analysis elaborated protocol

1 Software protocol

A protocol is created for the assay using the Seahorse Bioscience software as follows:



The instrument is switched on and the XF software was initiated to allow instrument to stabilize at 37°C.

2 Cell culture preparation

Cells were seeded in XFe96 Cell Culture Plates

- Cells were harvested by trypsinization (2 mL for T75), mixed before adding 4ml media to loosen clumps.(Add 4 mL media to T75 flask.)
- The flask was mixed well and the cell suspension was placed into a 15 mL centrifuge tube
- PBS (900 µL) was placed into a 1.5 mL Eppendorf tube and 100 µL of the cell mixture was added to this. Cells were counted using the Sceptor 2.0 Handheld cell counter. The answer was multiplied by 10 and the values entered into an excel spreadsheet.

Sample	HEPG2
Number of cells per mL	1896000
Desired cell seeding density (cells/well)	7500
Final volume of cells to be added to master mix	346
Final volume of medium to be added to mastermix	6654

- i. Master mixes were prepared and seeded: 80 μ L cells/well using a multichannel pipette and sterile reservoir or using a single-channel pipette.
- ii. The plate was allowed to stand at room temperature for 1 hour in the laminar flow cabinet before placing in the 5% CO₂ incubator at 37°C for 16 hours.
- iii. Time that cells were seeded: are shown in the table below
- iv. Time range – Seed 3 different plates on 3 different days:
- v. The 6 hours analysis was repeated to verify the effect of day to day analytical variation

3 Hours analysis	Time	Action	
Saturday 29/8/2015	18:00	Seed cells	
	19:00	Place in incubator	Hour 1
Sunday 30/8/2015	11:00	Add 40 μ l media	Hour 16
Monday 31/8/2015	8:00	Treat cells	Hour 37
	11:00	Seahorse analysis	Hour 40
6 Hours analysis	Time	Action	

Sunday 30/8/2015	15:00	Seed cells	
	16:00	Place in incubator	Hour 1
Monday 31/8/2015	08:00	Add 40µl media	Hour 16
Tuesday 01/09/2015	06:00	Treat cells	Hour 34
	12:00	Seahorse analysis	Hour 40
12 Hours analysis	Time	Action	
Monday 31/8/2015	15:00	Seed cells	
	16:00	Place in incubator	Hour 1
Tuesday 01/09/2015	08:00	Add 40µl media	Hour 16
Wednesday 02/09/2015	06:00	Treat cells	Hour 34
	12:00	Seahorse analysis	Hour 40
6 Hours analysis	Time	Action	
Tuesday 01/09/2015	21:00	Seed cells	0
	22:00	Place in incubator	Hour 1
Wednesday 02/09/2015	13:00	Add 40µl media	Hour 16
Thursday 03/09/2015	07:00	Treat cells	Hour 34
	13:00	Seahorse analysis	Hour 40

- a. Plate 1 = 3 hour incubation – 16 hours after cells were seeded, add 40 µL media. 37 hours after cells were seeded, add 100 µL treatment.
- b. Plate 2 = 6 hour incubation - 16 hours after cells were seeded, add 40 µL media. 34 hours after cells were seeded, add 100 µL treatment.

- c. Plate 4 = 24 hour incubation - 16 hours after cells were seeded, add 40 μ L media and 100 μ L treatment. Time of treatment: 8:00 (Thurs 27 Aug)

vi. Dilutions of compounds:

Blank Calculations					
Calculations	Stock solution	Ligand exchange	For WST-1 Dose 1 (100 μ L citrate, 120 μ L media)	Seahorse (use dose 2 (75 μ L))	Master mix
Citrate	38.8mM	C1V1=C2V2 (38.8mM)(2300 μ L)= C2 (102800 μ L) C2=0.87mM	C1V1=C2V2 (0.87mM)(220 μ L)=(38.8mM)V2 V2=5 μ L citrate, 95 μ L H2O x40 =200 μ L citrate, 3800 μ L H2O	C1V1=C2V2 (0.87mM)(75 μ L)=C2 (100 μ L) C2=0.6525mM	Per well Add 75 μ L (0.87mM) citrate to 25 μ L H2O Final volume 100 μ L x40 for stock (3000 μ L citrate, 1000 μ L H2O)
PVP	2.5mM	C1V1=C2V2 (1000 μ L)(2.5mM)=C2 (11000 μ L) C2=0.23mM	C1V1=C2V2 (0.23mM)(220 μ L)=(2.5mM)V2 V2=20 μ L, 80 μ L H2O x20 =400 μ L PVP, 1600 μ L H2O	(use dose 3 (50 μ L)) C1V1=C2V2 (0.23mM)(50 μ L)=C2 (100 μ L) C2=0.115mM	per well Add 50 μ L (0.23mM) PVP to 50 μ L H2O Final volume 100 μ L x40 for stock (2000 μ L PVP, 2000 μ L H2O)
PSSNa	1%	C1V1=C2V2 (500 μ L)(1%)=C2(10500 μ L) C2=0.048%	C1V1=C2V2 (0.048%)(220 μ L)=(1%)V2 V2=11 μ L, 89 μ L H2O x20 =220 μ L PSSNa, 1780 μ L H2O	(use dose 3 (50 μ L)) C1V1=C2V2 (0.048%)(50 μ L)=C2 (100 μ L) C2=0.024%	per well Add 50 μ L (0.024%) PSSNa to 50 μ L H2O Final volume 100 μ L x40 for stock (2000 μ L PSSNa, 2000 μ L H2O)
BSA	1mg/ml	C1V1=C2V2 (500 μ L)(1mg/ml)=C2 (10500 μ L) C2=0.048mg/ml	C1V1=C2V2 (0.048mg/ml)(220 μ L)=(1mg/ml)V2 V2=11 μ L, 89 μ L H2O x20 =220 μ L BSA 1780 μ L H2O	(use dose 3 (50 μ L)) C1V1=C2V2 (0.048mg/ml)(50 μ L) =C2(100 μ L) C2=0.024mg.ml	per well Add 50 μ L (0.024mg/ml) BSA to 50 μ L H2O Final volume 100 μ L x40 for stock (2000 μ L BSA, 2000 μ L H2O)
GSH	25mM	C1V1=C2V2 (500 μ L)(25mM)=C2 (10500 μ L) C2=1.19mM	C1V1=C2V2 (1.19mM)(220 μ L)=(25mM)V2 V2=11 μ L, 89 μ L H2O x10=110 μ L GSH, 890 H2O μ L	(use dose 4 (15 μ L)) C1V1=C2V2 (1.19mM)(15 μ L)=C2 (100 μ L) C2=0.1785mM	per well Add 15 μ L (1.19mM) GSH to 85 μ L H2O Final volume 100 μ L x40 for stock (600 μ L GSH, 3400 μ L H2O)
PEG	25mM	C1V1=C2V2 (700 μ L)(25mM)=C2 (10700 μ L) C2=1.64mM	C1V1=C2V2 (1.64mM)(220 μ L)=(25mM)V2 V2=14.4 μ L, 85.6 μ L H2O x20 =288 μ L PEG 1712 μ L H2O	(use dose 3 (50 μ L)) C1V1=C2V2 (1.64mM)(50 μ L)=C2 (100 μ L) C2=0.82mM	per well Add 50 μ L (0.82mM) PEG to 50 μ L H2O Final volume 100 μ L x40 for stock (2000 μ L PEG, 2000 μ L H2O)
MUA	1mM	C1V1=C2V2 (600 μ L)(1mM)=C2 (10600 μ L) C2=0.057mM	C1V1=C2V2 (0.057mM)(220 μ L)=(1mM)V2 V2=13 μ L, 87 μ L H2O x10=130 μ L GSH, 870 H2O μ L	(use dose 4 (15 μ L)) C1V1=C2V2 (0.057mM)(15 μ L)=C2 (100 μ L) C2=0.00855mM	per well Add 15 μ L (0.00855mM) MUA to 85 μ L H2O Final volume 100 μ L x40 for stock (600 μ L MUA, 3400 μ L H2O)

3 Sensor Cartridge Preparation for the XF96 Assay

- i. The XFe96 Flux Assay Kit was opened and the contents removed.
- ii. The Sensor Cartridge was placed upside down next to the Utility Plate.
- iii. Each well of the Utility Plate was filled with 200 μ L of Seahorse XF Calibrant.
- iv. The Sensor Cartridge was lowered onto the Utility Plate submerging the sensors in XF Calibrant.
- v. The XF Calibrant volume was sufficient to keep the sensors submerged.
- vi. The Utility Plate was placed in a non-CO₂ 37 °C incubator overnight. To prevent evaporation of the XF Calibrant. The incubator is to be properly humidified.

4 Mito stress test

Preparation of unbuffered assay medium (pH 7.4 at 37°C, 1000 ml)

1. 1.85 g NaCl was dissolved in 5 mL H₂O (filter sterilised once dissolved).
2. 1 g NaOH was dissolved in 50 mL H₂O, (filtered sterilised once dissolved, 0.5 M solution).
3. Tissue Culture-grade H₂O was autoclaved (990 mL).
4. One bottle of Sigma D5030 powder was dissolved into the prepared H₂O.
5. The prepared NaCl solution was added to the mixture to obtain a final concentration of 143 mM.
6. 0.6 mL of a 0.5% Phenol Red solution was also added to the mixture (Sigma P0290) for a final concentration of 3mg/L.
7. 10 mL of a 200 mM GlutaMAX solution was added (final concentration of 2 mM).
8. 1.7 mL 0.5 M NaOH was added.
9. Stored at 4°C. (Stable at 4°C for at least 3 months).

Preparation of cell culture plate

1. The Culture plate was rinsed using the XF Prep Station by using 140 mL of assay medium. The assay media was heated to 37°C and the pH was adjusted to 7.4 using NaOH or HCl.
2. The cells were observed under the microscope to:
 - Confirm cell health, morphology, seeding uniformity and purity (no contamination)
 - Ensure cells are adhered, and no gaps are present
 - Make sure no cells were plated in the background correction wells.

Cell culture medium was replaced with assay medium and incubated in non-CO₂ incubator

3. The cells were rinsed with assay medium
 - i. Approximately 300 mL ddH₂O was placed into the “H₂O” bottle and 200 mL 70% ethanol into the “Clean” bottle.
 - ii. Prime Manifold – First prime with “Clean” then prime with “H₂O”.
 - iii. Media Change – “Do Prime” and “Do Rinse”, and set final volume to 175 μ L.

- All wells, including Background Correction or blank wells, need to have vehicle or compound loaded in the port being used to ensure proper injection in all wells.
- To prevent the accidental discharge of compounds prior to starting the assay, the best practice is to hydrate the cartridge and load the injection ports adjacent to the XFe96 Analyzer

The hydrated XF assay cartridge must remain in the utility plate and be placed flat on the work surface throughout the loading procedure. Do not lift or angle the plate away from the bench while loading.

1. Orient the XF Assay Cartridge - The triangular notch will be in the bottom left-hand corner
2. Hold the base of the utility plate whenever handling the cartridge to avoid triggering discharge from the injection ports. Do not hold the cartridge and utility plate between your thumb and fingers
3. Use your fingertips to hold the outside edges of the loading guide to stabilize during loading so pipette tips do not dislodge the loading guide.
4. Position the pipette tips into the desired column in the loading guide, and orient the tips at a very slight angle ($<5^\circ$). Insert the tips as far as they will go without resistance into the holes and dispense the compound. Do not force the tips into the holes.
5. Dispense the compounds into the ports gently. Withdraw the tips from the ports carefully, stabilizing the loading guide throughout the procedure. Avoid creating air bubbles. Do NOT tap any portion of the cartridge in an attempt to alleviate air bubbles. This may cause compound leakage from the injection port.
6. Position yourself at eye level with the cartridge and visually inspect the injection ports for even loading. The liquid should be down at the bottom of the port, make sure there are no residual drops on top of the cartridge. Record the position of any ports which appear uneven for later data analysis.

E. Place cartridge & utility plate with calibration buffer into XF Analyzer. Run protocol from template to calibrate cartridge. Check cells under microscope. Upon completion of cartridge calibration, load cell culture plate into instrument. Continue to run assay protocol.